Bound and Continuum States

of

Diatomic Molecules

using the

R-matrix method

by

Susan E. Branchett

A thesis submitted to

THE UNIVERSITY OF LONDON

for the degree of

DOCTOR OF PHILOSOPHY

University College London   October 1991

ProQuest Number: 10609864

ProQuest 10609864

Abstract

Calculations are presented for electronic excitation of H_2 by electron impact. For the initial calculations, *ab initio* R-matrix scattering techniques are used to represent scattering from the ground to five low lying electronic states of H_2. Each target state is represented by a full configuration interaction treatment within a basis of Slater type orbitals, optimised to give accurate vertical excitation energies. All total symmetries including $^2\Phi_g$ are included in the scattering calculation. Eigenphase sums and integral cross sections are presented for this model together with assignments of the resonance structures produced.

This model is then extended to include the lowest seven electronic states of H_2 at the equilibrium geometry. Eigenphase sums and resonance feature analysis are presented for excitation from the ground to the six excited states included in the calculation. Integral cross sections are also presented for these processes and extensive comparison made with experimental data.

Differential cross sections calculated using the seven state model are presented for both resonant and non-resonant energy regions and comparison made with previous experimental and theoretical results.

A method of adapting scattering calculations to calculate bound states of molecules within the R-matrix method is presented. This method is based on atomic method of Seaton (1985). The results of test calculations on the bound states of CH and HeH, at fixed internuclear separation, are presented together with results for the vibrational bound states of HeH. The development of this method made it possible to calculate transition dipoles for excitation processes. Results for the transitions dipoles of H_2, as a function of internuclear separation, are presented and comparison made with available theoretical data.

2

Contents

4

List of Tables

7

List of Figures

10

Acknowledgements

Chapter 1

Introduction

1.1 General Introduction

In the last twenty years there has been a great interest in the area of electron-molecule collisions. These processes are not only of fundamental importance in the areas of physics and chemistry, where they are used in the study of fusion plasmas and radiation physics, but are also of importance in areas such as astronomy were a detailed knowledge of collision processes is necessary in order to understand interstellar matter and the earth's ionosphere. Recently the introduction of increased computing power and facilities has made it possible to develop new methods for solving the complex theory of molecule scattering.

Collisions between electrons and molecules are clearly more varied than between electrons and atoms. As well as electronic excitation, radiative recombination and ionisation, electron-molecule collisions can also give rise to rotational and vibrational excitation, dissociation, dissociative attachment and dissociative ionisation. For a summary of all the possible collision processes see Burke and Shimamura (1990). The non-spherical nature of the molecule makes the long range collision processes more complex than for the atomic case by introducing effects such as

multipole interactions between states of the same orbital angular momentum. The possibility of exciting nuclear degrees of freedom introduces important resonance effects which are not found in electron-atom collisions. Because of the increased complexity of the collision problem it became necessary to modify the methods used previously for studying electron-atom collisions and to introduce new ones. A brief discussion of some of the more useful methods developed to study molecule scattering and to calculate the bound states of a molecular system is given below.

1.2 Scattering Methods

Several methods have been developed to study low energy electron collisions with molecules. Some of these methods have used the laboratory frame as their frame of reference (Takayanagi and Geltman 1965), but these methods have so far only proved suitable for light, diatomic molecules due to the complex nature of the representation. Most of the methods used recently to produce successful results have used the molecular frame of reference with the internuclear distance assumed to be fixed. Relaxation of the fixed nuclei approximation and the effects of nuclear motion will be discussed later.

One of the techniques used to solve the fixed nuclei approximation is the single centre expansion technique. This method treats the target orbitals and the scattered electron as an expansion about the centre of mass of the molecule. The main problem associated with this method is that a large number of terms in the expansion are needed for convergence. For certain target molecules, including H_2, the static potential is straightforward to expand as a single centre expansion, but this is not true for all diatomic molecules. The method is, however, widely used in the study of polyatomic molecular targets. The representation of the exchange potential as a single centre expansion is far more complex, however, various methods

14

have been used to overcome these difficulties (Burke and Sinfailam 1970, Morrison 1979, McNaughten *et al* 1990).

Within the single centre expansion method, an iterative method was used to treat exchange by Collins, Robb and Morrison (1978) in the study of electron-H_2 scattering. These calculations produced good results for energies up to 1 eV. Morrison and co-workers went on to develop a method of treating exchange using a model exchange potential. These model exchange potentials are local potentials which imitate the exchange terms in the scattering equations. Morrison and Collins (1981) have made a comparison of two different model exchange potentials for a number of diatomic molecules. They conclude that a free electron gas type model potential treatment compares well with exact static exchange calculations. More recently Buckman *et al* (1991) used a method which treats exchange as separable, but non-local, to study vibration excitation of H_2. Very good agreement was obtained between these results and their experimental work for energies below 5 eV.

The single centre expansion method has also been used in combination with other methods such as the Linear Algebraic method and the Kohn Variational method.

The Linear Algebraic method was adapted by Collins and Schneider (1981) from similar techniques used to solve nuclear collision and electron-atom problems. By using Green's functions and reducing integrals to quadratures, it represents the electron-molecule system by a set of linear algebraic equations which are solved by an iteration-variation method. This method is well suited to vector super-computers and is useful for strong non-local potentials, though it shows no real advantage for local, multipolar potentials. This method is therefore most useful when the electron is close to the target molecule and suggests the division of space into two regions, an inner region where this method is appropriate and an outer

region where an alternative method would be more suitable. See for example the R-matrix method described below. The major disadvantage of the Linear Algebraic method is that the polarisation of the target molecule is treated as a separate potential and therefore the risk of over-polarisation can be large. This method was used to study electron-H_2 scattering (Schneider and Collins 1985), along with two other methods in a coordinated study which will be described below.

The Kohn variational method for electron-molecule collisions was developed by Collins and Robb (1980) from techniques used previously for nuclear collision and electron-atom problems. The method relies on having a good trial wavefunction for the system. It has been shown from the study of several diatomic molecules, including H_2 (Collins and Robb 1980), that the method is reasonably efficient and accurate for producing K-matrices, from which cross sections are calculated, and eigenphases over a wide range of energies. The method is susceptible to spurious singularities in the solution, however, Miller and Jansen op de Haar (1987) have produced a complex Kohn variational method which avoids these singularities. The Kohn variational method has also been employed by Armour and co-workers to study positron-molecule scattering. Results have been produced for positron-H_2 scattering (Armour and Baker 1987) and positron-N_2 scattering (Armour *et al* 1991) and the method is currently being extended to study other diatomic molecules.

The L^2 method for studying molecular scattering was developed from the use of bound state techniques and computer codes. The wavefunction of the system is expanded as a set of L^2 discrete basis functions which are square integrable. This method produces eigenphases of the system at discrete energies determined by the particular basis set used. The method assumes that only weakly coupled, low l values make significant contributions to the integral cross section and it is not possible to produce continuous values of eigenphases with a single basis represen-

tation. The method has been applied to electron-H_2 and electron-N_2 scattering (McCurdy *et al* 1976). The results agree well with previous theoretical studies which use the *l*-spoiling approximation. This method has also been incorporated into the R-matrix, and various T-matrix methods, where it is used to represent polarisation effects sufficiently accurately to enable the study of resonances.

The Schwinger variational method was developed for studying molecule scattering by Takatsuka and McKoy (1981, 1984). It produces the T-matrix of the system. The main advantage of this method over the Kohn variational method is that the trial function does not have to have the correct asymptotic form as long as it is a good approximation to the exact wavefunction in the region of the effectiveness of the potential. The single centre expansion is frequently used in this method and better convergence for long range potentials is achieved by an iterative procedure. The Schwinger multichannel variational method has been used to study electron scattering from H_2 by Lima *et al* (1985,1988), Gibson *et al* (1984,1987), and more recently by Huo and Weatherford (1991). As with the Linear Algebraic treatment of this system, the major weakness of this method is the representation of the correlation and polarisation effects.

Another method which has been used to study electron-molecule collisions by calculating the T-matrix is the distorted wave approximation developed by Rescigno *et al* (1974). In this approximation both the incident and the scattered electronic wavefunctions are represented by distorted waves. The effective distorting potential is obtained by averaging over the internal degrees of freedom of the target molecule. As the collision energy decreases the distortion will increase until this method is no longer appropriate, however, it has also been extended to the study of low energy collision processes. The major disadvantage of this method is that, although correlation effects can be represented by a distorted wave representation, polarisation effects cannot. This method has been used to study the

17

electron-H_2 system by Fliflet and McKoy (1980) and Lee *et al* (1982, 1990) and the results produced were in good agreement with results obtained using a Schwinger variational method neglecting polarisation effects.

The R-matrix method, along with the Schwinger variational method, is the method that would seem to be the most useful for further study of diatomic and polyatomic collision processes. The R-matrix was originally used by Wigner (1946 a, b) and Wigner and Eisenbud (1947) for the study of nuclear collisions and later adapted for use in electron-atom collisions by Burke *et al* (1971). It has been used in the field of atomic collisions for the study of various processes including scattering, photoionisation, atomic polarisabilities, spectral line shifts, free-free transitions and photoabsorption, reviews of which are found in Burke and Robb (1975) and Burke (1982).

The R-matrix method was developed for use in the study of electron-molecule collisions by Schneider (1975) and Burke *et al* (1977) and it is this treatment that is of interest here. The molecular R-matrix method has been used previously to study integral and momentum transfer cross sections for electron scattering from various diatomic molecules, reviews of which are given by Buckley *et al* (1984) and Burke and Noble (1986). The method has also been extended to the study of positron-molecule collisions by Tennyson (1986), Tennyson and Morgan (1987) and Danby and Tennyson (1990).

The main feature of the R-matrix method is that it divides space into an internal and an external region separated by a sphere of radius a, centred on the centre of mass of the target molecule. The sphere is chosen to just enclose the target charge distribution. This is very similar to the frame transformation method used by Chang and Fano (1972). In the internal region the potential is strong and multicentred, and exchange and correlation effects between the incident electron and the target are important. In the external region exchange and correlation

18

effects are neglected and only the long range polarisation potential is important.

In order to express the complex process in the internal region Schneider (1975) used a set of prolate spheroidal coordinates with which to expand the wavefunction. These prolate spheroidal coordinates give good results for diatomic molecules, but are not appropriate for polyatomic molecules. Burke *et al* (1977) however favoured a multicentre, discrete basis representation in the internal region. This method used sets of Slater-type orbitals, with effectively negligible amplitude at the boundary, centred on the atomic centres, and a set of Slater type orbitals which did not vanish at the boundary, centred on the centre of mass of the target molecule. The molecular orbitals were then defined in terms of the orbitals centred on the atomic centres and the continuum molecular orbitals were expressed in terms of all the sets of orbitals (*i.e.* three sets for the diatomic case). The set of orbitals centred on the centre of mass of the molecule in the inner region provides the link between the multicentred treatment in the inner region and the single centre expansion approach in the external region.

The R-matrix method employed here uses a set of numerical basis functions, instead of Slater type orbitals, centred on the centre of mass of the target molecule (Gillan *et al* 1987). Slater type orbitals are difficult to integrate over due to the cusp at the origin. Indeed no integral package has yet been written which uses Slater type orbitals to deal with non-planer molecules. The numerical basis functions used here, however, are more suitable for integration. The use of these numerical basis functions means, however, that a Bloch operator (Bloch 1957) must be added to the Hamiltonian matrix to ensure that the Hamiltonian is Hermitian. The method is therefore no longer a strictly variational one, as the Buttle correction is based on perturbation theory. However, in practice the method still behaves in a variational manner.

By setting up and diagonalising the Hamiltonian matrix in the internal region

19

a set of eigenenergies and eigenvectors can be produced. These eigensolutions can then be used to form the basis set in the inner region from which all the physical solutions of the wave equation can be expanded. The great advantage of this method is that the diagonalisation only has to be performed once for each symmetry of the electron-molecule system, and solutions at all energies can then be found at comparatively little cost.

The inner region functions are matched to the outer region functions at the R-matrix boundary by a matrix known as the R-matrix. The R-matrix relates the functions at the boundary to their derivatives as will be explained in more detail in the next chapter. This matching can then be used to produce the K-matrix (reactance matrix) and the T-matrix from which scattering information is determined.

Nesbet *et al* (1986) developed a method which combines the R-matrix method with a matrix-variational approach. This method divides space in a similar way to the R-matrix method, but uses numerical asymptotic functions for the continuum basis functions. As with the matrix-variational method the continuum basis functions are energy dependent which means that the inner region calculation has to be repeated for each energy range. The number of continuum functions used is therefore kept to a minimum. This method has produced results which compare reasonably well with experimental data for elastic electron-H_2 scattering, but has not yet been extended to include nuclear motion or applied to any other system.

1.3   A Comparative Study

The R-matrix method was used to study electron-H_2 scattering by Baluja *et al* (1985) in a coordinated study to compare the R-matrix method, the Linear Algebraic method (Schneider and Collins 1985) and the Schwinger multichannel vari-
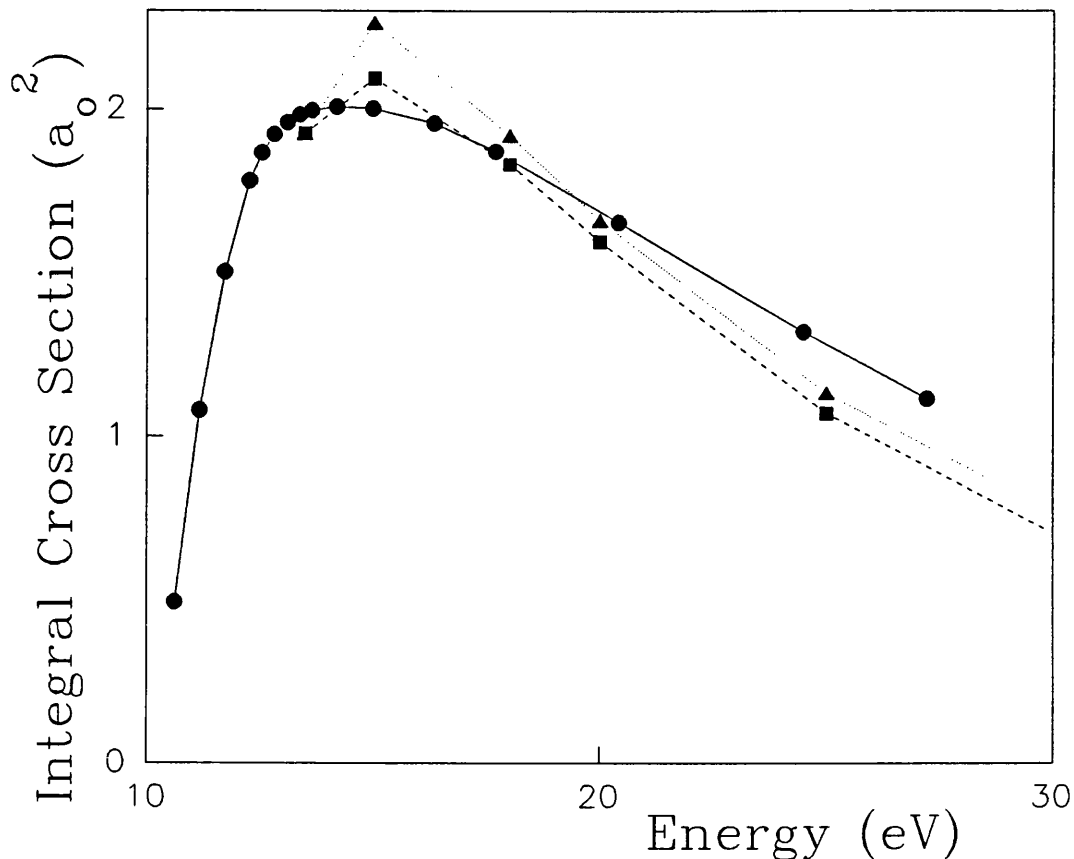
Figure 1.1: Integral cross section for excitation from the ground to the b $^3\Sigma_u^+$ state of H_2. The solid curve represents the work of Baluja et al (1985), the dashed curve that of Schneider and Collins (1985) and the dotted curve that of Lima et al (1985).

ational method (Lima et al 1985) for a specific model. The three methods were used to represent elastic scattering and electronic excitation from the ground to the first excited state of H_2, the b $^3\Sigma_u^+$ state. This transition is of interest as it is spin forbidden and can only take place by exchange. It therefore represents a good test of the effectiveness of the method of including exchange effects. The models used also included electron correlation effects to relax the strict orthogonality condition between the bound and continuum states. The integral cross sections produced by these three models are shown in figure 1.1. It can be seen

that the results produced were in good agreement with each other. They were also in reasonable agreement with experimental data.

This study was able to demonstrate the importance of including exchange and correlation effects. Previous calculations which did not include these effects gave integral cross sections that were significantly too low. The only one of these three methods that attempted to include polarisation effects was the R-matrix method. Including polarisation lead to a reduction in the integral cross section at low energies, however, in chapters 3, 4 and 5, it has been shown that the representation used was insufficient. By improving the polarisation representation the integral cross section at higher energies are reduced and resonance information can be obtained.

1.4 Bound states

The calculation of bound states of molecules has also been an active area of research since the introduction of improved computing power and facilities. A large amount of bound state information is necessary in order to calculate properties such as radiative transition probabilities, photoionisation cross sections and opacities in stellar atmospheres and interiors.

Quantum chemical methods for producing molecular bound states have proved very successful for studying low lying bound states. These methods generally represent the target molecule by using a linear combination of atomic orbitals and Gaussian type orbitals and using a configuration interaction (CI) technique. Very large CI expansions are used, often employing millions of configurations. However, these methods are not suitable for producing the high lying Rydberg states just below the ionisation energy of the molecule. An alternative method was therefore needed and recently Kaufmann *et al* (1989) adapted a Gaussian

type orbital expansion to look at Rydberg series.

The R-matrix codes developed for scattering calculations are ideally suited to the calculation of bound states as the complex internal region calculation is the same for both cases. The difference lies in the calculation of the external region wavefunction and the matching conditions at the R-matrix boundary. Within the field of the atomic R-matrix method Ojha and Burke (1983) developed a method of searching for bound states, but it had the limitation that only bound states with energies close to the R-matrix poles could be found. This method was later adapted for the molecular case, see for example the work on H_2 by Tennyson *et al* (1986) and on CH by Tennyson (1988), but was again unsuitable for calculating the Rydberg states of the system.

The method described by Seaton (1985) for the calculation of atomic bound states using the R-matrix method, however, is able to produce the bound states of a system from a single construction of the R-matrix. In the internal region the wavefunctions are set up as described for the scattering case. Solutions in the outer region must tend to zero as r, the distance of the electron from the centre of mass of the target, tends to infinity and must be able to be matched to the inner region functions at the R-matrix sphere. These outer region functions can be found by a combination of analytical and simple numerical methods. By imposing suitable boundary conditions and matching the inner and outer region functions, all the bound states of the system can in principle be calculated. This method has proved very useful in the study of atomic systems and was used for the Opacity Project (Seaton 1987, Berrington *et al* 1987) which produced large numbers of atomic ion bound states.

This method has been converted to find the bound state energies of molecules, see Chapter 6. Once the molecular wavefunctions in the inner and outer region have been calculated the method of matching the solutions is identical for the

atomic and molecular cases. In order to find the atomic bound state energies Seaton (1985) used a search for zeros of the matching matrix, which indicates a bound state, over a range of quantum defect number. For each principal quantum number there are only a small number of bound states for a given symmetry in the atomic case, however, this is not in general true for the molecular case and therefore a modification to the searching procedure had to be developed. This will be discussed in some detail later.

1.5 Nuclear motion

The fixed nuclei approximation, frequently used in the methods described above, is valid when the time of interaction between the electron and the molecule is small compared to the vibration and rotational period of the molecule. This is usually the case except near to the threshold of a channel or near to a resonance position where the time of interaction is greatly increased. Even when these conditions are not satisfied it is still possible to use the fixed nuclei approximation as rotational and vibrational effects can be corrected for in a second part of the calculation. This is known as the adiabatic-nuclei or Born-Oppenheimer approximation and it relies on the assumption that the electronic and the nuclear motion can be treated separately.

When this assumption is no longer valid, for example in the region of a resonance or close to the ionisation energy of the target molecule, the non-adiabatic effects have to be included. A method for including vibrational non-adiabatic effects was developed within the R-matrix method by Schneider *et al* (1979). The wavefunction of the system is expanded as products of fixed-nuclei functions and basis functions representing the nuclear motion. This treatment has been used to study systems such as N_2 (Morgan 1986, Gillan *et al* 1987) and *HCl* (Morgan *et*

al 1990).

In order to include the effects of rotational motion of the target molecule, Arthurs and Dalgarno (1960) introduced a rigid rotor model for the target molecule. This method neglects the vibrational motion of the target and uses the laboratory frame to obtain the correct asymptotic form of the wavefunction. The total angular momentum of the electron-target system is a constant and the eigenfunctions of the total angular momentum vector are used as a basis to expand the wavefunction of the system. This method, however, is not suitable for use within the molecular R-matrix method as it employs the laboratory frame and not the molecular frame of reference used in the inner region of the R-matrix method. An alternative method was used by Tennyson and Morgan (1987) for the study of positron-CO scattering within the R-matrix method. They used the multipole-extracted adiabatic-nuclei approximation which models rotational motion by using the static, space-fixed, first Born approximation. This method gave reasonably good results for scattering energies below the positronium formation threshold energy, but the results were less pleasing at higher energies.

1.6   Present work

In this work the molecular R-matrix method has been used to study the integral and differential cross sections for electron-H_2 scattering. Elastic scattering and scattering from the ground to the first six electronically excited states of H_2 have been considered. Chapter 2 sets out the theory of the molecular R-matrix method and gives a description of the computer codes used in this work. Chapter 3 presents preliminary results for a six state model and outlines some of the difficulties encountered when trying to produce this data. Chapter 4 discusses the integral cross sections for the full seven state model with special reference to the resonance fea-

tures found. Chapter 5 presents the differential cross sections calculated for the full seven state model. These calculations represent an improvement on previous studies of the system in two respects: firstly the target representation is a full CI representation and secondly, previous calculations were restricted to the study of two target states whereas these calculations consider the lowest seven states.

The molecular R-matrix method can also be used to find the bound states of molecules. Following the algorithm set out in Seaton (1985) for the calculation of atomic bound states using the R-matrix method, a computer program module has been developed to calculate molecular bound states together with a module to calculate the transition moments between them. These program modules, and results obtained for the diatomic molecules H_2, HeH and CH which demonstrate the effectiveness of the method, are presented in Chapter 6.

Chapter 2

Molecular R-matrix theory

As has already been mentioned the basic feature of the R-matrix method is that space is divided into two regions separated by a sphere of radius a. The complex inner region calculation follows the same theory for both scattering and bound state calculations and this will be discussed in some detail. The theoretical method used to obtain scattering information in the outer region will be presented as well as the theory, adapted from Seaton (1985), which was used in the computer program module to calculate the bound states of molecules. The use of these bound state in the calculation of transition dipoles is also described. The various modules of the computer package used in this work will be discussed in relation to the relevant theory.

2.1 Inner region

In the inner region the target molecular orbitals ϱ_i are represented by the expansion:

$$\varrho_i = \sum_l D_{li}\rho_l, \tag{2.1}$$

27

where ρ_l are Slater type orbitals (STOs) centered on the nuclear centres of the target molecule and D_{li} are coefficients which are found by performing a self consistent field (SCF) calculation. The functions ϱ_i are then known as LCAO-MO-SCF or linear combination of atomic orbitals molecular orbitals in the SCF approximation. The SCF approximation involves including electron–electron interaction in an average field approximation. The forces on a particular electron within the average field of all the other target particles are calculated and the electron is allowed to move in this field. This, however, affects the average field exerted on the other electrons, which are then allowed to alter their positions in turn. This process is repeated until some minimum energy for the system within the SCF approximation is reached.

In order to perform a target CI calculation configurations of the N electron target molecule ϕ_i^N have to be built up from the SCF target molecular orbitals. The target molecular wavefunctions ψ_I^N are then expanded as a linear combination of these configuration:

$$\psi_I^N = \sum_i c_{iI} \phi_i^N. \tag{2.2}$$

The coefficients c_{iI} are calculated by diagonalising the N electron Hamiltonian H^N:

$$\langle \psi_I^N | H^N | \psi_{I'}^N \rangle = e_I \delta_{II'}, \tag{2.3}$$

where the e_I are the target energies.

The target molecular orbitals ϱ_i must be augmented by a set of continuum orbitals in the inner region in order to perform an $N+1$ electron calculation. This is achieved by first setting up effective atomic orbitals u_i centred on the centre of mass of the target molecule. These u_i take the form of numerical basis functions which satisfy the equation:

$$\left(\frac{d^2}{dr^2} - \frac{l_i(l_i+1)}{r^2} + V_o(r) + k_i^2\right)u_i(r) = 0, \tag{2.4}$$

subject to the boundary conditions

$$u_i(0) = 0 \qquad (2.5)$$

and

$$\left.\frac{a}{u_i}\frac{du_i}{dr}\right|_{r=a} = b, \qquad (2.6)$$

where $k_i^2 = 2e_i$, V_o is a suitable potential (for example the Coulomb potential) and b is an arbitrary constant taken to be zero in this work.

The continuum molecular orbitals η_j for a diatomic molecule can then be represented in the inner region by the partial wave expansion:

$$\eta_j(\mathbf{r}) = \sum_i r^{-1} u_i(r) Y_{l_j m_{l_j}}(\hat{\mathbf{r}}) A_{ij} + \sum_i \rho_i^A B_{ij} + \sum_i \rho_i^B C_{ij}, \qquad (2.7)$$

where the $Y_{l_j m_{l_j}}$ are spherical harmonics, ρ_i^A and ρ_i^B are Slater type orbitals centred on the target nuclei A and B. The coefficients A_{ij}, B_{ij} and C_{ij} are determined by Schmidt and Lagrange orthogonalisation (Tennyson et al 1987).

The eigenstate wavefunctions ψ_k^{N+1} of the inner region N+1 electron system, with eigenenergies e_k in Hartrees, can then be represented by the expansion:

$$\psi_k^{N+1} = \mathcal{A} \sum_{i,j} \phi_i^N(\mathbf{x}_1...\mathbf{x}_N) \bar{\eta}_j(\mathbf{r}_{N+1}\sigma_{N+1}) \alpha_{ijk} + \sum_m \chi_m(\mathbf{x}_1...\mathbf{x}_{N+1}) \beta_{mk}, \qquad (2.8)$$

where $\mathcal{A}$ is the antisymmetrisation operator and $\mathbf{x_n} = (\mathbf{r_n}, \sigma_n)$, where $\mathbf{r_n}$ is the spatial coordinate of the nth electron and σ_n is its spin coordinate. The $\bar{\eta}_j$ are formed by coupling the spin function of the scattered electron to the continuum molecular orbitals η_j. The first term in equation (2.8) therefore represents a summation over all configurations where the target electrons are in a target configuration and the $N + 1^{th}$ electron is in one of the continuum orbitals.

The functions χ_i in equation (2.8) correspond to configurations where all $N + 1$ electrons are placed in the target molecular orbitals. They are added to allow for short range correlation and polarisation effects between the scattered electron and the target molecule.

29

The coefficients α_{ijk} and β_{ik} are determined by diagonalising the Hamiltonian matrix in the inner region so that

$$\langle \psi_k^{N+1} | H_{N+1} + L_{N+1} | \psi_{k'}^{N+1} \rangle = e_k \delta_{kk'}, \qquad (2.9)$$

where H_{N+1} is the Hamiltonian of the N+1 electron system and L_{N+1} is the Bloch operator (Bloch 1957) included to ensure that the Hamiltonian is hermitian in the inner region. It is defined by the equation:

$$L_{N+1} = \frac{1}{2} \sum_{i=1}^{N+1} \sum_j |\psi_j^N(\mathbf{r}_i^{-1}) Y_{l_j m_{l_j}}(\hat{\mathbf{r}}_i) \rangle \delta(r_i - a) (\frac{d}{dr_i} - \frac{b}{r_i}) \langle \psi_j^N(\mathbf{r}_i^{-1}) Y_{l_j m_{l_j}}(\hat{\mathbf{r}}_i) | \quad (2.10)$$

A CI target representation can be used to reduce the size of the Hamiltonian matrix to be diagonalised. If the coefficients α_{ijk} in equation (2.8) are not allowed to vary fully, so that only the N electron configurations ϕ_i^N included in the CI target representation are included, then equation (2.8) may be rewritten:

$$\psi_k^{N+1} = \mathcal{A} \sum_I \psi_I^N(\mathbf{x_1}...\mathbf{x_N}) \sum_j \bar{\eta}_j(\mathbf{r_{N+1}} \sigma_{N+1}) \alpha_{Ijk} + \sum_m \chi_m(\mathbf{x_1}...\mathbf{x_{N+1}}) \beta_{mk},$$

$$(2.11)$$

where the N electron target wavefunctions ψ_I^N are given by equation (2.2). By defining the Hamiltonian matrix element $H_{iji'j'}$ for going from configuration $\phi_i^N \eta_j$ to $\phi_i'^N \eta_j'$ by:

$$H_{iji'j'} = \langle \phi_i^N \eta_j | H | \phi_i'^N \eta_j' \rangle, \qquad (2.12)$$

for going from configuration $\phi_i^N \eta_j$ to χ_m by:

$$H_{ijm} = \langle \phi_i^N \eta_j | H | \chi_m \rangle, \qquad (2.13)$$

and for going from configuration χ_m to χ_m' by:

$$H_{mm'} = \langle \chi_m | H | \chi_m' \rangle, \qquad (2.14)$$

a Hamiltonian matrix of reduced size can be defined by the three equations:

$$H_{IjI'j'}^* = \sum_{ii'} c_{iI} H_{iji'j'} c_{i'I'}, \qquad (2.15)$$

30

$$H^*_{Ijm} = \sum_i c_{iI} H_{ijm}, \tag{2.16}$$

and

$$H^*_{mm'} = H_{mm'}, \tag{2.17}$$

where the coefficients c_{iI} are those of equation (2.2). It can be seen that no saving is made for configurations where all the electrons are in target molecular orbitals, but the number of these is typically much smaller than the number of configurations where the $N + 1^{th}$ electron is in a continuum orbital. As an example the seven target state work on electron–H_2 scattering discussed in Chapter 4 generated a Hamiltonian matrix that was 5396 × 5396 elements large for the $^2\Sigma_g$ symmetry. Using this contraction method the size was reduced from 5396 configurations squared to 428 configurations squared of which 209 of the configurations where of the type where all $N + 1$ electrons are in the target molecular orbitals.

The Schrödinger equation of the $N + 1$ electron system in the inner region is given by:

$$(H_{N+1} + L_{N+1} - E)\Psi = L_{N+1}\Psi. \tag{2.18}$$

where Ψ is the total wavefunction of the system. This has the solution:

$$\Psi = (H_{N+1} + L_{N+1} - E)^{-1} L_{N+1}\Psi. \tag{2.19}$$

The inverse operator can be expanded in the basis defined by equations (2.8) and (2.9) so that:

$$|\Psi\rangle = \sum_k \frac{|\psi_k^{N+1}\rangle\langle\psi_k^{N+1}|L_{N+1}|\Psi\rangle}{(e_k - E)}. \tag{2.20}$$

Premultiplying this equation by the channel function $< \psi_I^N Y_{l_i m_{l_i}}|$ and defining the reduced radial functions F_i as:

$$F_i(r) = \langle\psi_I^N Y_{l_j m_{l_j}}|\Psi\rangle, \tag{2.21}$$

the surface amplitudes f_{ik} by:

$$f_{ik} = \langle\psi_I^N Y_{l_j m_{l_j}}|\psi_k\rangle \tag{2.22}$$

31

and using the Bloch operator defined by equation (2.10) it follows that at the R-matrix boundary:

$$F_i(r) = \sum_j R_{ij}(E)(a\frac{dF_j}{dr} - bF_j)_{r=a},$$ (2.23)

which defines the R-matrix given by

$$R_{ij}(E) = \frac{1}{2a}\sum_k f_{ik}(a)(e_k - E)^{-1}f_{jk}(a).$$ (2.24)

In practice it is not possible to include an infinite number of states ψ_k^{N+1}, and the sum in equation (2.24) has to be truncated to a finite number of terms N_{il} for each value of ℓ. The error produced by this truncation is particularly important in this case due to the artificial boundary conditions (equations (2.5) and (2.6)) at the R-matrix sphere. The Buttle correction (Buttle 1967, Shimamura 1978) is therefore added to the diagonal terms of the R-matrix to remove the error incurred and is defined as:

$$B_{ll}(E) = \frac{1}{2a}\sum_{i=N_{li}+1}^{\infty} \frac{[u_{li}(a)]^2}{\frac{1}{2}k_{li}^2 - E},$$ (2.25)

where u_{li} is the ith eigensolution of equation (2.4) and $k_{li}^2 = 2e_{ki}$ the relevant eigenenergy.

2.2   Inner region program suite

The computer program suite used in this work to solve the inner region problem was adapted from the quantum chemical package ALCHEMY (McLean 1971, Noble 1982). A flow chart of this suite is given in figure 2.1.

The module SCF is where the atomic Slater type orbitals are input and a self consistent field target calculation is performed. The module outputs target molecular orbitals which are linear combinations of the atomic orbitals as in equation (2.1).

32
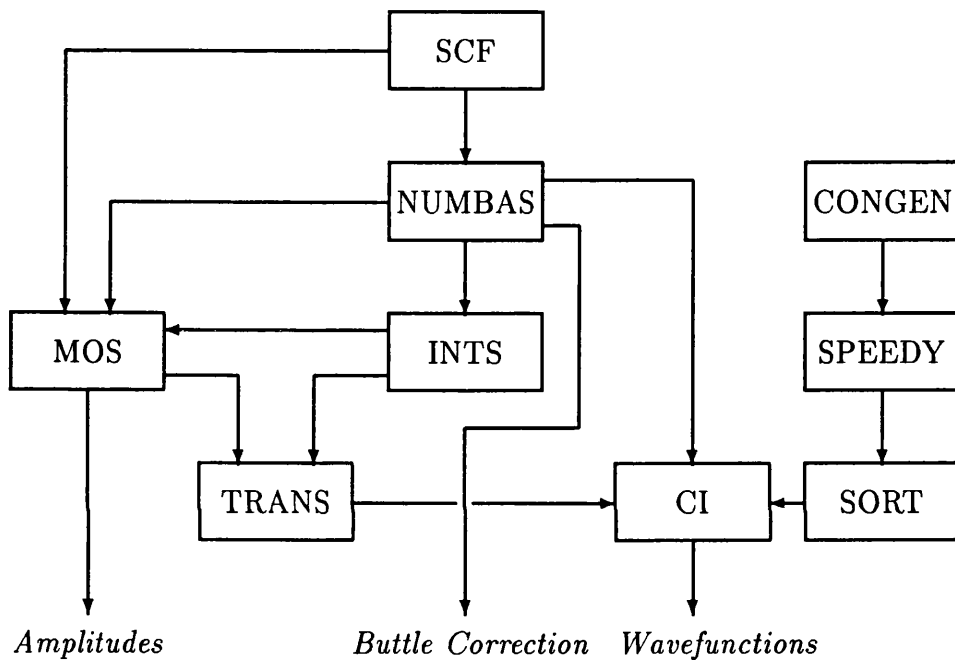
Figure 2.1: Inner region flow chart.

The module NUMBAS is where the numerical continuum orbitals are generated in accordance with equations (2.4), (2.5) and (2.6). The potential V_o can be input separately or the module has the capability of calculating several simple potentials. The maximum number of partial waves retained must be input and no attempt is made to orthogonalise the orbitals to the target. This module also calculates the Buttle correction defined by (2.25).

INTS generates the 1-electron, 2-electron and property integrals over the restricted inner region.

MOS produces molecular orbitals and their boundary amplitudes, given by equation (2.22), from the target orbitals generated by SCF and the continuum orbitals generated in NUMBAS. MOS can be used to Schmidt orthogonalise the target orbital set, or the target-continuum orbital set and it can also be used to Lagrange Orthogonalise the continuum orbitals to a specified number of target orbitals of the same symmetry (Tennyson *et al* 1987). This procedure may be needed to eliminate linear dependance.

TRANS orders the atomic orbital integrals generated by INTS and transforms them into molecular orbital integrals using the molecular orbital coefficients generated in MOS.

In the module CONGEN electron configurations to be included in the CI calculation are picked by hand. It is therefore used to determine which terms are included in the expansions of equation (2.8). SPEEDY determines which integrals, computed by INTS and transformed by TRANS, will be needed for the configurations generated in CONGEN. SORT then sorts these integrals into the most convenient order for the module CI. CI performs a configuration interaction calculation. It diagonalises the Hamiltonian as in equation (2.9) to yield the eigenenergies e_k and the coefficients α_{ijk} and β_{ik} of equation (2.8). In the case of a CI target calculation this yields the coefficients α_{Ijk} and β_{ik} of equation (2.11).

The other module of interest here is TMT which is used to produce the dipole and quadrupole moments of the target, required in the outer region calculation, from data generated in the inner region and inner region moments for $N + 1$ electron transitions. This module will be discussed in more detail in section 2.7.

2.3 Outer region scattering calculation

In the outer region it is assumed that the effects of electron exchange between the scattering electron and the target can be ignored and that the wavefunction can be expanded in the single centre, close coupling form:

$$\Psi = \sum_i \bar{\phi}_i(\mathbf{x_1}..\mathbf{x_N}, \sigma_{N+1}) r^{-1} G_i(r_{N+1}) Y_{l_i m l_i}(\hat{\mathbf{r}}_{N+1}). \tag{2.26}$$

Following the method used in the inner region this equation can be substituted into the Schrödinger equation and projected onto the channel functions to give a set of coupled differential equation for the reduced radial functions G_i for a given internuclear separation:

$$\left(\frac{d^2}{dr^2} - \frac{l_i(l_i + 1)}{r^2} + k_i^2\right) G_i(r) = 2 \sum_j V_{ij}(r) G_j(r), \tag{2.27}$$

where

$$k_i^2 = 2(E - E_i^N), \tag{2.28}$$

E_i^N are the eigenenergies associated with the target state ϕ_i^N and V_{ij} is the potential in the outer region.

For a scattering calculation the equations (2.26) are subject to the asymptotic boundary conditions $(r \to \infty)$

$$G_{ij} \to k_i^{-\frac{1}{2}}(sin\theta_i \delta_{ij} + cos\theta_i K_{ij}) \qquad \text{for open channels} \tag{2.29}$$

$$G_{ij} \to 0 \qquad \text{for closed channels} \tag{2.30}$$

which also define the K-matrix K_{ij} that couples the open channels. The θ_i are given by:

$$\theta_i = k_i r - \frac{1}{2} l_i \pi + \frac{z}{k_i} \ln 2k_i r + arg\Gamma(l_i + 1 - i\frac{z}{k_i}), \qquad (2.31)$$

where $\Gamma(l_i + 1 - iz/k_i)$ is a complex gamma function and z is the residual charge of the molecule. From the K-matrix the eigenphase sum δ is given by

$$\delta = \sum_i \arctan(K_{ii}^D) \qquad (2.32)$$

where K_{ij}^D is the diagonalised K-matrix. The T-matrix can be obtained from the matrix equation

$$\mathbf{T} = \frac{2i\mathbf{K}}{1 - i\mathbf{K}}. \qquad (2.33)$$

From the T-matrix the integral cross-section $\sigma(i \rightarrow i')$, for going from state i to state i', can be found for a linear molecule (Burke 1979) from the equation

$$\sigma(i \rightarrow i') = \frac{\pi}{k_i^2} \sum_S \frac{(2S + 1)}{2(2S_i + 1)} \sum_{\Lambda ll'} |T_{i l i' l'}^{\Lambda S}|^2, \qquad (2.34)$$

where S is the total spin angular momentum, S_i is the spin angular momentum of state i and Λ is the total electronic angular momentum projected onto the molecular axis. The T-matrix can also be used to calculate the differential cross section, see Malegat (1990).

In the present work the outer region functions were obtained by first propagating the R-matrices (Baluja *et al* 1982, Morgan 1984) to a suitable radius and then using (Gailitis) asymptotic expansion techniques (Noble and Nesbet 1984) to solve equation (2.27).

2.4 Outer region program suite

Figure 2.2 shows the flow diagram for the outer region suite of programs used. It should be noted that inner region modules of figure 2.1 are individual programs
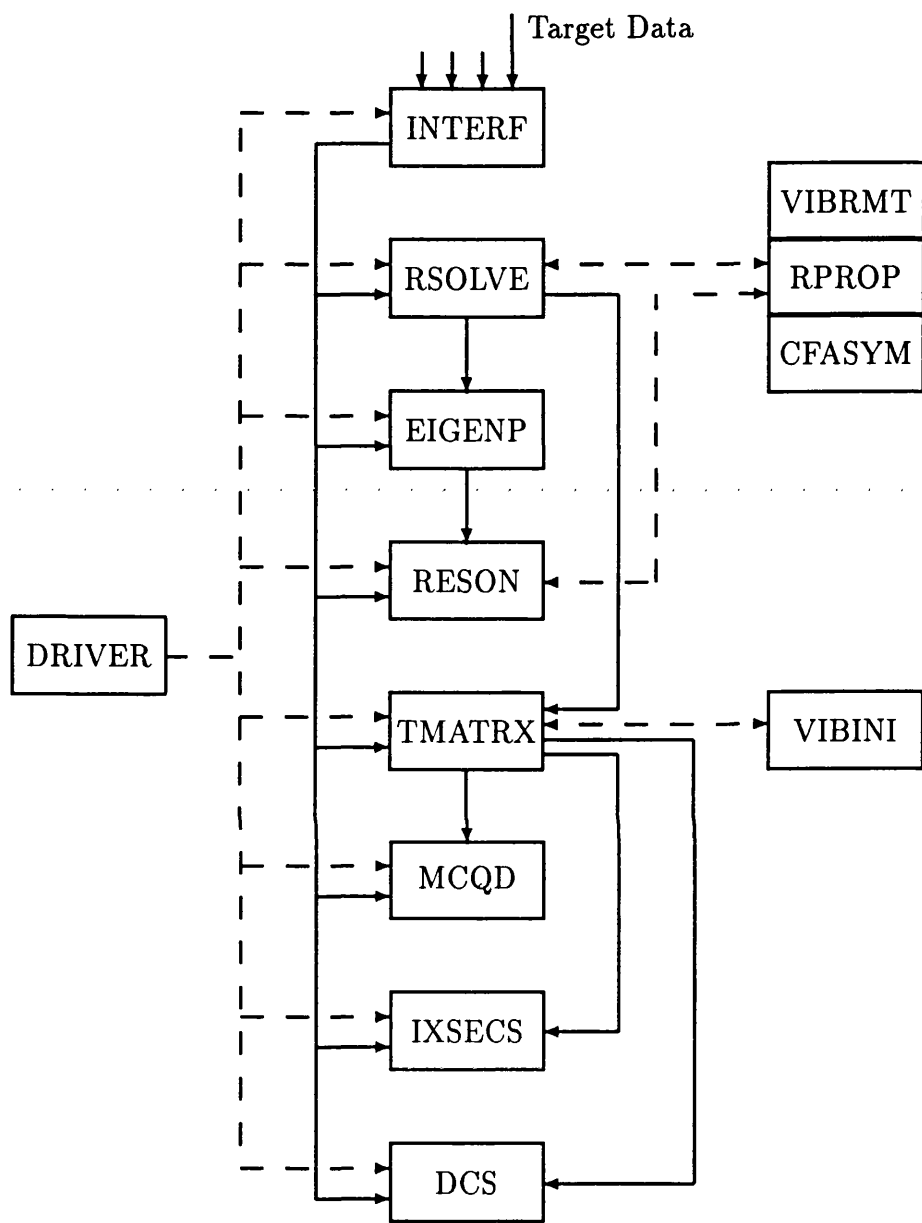
Figure 2.2: Outer region scattering flow chart.

that are the run separately and independently of one another. The solid lines linking the various modules are data flow indicators. However, the outer region package is one program that is divided into modules. The solid lines in figure 2.2 again indicate data flow, but the dashed lines represent calls to modules from within other modules.

The outer region program is managed by the module DRIVER which sets up computer memory allocations and calls the various modules.

The module INTERF is used to interface between the inner and the outer region codes. It takes the input from the inner region together with additional target data, including internuclear separation, energy levels of the target states and multipole moments. It constructs the surface amplitudes f_{ik} given by equation (2.22) at the R-matrix boundary from the information generated in the inner region and adds in the Buttle correction of equation (2.25).

RSOLVE is the main driving module of the outer region which produces the K-matrices of the system (equation (2.29)). It makes calls to VIBRMT, which sets up the necessary data if a non-adiabatic calculation is being performed, RPROP which propagates the R-matrix to a given radius and CFASYM which calculates wavefunctions in the asymptotic region.

EIGENP produces eigenphases from K-matrices using equation (2.32) and RESON is an automatic resonance detection program which produces resonance positions and widths by fitting detected resonances to a Breit-Wigner form (Tennyson and Noble 1984). Within this form the eigenphase η is expressed as a function of the scattering energy, E, in the form:

$$\eta(E) = \sum_{i=1}^{M} tan^{-1} \left[\frac{\Gamma_i^{res}}{(E - E_i^{res})} \right] + \sum_{i=0}^{N} a_i(E)^i, \qquad (2.35)$$

where Γ^{res} is the width and E^{res} is the position of the resonance. The second sum in this equation is a power series used to represent the underlying trend of the eigenphase across the region of the resonance.

38

TMATRX is used to produce the T-matrices of the system (see equation (2.33)) from the K-matrices and additional vibrational data via a subroutine call to VIB-INI if a non-adiabatic calculation is being performed. From the T-matrices MCQD computes multichannel quantum defects (see section 2.5), the integral cross sections are computed by the module IXSECS and the differential cross sections by the module DCS (Malegat 1990).

2.5 Bound state calculation

In the inner region the total wavefunction of the bound $N + 1$ electron system Ψ_i can be expanded in terms of the complete set of functions ψ_k^{N+1} of equation (2.8):

$$\Psi_J = \sum_k \psi_k^{N+1} C_{kJ}.$$ (2.36)

The coefficients C_{kJ} are known as the bound state coefficients. In order to calculate these bound states, the outer region functions must tend to zero as the distance of the scattering electron tends to infinity. Within the R-matrix method they must also be able to be matched to the inner region functions at the R-matrix boundary. In the present work these outer region functions were obtained by first using a Gailitis expansion technique (Noble and Nesbet 1984) at a suitable radius, and then propagating inwards to the R-matrix boundary using the Runge Kutta Nystrom method to solve the asymptotic equations numerically.

The matching conditions, at the R-matrix boundary, for a bound state are:

$$F_i = \sum_j P_{ij} X_j$$ (2.37)

and

$$\frac{dF_i}{dr} = \sum_j \frac{dP_{ij}}{dr} X_j,$$ (2.38)

where the F_i are the reduced radial functions described in section 2.1, the P_{ij} are the outer region functions and X_j is a column vector needed to construct the

bound state coefficients C_{kJ} given by the equation:

$$C_{kJ} = \sum_i \frac{f_{ik}}{2(e_k - E)} \sum_j (\frac{dP_{ij}}{dr} - \beta P_{ij})X_j. \qquad (2.39)$$

By combining equations (2.23), (2.37) and (2.38) the standard form of the matching condition is given by:

$$\sum_j B_{ij}X_j = \sum_j (P_{ij} - [\sum_k R_{ik}(E)Q_{kj}])X_j = 0, \qquad (2.40)$$

where

$$Q_{kj} = \frac{dP_{kj}}{dr} - \beta P_{kj}. \qquad (2.41)$$

Equation (2.40) has the standard form of an eigenvalue equation and it therefore only has solutions at discrete values of energy E, the bound state energies, where the determinant of the matrix B_{ij} will be zero.

A problem arises at energies E close to the R-matrix pole energies e_k. At these energies the R-matrix (equation (2.24)), and hence the matrix B_{ij} (equation (2.40)), is undefined. It therefore becomes necessary to eliminate these poles and this is done using the method described by Burke and Seaton (1984).

Equation (2.24) is first rewritten as:

$$R_{ij} = \frac{S_{ij}}{2a(e_K - E)} + T_{ij}, \qquad (2.42)$$

where the total energy E is close to the pole energy e_K,

$$S_{ij} = f_{iK}(a)f_{jK}(a) \qquad (2.43)$$

and

$$T_{ij} = \sum_{k \neq K} \frac{1}{2a}f_{ik}(a)(e_k - E)^{-1}f_{jk}(a). \qquad (2.44)$$

A solution of the eigenvalue problem:

$$\sum_j S_{ij}U_{jk} = \sum_k U_{ik}s_k \qquad (2.45)$$

is then sought. It can be shown (Burke and Seaton 1984) that this equation is satisfied when U_{ij} is given by:

$$\text{for } j = 1 \text{ to } (I-1) \qquad U_{ij} = \begin{cases} f_{iK}f_{j+1K}/\Gamma_j\Gamma_{j+1} & \text{for } i = 1 \text{ to } j \\ -\Gamma_j/\Gamma_{j+1} & \text{for } i = j+1 \\ 0 & \text{for } i > (j+1) \end{cases} \qquad (2.46)$$

and

$$\text{for } j = I \qquad U_{iI} = f_{iK}/\Gamma_I, \qquad (2.47)$$

for $i = 1$ to I where I is the total number of channels and

$$\Gamma_j = (\sum_{i=1}^{j} f_{iK}^2)^{\frac{1}{2}}. \qquad (2.48)$$

The matrix U_{ij} is normalised to

$$\sum_l U_{il}^T U_{lj} = \delta_{ij}, \qquad (2.49)$$

where U_{ij}^T is the transpose of U_{ij}. The solution for s_k is then:

$$s_k = \delta_{kI}\Gamma_I^2. \qquad (2.50)$$

By combining equation (2.40) with equation (2.42) and premultiplying by the matrix U_{ij}^T the matching condition becomes:

$$\text{for } i = 1 \text{ to } (I-1) \qquad \sum_{i'=1}^{I} L_{ii'}X_{i'} = 0 \qquad (2.51)$$

and

$$\sum_{i'=1}^{I}[L_{Ii'} - \frac{1}{2a(e_K - E)}\Gamma^2 M_{Ii'}]X_{i'} = 0, \qquad (2.52)$$

where

$$L_{ij} = \sum_l U_{il}^T (P_{lj} - [\sum_m T_{lm}Q_{mj}]) \qquad (2.53)$$

and

$$M_{ij} = \sum_l U_{il}^T Q_{lj}. \qquad (2.54)$$

41
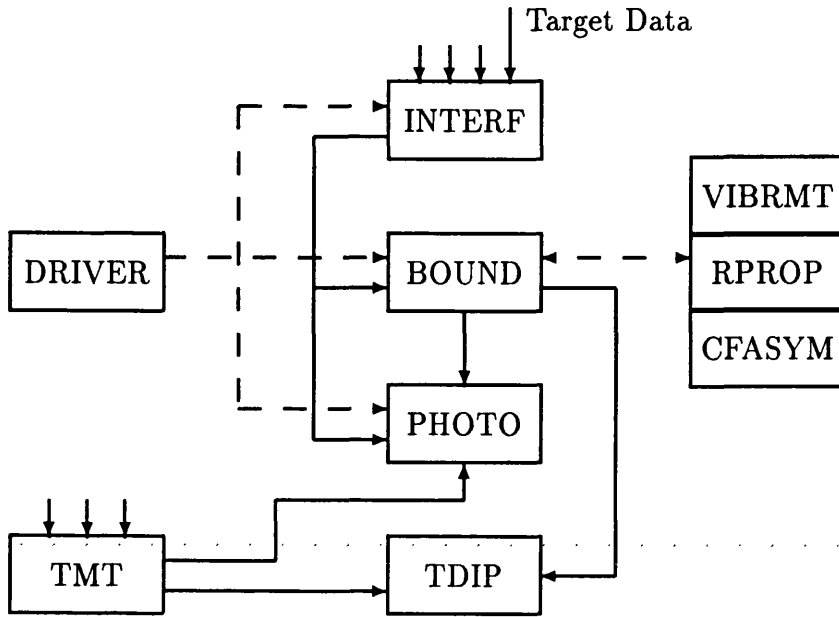
Figure 2.3: Outer region bound state flow chart.

The quantity $(e_K - E)$ now only appears in one of the matching equations (equation (2.52)). This equation can then be multiplied by the $(e_K - E)$ factor to redefine the matrix B_{ij}:

$$\text{for } i = 1 \text{ to } (I - 1) \qquad B_{ii'} = L_{ii'} \qquad (2.55)$$

and

$$B_{Ii'} = (e_K - E)L_{Ii'} - \Gamma^2 M_{Ii'}, \qquad (2.56)$$

thus eliminating any singularities.

The bound states of a system are found using the computer module BOUND shown in figure 2.3. As for the scattering case DRIVER is the control module and the module INTERF provides the interface between the inner and the outer region calculations. The module BOUND makes calls to subroutines VIBRMT,

RPROP and CFASYM in order to include vibrational information, propagate the R-matrix and perform the asymptotic calculations respectively in exactly the same way that the scattering module RSOLVE did. The calculation of the bound states is performed within the module BOUND itself.

Zero's of the determinant of B_{ij}, defined by equations (2.55) and (2.56), can be searched for by calculating the determinant at successive energy points and detecting any change in sign of the determinant. In practice, for ionic molecules, it is often more convenient to search over effective quantum number ν (Seaton 1966, 1985) given by:

$$E = E_l - \frac{z^2}{2\nu^2},\tag{2.57}$$

where E_l is the energy of the lowest molecular state. The effective quantum number is related to the principal quantum number n by the equation:

$$\mu = n - \nu \tag{2.58}$$

and μ is the quantum defect. In the atomic case there are only a small number of bound states for a given value of the principal quantum number n, but for molecules this is not necessarily the case. It was therefore necessary to develop a new method of searching for bound state energies.

For a given value of n an estimate for the number of poles likely to be found was calculated by considering the number of open channels with allowed values of ℓ. This information was then used to construct an evenly spaced grid in quantum defect space of effective numbers from $n - \frac{1}{2}$ to $n + \frac{1}{2}$. For each grid point the R-matrix pole nearest in energy to the grid point was found and the determinant of the matrix B_{ij}, given by equations (2.55) and (2.56), was calculated. If there was no change of sign in the determinant between successive grid points then a check was made for the possibility of two poles between the grid points by fitting the determinant function to a quadratic. Once a change in sign had been detected a

Newton-Raphson search was performed to obtain an initial estimate of the bound state energy.

This initial estimate of the bound state energy, E_1, was then assumed to be very close to the true value, E_o and the first two terms of a Taylor series expansion were used to set up the standard eigenvalue equation:

$$\sum_j B_{ij}(E)X_j = \sum_j (B_{ij}(E_1) + (E_o - E_1)\frac{dB_{ij}(E_1)}{dE})X_j = 0. \qquad (2.59)$$

This relation was then applied recursively (Seaton 1985, appendix 3) until the change in the energy produced for one application of the formula was below a certain value.

Since the calculation of the determinant of B_{ij} takes a considerable amount of computer time an option was added so that instead of setting up an even grid of effective quantum number a grid could be used that was dense around the points where a bound state might be expected and sparse in between these points. This was made possible by the use of a quantum defect grid instead of an energy grid, since for each value of n there is likely to be a bound state energy with approximately the same value of quantum defect number as for $n - 1$ (Seaton 1966). See figure 2.4. The arrows represent the bound state quantum defect values and the vertical lines represent the grid points. Thus for a given value of n, bound state energies are searched for near to the bound state energies found for $n - 1$, by adding 1 onto their effective quantum numbers.

For molecules with no residual charge the use of a quantum defect grid is not possible. An option was therefore included to set up an energy grid instead which could be used for all types of molecular targets.

44
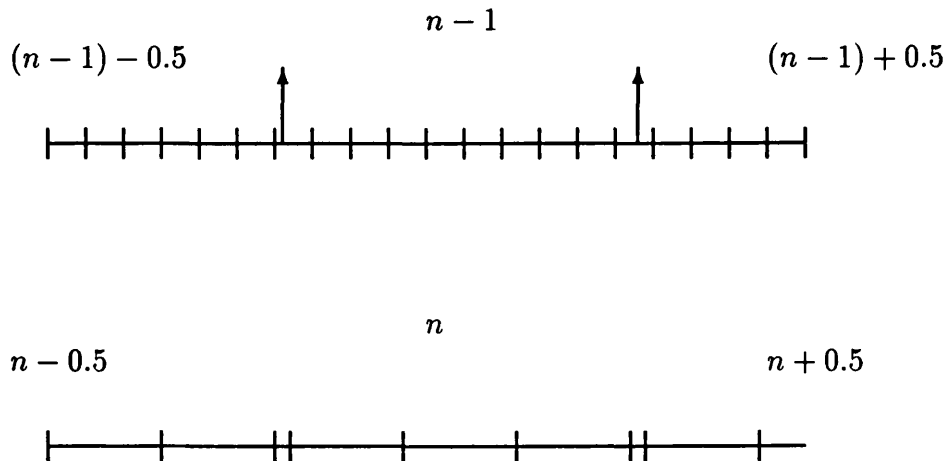
Figure 2.4: Quantum Defect grid.

2.6 Calculation of transition dipoles

The development of the bound state computer module made it possible to calculate photoionisation cross sections using the module PHOTO and to develop another module TDIP to calculate transition dipoles from which oscillator strengths can be calculated, see figure 2.3.

Previously the module TMT was used to calculate dipole and quadrupole moments of the N electron system for use in the outer region program package to produce both scattering information and bound state. It can also be used to calculate inner region transition moments of the $N + 1$ electron system. In order to do this the module TMT requires input from the inner region packages (see figure 2.1). It requires the transformed property integrals generated in the module TRANS, the sorted energy expression generated in SORT and the CI wavefunction information generated in the module CI. TMT then produces a transition matrix

$T_{kk'}$ using the dipole length approximation:

$$T_{kk'} = \langle \psi_k^{N+1} | \sum_{i=1}^{N+1} e_i r_i | \psi_k'^{N+1} \rangle. \qquad (2.60)$$

The module BOUND is then used to generate bound states Ψ_i of the $N+1$ electron system with bound state coefficients C_{kJ}, see equation (2.36).

The transition dipole t for going from state i to state i' is given by:

$$t_{ii'} = \langle \Psi_i | \sum_{i=1}^{N+1} r_i | \Psi_i' \rangle = \sum_{kk'} C_{ki} T_{kk'} C_{k'i'}, \qquad (2.61)$$

From the transition dipole the oscillator strength $f_{ii'}$ can be calculated using the definition (Schadee 1978):

$$f_{ii'} = \frac{2}{3} \frac{(2 - \delta_{0,\Lambda+\Lambda'})}{(2 - \delta_{0,\Lambda})} (E_i' - E_i) |t_{ii'}|^2, \qquad (2.62)$$

in atomic units. At present the module TMT can only be used for non-CI targets.

Chapter 3

Six state model for H_2

Even for the seemingly simple H_2 molecule there are still several areas where our knowledge of its characteristics is weak (McConkey *et al* 1988). These areas include the electronic excitation integral cross sections, dissociative recombination and differential cross section. An attempt has been made here to produce accurate results for the integral (and in Chapter 5 differential) cross sections for electronic excitation of molecular hydrogen by electron impact using the R-matrix method described in Chapter 2.

Several recent experimental studies have concentrated on integral cross section measurement (Watson and Anderson 1977, Ajello *et al* 1982, 1984, Hall and Andric 1984, Pasquerault *et al* 1985, Mason and Newell 1986b, Khakoo and Trajmar 1986b, Nishimura and Danjo 1986, Khakoo *et al* 1987), a review of which has recently been made by Tawara *et al* (1990). These measurements are very difficult to make and, therefore, the integral cross section results are not always reliable. There has also been considerable theoretical effort in this area (Fliflet and McKoy 1980, Arrighini *et al* 1980, Lee *et al* 1982, Redmon *et al* 1985, Baluja *et al* 1985, Schneider and Collins 1985, Lima *et al* 1985, Gibson *et al* 1987, Rescigno and Schneider 1988, Lima *et al* 1988, Lee *et al* 1990). In this chapter and the next

these results are compared with the ones obtained in this work.

Previous experimental studies of molecular hydrogen have shown that the integral cross section for several excitation processes displays a highly resonant character in the 10–15 eV energy region. These studies (Comer and Read 1971, Schulz 1973, Spence 1974, Weingartshofer *et al* 1975, Böse and Linder 1979, Mason and Newell 1986a), have produced a large amount of data which has revealed features associated with several series of resonances. Theoretically, stabilisation and Feshbach methods have been used (Eliezer *et al* 1967, Buckley and Bottcher 1977, Bardsley and Cohen 1978, DeRose *et al* 1988) in this energy region and recently scattering techniques (da Silva *et al* 1990) have also been used to study this resonance structure. However, there has still not yet been a consistent explanation for the structure. The present calculations were found to be sufficiently detailed to be able to produce resonance information which is discussed here.

3.1 Representation of the target molecule

Previous attempts to calculate electronic excitation cross sections for H_2 have been restricted to studying two states of the target molecule at a time (Baluja *et al* 1985, Schneider and Collins 1985, Lima *et al* 1985, Gibson *et al* 1987, Rescigno and Schneider 1988). These attempts used a single-configuration wave function representation for the electron states considered. Recently studies including several coupled channels (da Silva *et al* 1990) and target correlation (Lee *et al* 1990) have been carried out and it is clear that improved data can only be obtained by adopting a similar approach. In this calculation the target molecule was represented by six target states, which made it possible to calculate excitation from the ground to five low lying excited states of H_2 using the same model. Each electronic state was represented by a full CI wavefunction within the basis of STOs used.

In order to achieve this six state representation it was first necessary to choose a set of STOs. The $(1s, 2s, 2p_\sigma)$ set of σ_g orbitals, optimised for the $X^1\Sigma_g^+$ ground state of H_2 by Fraga and Ransil (1961), were used. Initially the σ_u orbital exponents were chosen to be the same as those for the σ_g orbitals. The π_g orbitals used were those of Nesbet $et\ al$ (1986) for a $(2p_\pi, 3p_\pi, 3d_\pi)$ set and the π_u orbital exponents were chosen to be the same as those of the π_g set. This was the first basis set used and the target molecular orbitals produced by an SCF calculation were then used to perform a full CI target calculation for the $X^1\Sigma_g^+$, $b^3\Sigma_u^+$, $a^3\Sigma_g^+$, $c^3\Pi_u$, $B^1\Sigma_u^+$ and $C^1\Pi_u$ state of H_2. For a full CI calculation all possible electron configurations that are allowed for a given symmetry and within the basis of molecular orbitals chosen are included. The target state energies produced at a fixed internuclear separation of 1.4 a_o for this first basis, together with a comparison with effectively exact quantum-chemistry calculations are given in table 3.1.

The aim of this calculation was to obtain a good representation for all six target states using the same, small set of molecular orbitals. It can be seen that this first basis was not particularly effective and a great deal of time was spent in order to improve the target representation. The program SCF is capable of optimising orbitals for a given symmetry, but some trial and error methods of optimisation were also required to reach the final representation.

The σ_u orbital exponents were optimised by performing an SCF calculation on the lowest state of $^1\Sigma_u^+$ symmetry and the same procedure was used to find the exponents of a $(2p_\pi, 3p_\pi, 3d_\pi)$ set of π_u orbitals using the lowest state of $^1\Pi_u$ symmetry. The results of these successive optimisation ($i.e.$ basis 2 to basis 4) can be seen in table 3.1. This set of orbitals, however, was not able to represents diffuse target states accurately, so the diffuse $2s(\sigma_g)$ orbital was added to the σ_g orbital set (basis 5). Table 3.2 gives the exponents of all the orbitals used in the fifth basis on which the results of this chapter are based.

49

State	1st Basis	2nd Basis	3rd Basis	4th Basis	5th Basis	'Exact'
$X^1\Sigma_g^+$	-1.17060	-1.17018	-1.16553	-1.16569	-1.165844	-1.1744744^a
$b^3\Sigma_u^+$	10.80	11.13	10.44	10.45	10.45	10.62^a
$a^3\Sigma_g^+$	19.81	22.05	21.96	21.96	12.77	12.54^b
$c^3\Pi_u$	13.38	13.33	12.65	12.58	12.59	12.73^c
$B^1\Sigma_u^+$	13.94	15.50.	13.17	13.16	13.15	12.75^b
$C^1\Pi_u$	14.56	14.46	13.09	13.11	13.10	13.23^d

[a]Kołos and Wolniewicz (1965)

[b]Kołos and Wolniewicz (1968)

[c]Kołos and Rychlewski (1977)

[d]Rothenberg and Davidson (1966)

Table 3.1: Ground state energies (in Hartrees) and vertical excitation energies (in eV) of H_2 for several different target representations.

Orbital	Exponent	Orbital	Exponent
$1s\sigma_g$	1.378	$1s\sigma_u$	1.081
$2s\sigma_g$	1.176	$2s\sigma_u$	0.800
$2s\sigma_g$	0.800		
$2p\sigma_g$	1.820	$2p\sigma_u$	1.820
$2p\pi_u$	0.574	$2p\pi_g$	1.084
$3p\pi_u$	0.636	$3p\pi_g$	1.084
$3d\pi_u$	1.511	$3d\pi_g$	2.470

Table 3.2: Exponents of the STOs used in the six state target representation of H_2.

It can be seen from table 3.1 that the vertical excitation energies obtained agree with the 'exact' results to within 0.4 eV. These small differences were corrected for by shifting the diagonal elements of the Hamiltonian matrix by the appropriate amounts.

3.2 Scattering calculation

Having obtained a target representation, a set of continuum orbitals was generated numerically as described in Chapter 2, with $V = 0$. Some investigation was done to see which model potential used to generate the numerical basis functions gave the best results, but the model was found not to be very sensitive to this. The best possible number of continuum orbitals to include was also the subject of considerable investigation. Including too few would result in inaccurate calculations, but

including too many could cause computational problems. The program module which is most affected by this is TRANS where all the molecular integrals required to construct the Hamiltonian matrix are computed. Table 3.3 shows the effect of varying the number of continuum orbitals used, by choosing the maximum energy solution to be included, on a 24 configuration CI test single target state calculation with an R-matrix radius of 20 a_o and total symmetry $^2\Sigma_g$ using the fourth basis set of table 3.1. It can be seen that the eigenphase sums are approximately stable for values of the maximum energy that are greater than 5, but not below.

In the present calculation all solutions below 5 Ryd with $\ell \leq 6$ and $m \leq 3$ were included in the inner region calculation which meant that the calculations ran close to the limit of the Rutherford Cray XMP scratch disk space.

Directly related to this problem is the one of R-matrix sphere size. A large radius was required in this work because of the diffuse nature of the target, however, increasing the radius also increases the number of continuum orbitals needed for an accurate representation of the scattering process. Table 3.4 shows the effect of changing the R-matrix radius on the number of numerical basis functions generated for a 2 CI target calculation using basis 4 and for a total symmetry of $^2\Sigma_g$. It can be seen that increasing the R-matrix radius dramatically increases the number of basis functions and, therefore, the size of the calculation. It can also be seen that size of the R-matrix sphere also changes the energy of the lowest R-matrix pole.

Some experimentation was, therefore, required to obtain the most suitable radius and it was found that an R-matrix radius of 20 a_o provided the best compromise for these calculations. This large radius, approximately double the usual size for a molecular calculation, meant that the number of quadrature points needed to evaluate the long-range portions of the necessary integrals (Noble 1982) had to be increased and after further tests approximately double the default number of

Maximum Energy (Ryd)	10	8	6	5	4
No. of continuum functions	55	49	43	37	34
Lowest R-matrix pole (Hartrees)	-1.129639	-1.129639	-1.129638	-1.129637	-1.129636
Scattering Energy (eV)	Eigenphase Sum (radians)				
1.22	-0.6160	-0.6159	-0.6160	-0.6163	-0.6192
3.40	-0.9764	-0.9769	-0.9778	-0.9802	-0.9758
6.67	-1.272	-1.272	-1.271	-1.271	-1.282
11.02	1.639	1.638	1.636	1.631	1.641
13.61	1.547	1.547	1.547	1.548	1.532
14.97	1.507	1.507	1.508	1.510	1.487
16.33	1.470	1.470	1.470	1.469	1.455
20.41	1.381	1.379	1.375	1.366	1.391

Table 3.3: Effect of changing the maximum energy of the solutions generated for the continuum functions on the target representation.

R-matrix radius	10	12	20
No. of continuum functions	27	33	57
Lowest R-matrix pole (Hartrees)	-1.115336	-1.122450	-1.131470

Table 3.4: Effect of changing the R-matrix radius on the target representation.

points were found to be necessary.

A great deal of time was spent on determining the best possible method of orthogonalisation. If insufficient orthogonalisation procedures are taken out the effects of linear dependence can be to produce R-matrix poles that are too low in energy. If too much orthogonalisation is used then too much is omitted from the calculation and the resulting representation is not adequate. Tests were carried out using no Lagrange orthogonalisation, Lagrange orthogonalisation to one target orbital and Lagrange orthogonalisation to two target orbitals for the σ_g, σ_u, π_g and π_u orbital sets. In the final six state calculations one orbital from the σ_g, σ_u and π_g and two orbitals from the π_u sets were Lagrange orthogonalised to the target orbitals of the same symmetry. This gave a set made up of 49 σ_g, 38 σ_u, 37 π_u, 35 π_g, 36 δ_g, 25 δ_u, 25 ϕ_u and 23 ϕ_g continuum orbitals. The full set of target and continuum orbitals was then Schmidt orthogonalised to the set of target orbitals to give an orthonormal set of molecular orbitals.

In the inner region all possible configurations, for a given total symmetry, where the target electrons were in target orbitals and the scattered electron was in a continuum orbital, were included. All possible configurations with all electrons in the target molecular orbitals were also included in order to allow for high-ℓ terms. Because a full CI target representation was used, all these configurations could be included without the risk of over correlation. The inner region Hamiltonian matrix

54

was then set up, reduced and diagonalised as described in Chapter 2.

The memory problems caused by the size of these calculations lead to the modification of the program module CI (Tennyson 1990) described in the previous chapter. In the previous version the uncontracted Hamiltonian matrix was constructed and written to disk. The full Hamiltonian was then read into core in order to perform the contraction process described in Chapter 2. In the new version the uncontracted Hamiltonian elements are read into core a band at a time and the contraction process vectorised.

In the outer region solutions were obtained by setting up the R-matrix at the R-matrix boundary and then propagation it (Morgan 1984) to a suitable radius. Solutions were then obtained by applying asymptotic expansion techniques (Noble and Nesbet 1984). Some experimentation was needed to determine the best propagation radius to use. Too small a radius produces errors caused by matching conditions at the boundary not being fulfilled, but increasing the radius increases the amount of computational work that has to be done in the outer region. The radius of propagation was gradually increased until no mismatching occurred and the results obtained here are for a propagation radius of 100 a_o. All diagonal and off-diagonal dipole and quadrupole moments, calculated using the module TMT, were retained. From these results K-matrices, eigenphase sums, T-matrices and integral cross sections were calculated as described in Chapter 2.

3.3 Results

Figures 3.1 to 3.8 show the eigenphase sums obtained for each total symmetry up to Φ_g. The filled triangles indicate the threshold energies of the excited states of the target molecule. The curves are all plotted on a grid of scattering energies separated by 0.01 eV with small gaps at the threshold energies. The results have

Symmetry	E_{res} (eV)	Γ_{res} (eV)	Assignment
$^2\Sigma_g^+$	10.96	1.39	$1\sigma_g^1 1\sigma_u^2$
	12.30	0.073	a
$^2\Sigma_u^+$	10.62		b $^3\Sigma_u^+$ threshold
	10.97		'feature'
	12.76		c $^3\Pi_u$ threshold
$^2\Pi_u$	12.60	0.066	c
$^2\Pi_g$	10.62		b $^3\Sigma_u^+$ threshold
	11.06	0.46	
	11.78	0.96	

Table 3.5: Resonance positions, E_{res}, and widths Γ_{res} for H_2.

been smoothed using the fact that the eigenphases are arbitrary to a factor of modulo π.

These eigenphases were then used in the program module RESON to produce resonance information. Two terms were used in the polynomial fit to the background (see equation (2.35)). A summary of the most significant results obtained below the energy of the C $^1\Pi_u$ threshold, is given in table 3.5. In order to obtain these final results it was necessary, in certain cases, to repeat the scattering calculation at a much smaller energy separation, but there still remained some features which could not be fitted to a resonance form. This will be discussed in the next section along with the assignments given in the table.

The remaining figures in this chapter represent integral cross sections. Figure
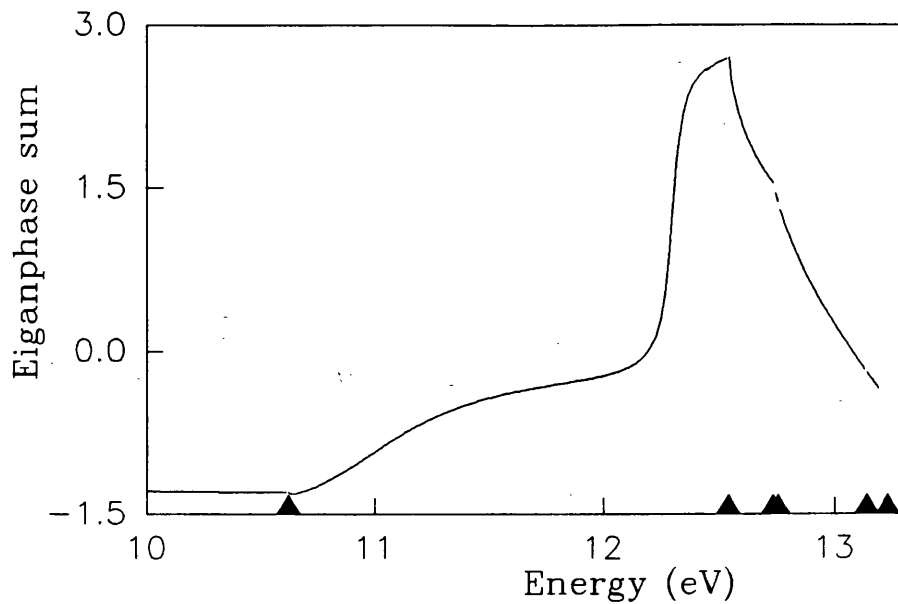
Figure 3.1: $^2\Sigma_g^+$ eigenphase sums for electron-H_2 collisions as a function of scattering energy in eV.
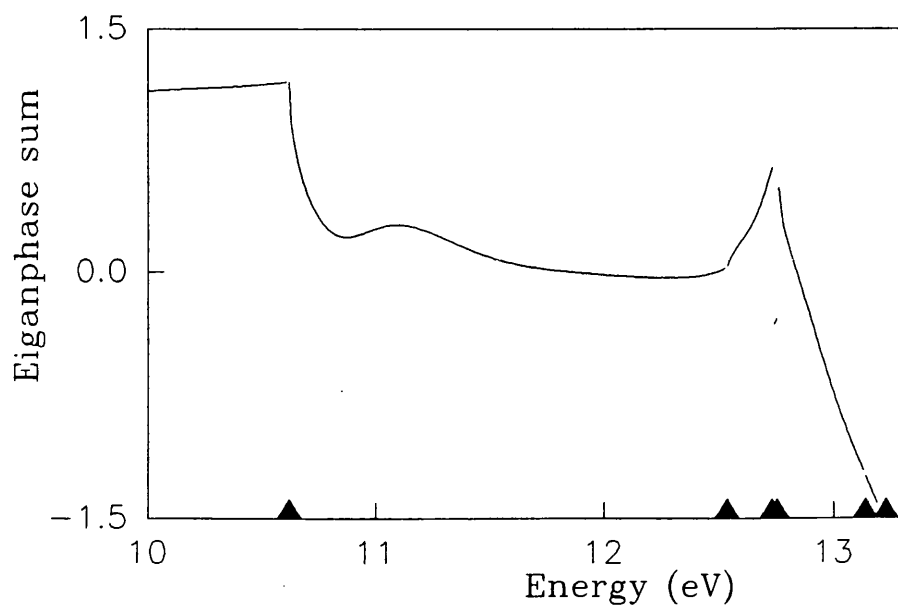
Figure 3.2: $^2\Sigma_u^+$ eigenphase sums for electron-H_2 collisions as a function of scattering energy in eV.
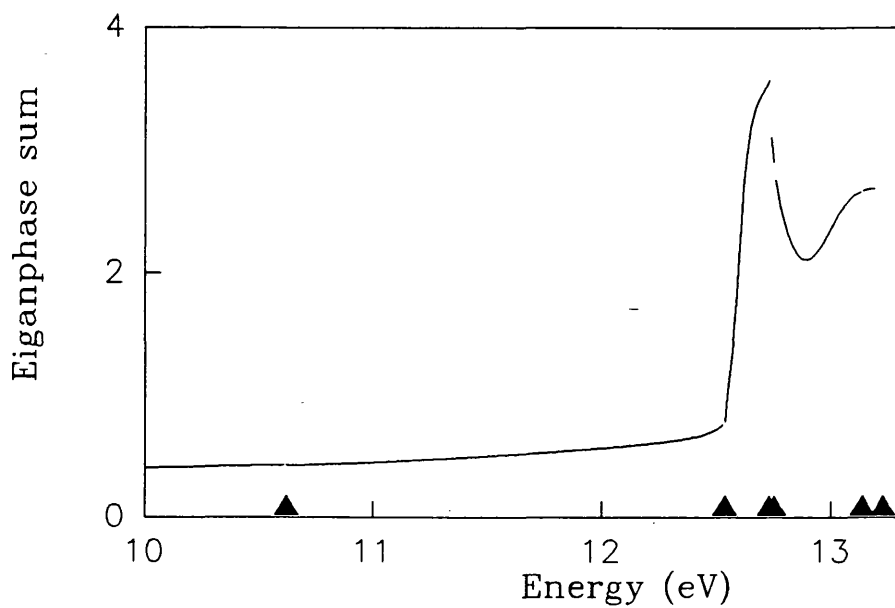
Figure 3.3: $^2\Pi_u$ eigenphase sums for electron-H_2 collisions as a function of scattering energy in eV.
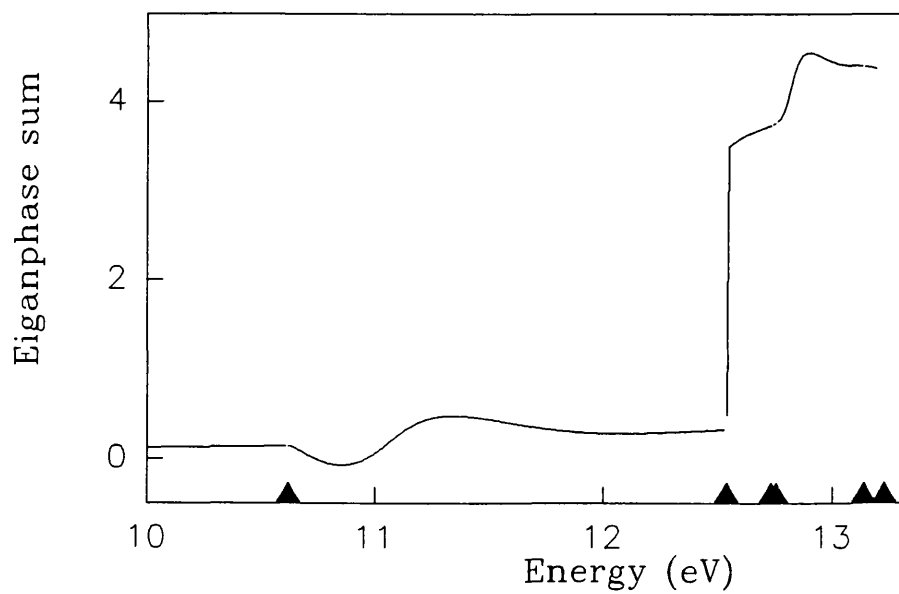
Figure 3.4: $^2\Pi_g$ eigenphase sums for electron-H_2 collisions as a function of scattering energy in eV.

58
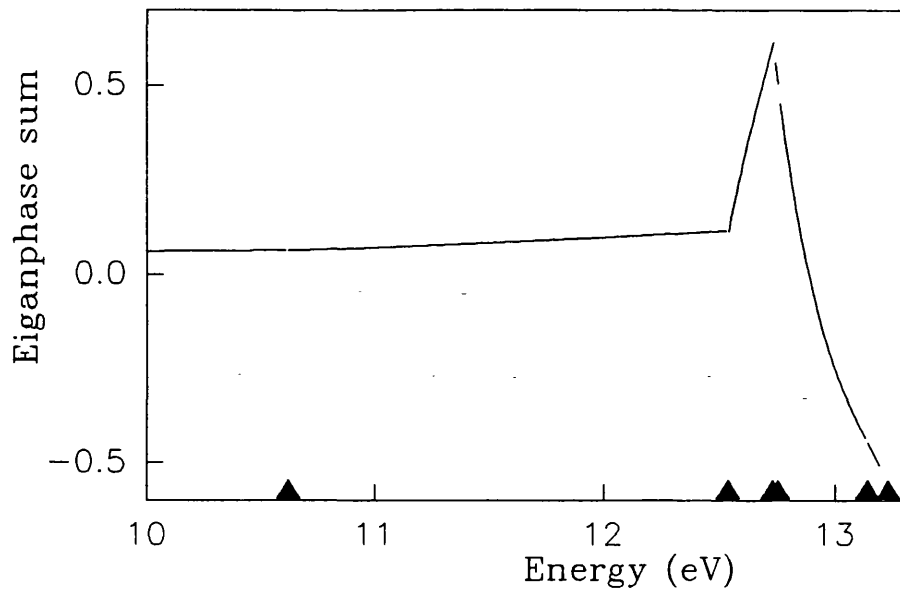
Figure 3.5: $^2\Delta_g$ eigenphase sums for electron-H_2 collisions as a function of scattering energy in eV.
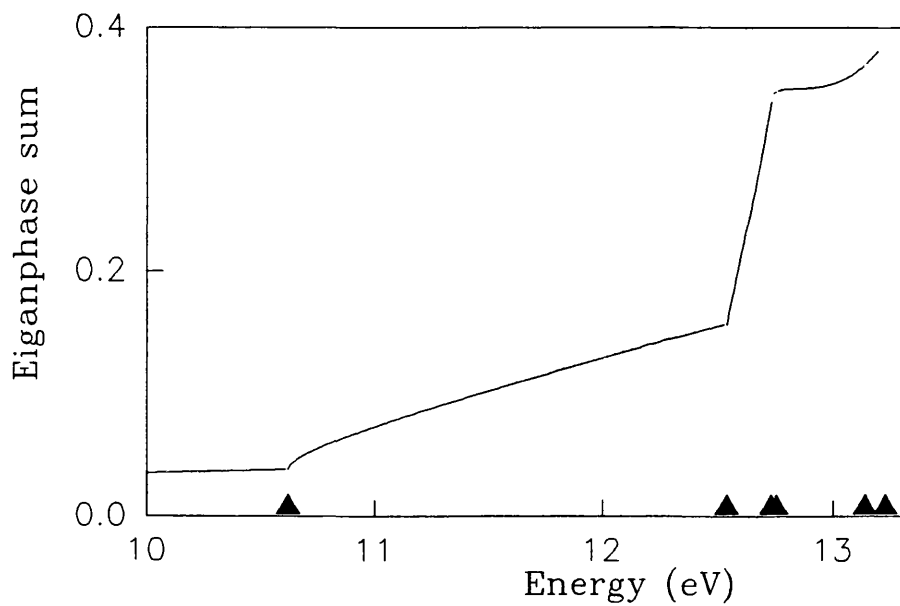
Figure 3.6: $^2\Delta_u$ eigenphase sums for electron-H_2 collisions as a function of scattering energy in eV.
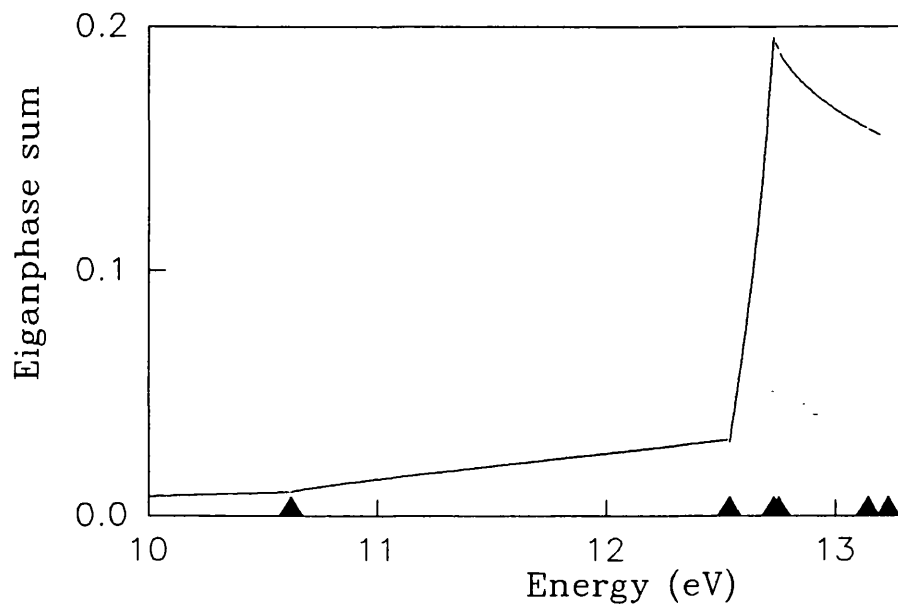
Figure 3.7: $^2\Phi_u$ eigenphase sums for electron-H_2 collisions as a function of scattering energy in eV.
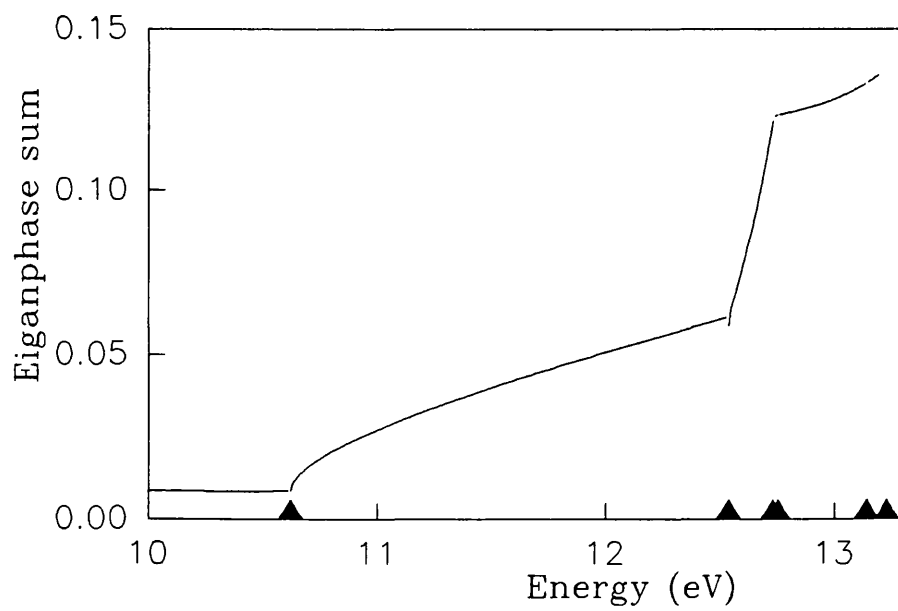
Figure 3.8: $^2\Phi_g$ eigenphase sums for electron-H_2 collisions as a function of scattering energy in eV.

3.9 shows the effect on the shape of the cross section for excitation from the ground to the first excited state of H_2, considering the $^2\Sigma_g$ symmetry only, of increasing the number of target states in the representation. Results are given for two state (X $^1\Sigma_g^+$, b $^3\Sigma_u^+$), four state (X $^1\Sigma_g^+$, b $^3\Sigma_u^+$, a $^3\Sigma_g^+$, B $^1\Sigma_u^+$) and six state (X $^1\Sigma_g^+$, b $^3\Sigma_u^+$, a $^3\Sigma_g^+$, B $^1\Sigma_u^+$, c $^3\Pi_u$, C $^1\Pi_u$) calculations. The two state calculations of Baluja *et al* (1985) are also shown for comparison.

Figures 3.10 to 3.14 show the integral cross sections for excitation from the ground to the five excited states considered in this model. The contributions from all eight symmetries up to $^2\Phi_g$ have been included.

3.4 Discussion

The eigenphase sums given in figures 3.1 to 3.8 display a large number of features previously only observed in atomic collision calculation (*e.g.* Clarke and Taylor 1982). This is a result of the sophistication of the model used and the fact that the R-matrix method is ideally suited to this sort of calculation where a large number of scattering energies must be considered. This ability to repeat the calculations at many energies made it possible to map out resonance features to determine their positions and widths.

The results of the resonance analysis are found in table 3.5. In several cases resonance like features were found just below threshold energies, but the jump in eigenphase sum was less than that associated with a true resonance (*i.e.* π). This was particularly noticeable just above the b $^3\Sigma_u^+$ threshold in both the $^2\Sigma_u$ and the $^2\Pi_g$ symmetries. Another resonance like feature was found in the $^2\Sigma_u$ symmetry against a sharply falling background which made it impossible to fit the resonance using the program module RESON. The broad resonance in the $^2\Sigma_g$ symmetry is due to the well known (Schulz 1973) repulsive $1\sigma_g^1 1\sigma_u^2$ state of H_2^-.
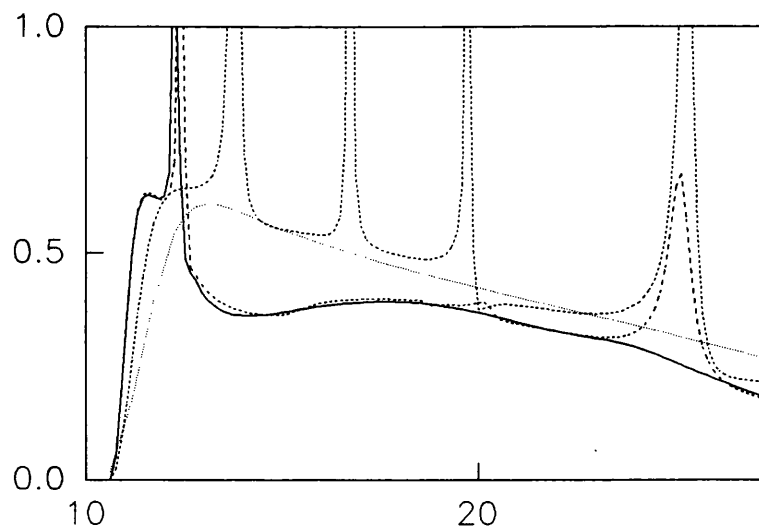
Figure 3.9: Integral cross section, in a_o^2, for excitation from the X $^1\Sigma_g^+$ state to the b $^3\Sigma_u^+$ state, as a function of energy, in eV, considering only the $^2\Sigma_g$ contribution. Theory: solid curve, six state model; long dashed curve, four state model; short dashed curve, two state; dotted curve, Baluja *et al* (1985).
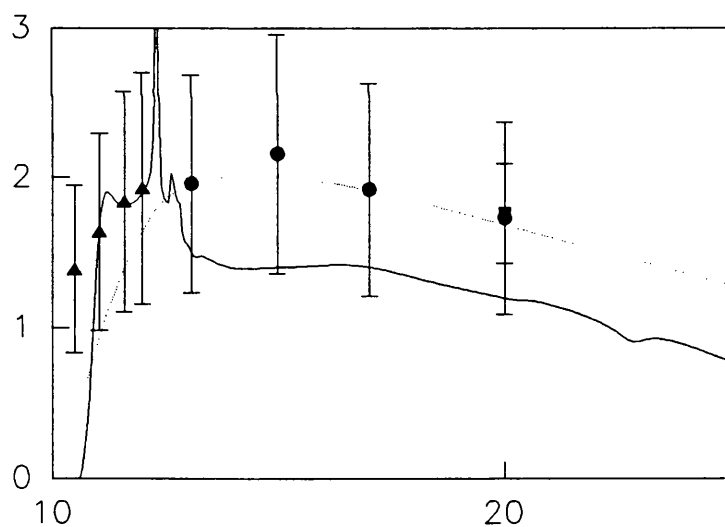
Figure 3.10: Integral cross section, in a_o^2, for excitation from the X $^1\Sigma_g^+$ state to the b $^3\Sigma_u^+$ state, as a function of energy, in eV. Theory: solid curve, six state model; dotted curve, Baluja *et al* (1985). Experiment: solid circle, Nishimura and Danjo (1986); solid square, Khakoo *et al* (1987); solid triangle, Hall and Andric (1984).
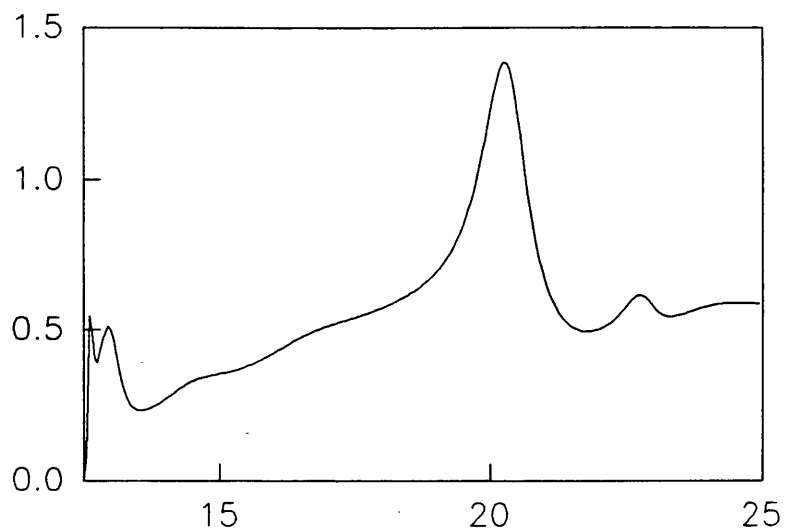
Figure 3.11: Integral cross section, in a_o^2, for excitation from the X $^1\Sigma_g^+$ state to the a $^3\Sigma_g^+$ state, as a function of energy, in eV.
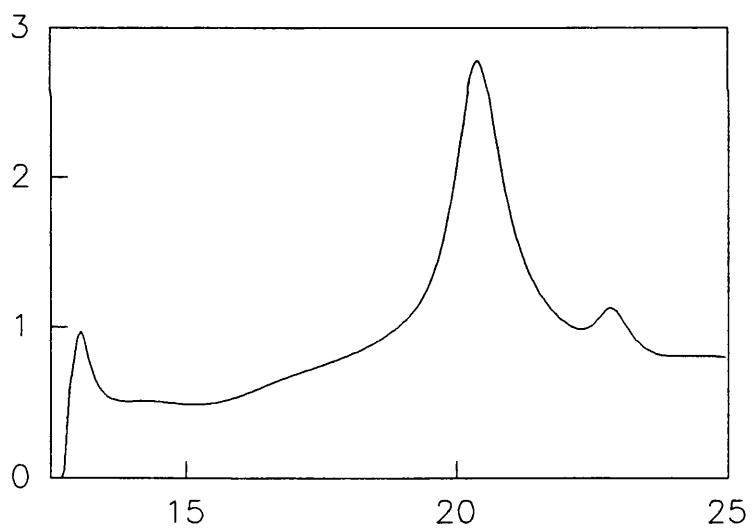
Figure 3.12: Integral cross section, in a_o^2, for excitation from the X $^1\Sigma_g^+$ state to the c $^3\Pi_u$ state, as a function of energy, in eV.
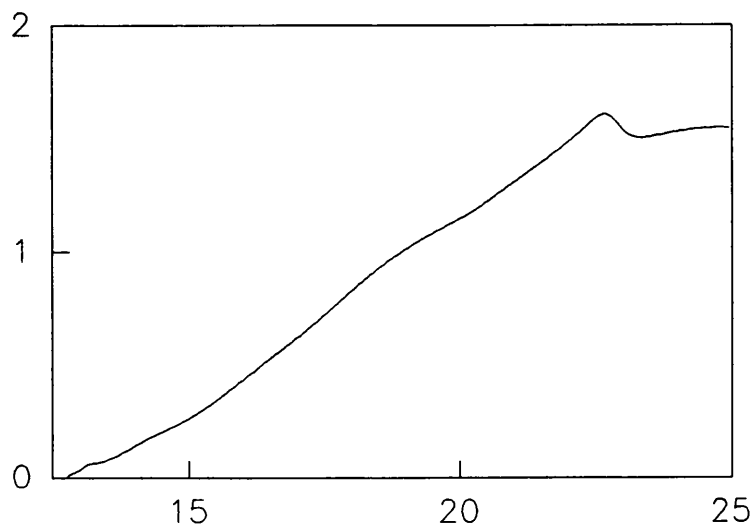
Figure 3.13: Integral cross section, in a_o^2, for excitation from the X $^1\Sigma_g^+$ state to the B $^1\Sigma_u^+$ state, as a function of energy, in eV.
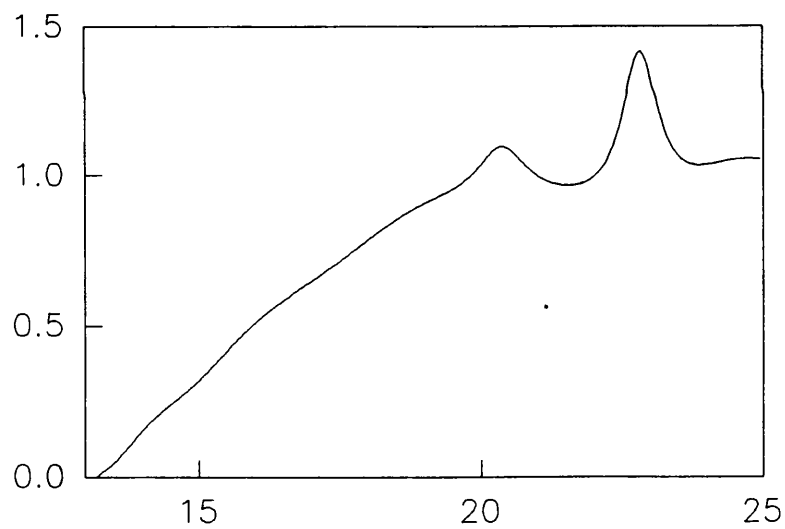
Figure 3.14: Integral cross section, in a_o^2, for excitation from the X $^1\Sigma_g^+$ state to the C $^1\Pi_u$ state, as a function of energy, in eV.

The results here were obtained for fixed nuclei. In order to compare these results with experimental resonances labeled a to g (Schulz 1973) the present results must be shifted by the difference in energy between the vertical excitation energy and the adiabatic excitation energy of the parent state. The a and c resonances both have the parent state c $^3\Pi_u$ shifting the resonance positions to 11.29 eV and 11.59 eV for the $^2\Sigma_g$ and $^2\Pi_u$ respectively. These results agree well with the previous experimental results of Schulz 1973 and Mason and Newell (1986a) who found the resonances in the 11.28–11.34 and 11.43–11.50 eV range and with the theoretical results of Buckley and Bottcher (1977) who found the two resonances at 12.16 and 12.70 eV respectively and Eliezer et al (1967) who found the a series resonance at 12.32 eV.

These calculations did not show any evidence for the b series resonance of Comer and Read (1971) and Buckley and Bottcher (1977) with parent state B $^1\Sigma_u^+$, nor did it find the d, e or higher series of resonances.

Figure 3.9 shows the effect of including more target states in the calculation. It can be seen that the present two state calculation agrees well with the two state calculation of Baluja et al (1985) if the sharply peaked resonances are ignored. These pseudoresonances are caused by neglecting open channels in the calculation. By including more target states the cross section becomes larger close to threshold and smaller at large energies. This is due to the improved representation of the target polarisation and to the loss of flux to other processes allowed for in the more complex target representation. The resonance close to the threshold in the four and six state calculations do not appear to be pseudoresonances, but are physical in origin. This type of resonance is also seen in several other symmetries which lead to the resonance analysis described above.

Figure 3.10 shows the integral cross sections obtained for the excitation process X $^1\Sigma_g^+$ $\rightarrow$ b $^3\Sigma_u^+$ state. The results obtained by Baluja et al (1985) are again

smaller at low energies and larger at high energies. Experimental results have also been given, but it can be seen that the experimental errors and the number of experimental points available mean that it is impossible to resolve the resonant structure close to threshold.

Figures 3.11 to 3.14 show cross sections for excitation to the other four excitation processes. No experimental data has been plotted since this will be discussed in the next chapter where a more complex model has been used. These figures do, however, show distinct resonance features. Like the X $^1\Sigma_g^+ \to$ b $^3\Sigma_u^+$ process the X $^1\Sigma_g^+ \to$ a $^3\Sigma_g^+$ process and the X $^1\Sigma_g^+ \to$ c $^3\Pi_u$ excitation process also display resonance features close to threshold.

In this chapter results have been presented for electron-H_2 scattering using a full CI six target state calculation. Integral cross sections have been calculated for excitation from the ground to the five excited states included in the calculation. The calculations were sufficiently complex to allow an investigation into the resonant structure of the integral cross sections and the agreement between these results and those of previous experimental and theoretical work has been acceptable. In the next chapter a more sophisticated model is used to study the same cross sections and resonances and a more detailed comparison with previous work is given.

Chapter 4

Integral cross sections for H_2

The seven state target calculations discussed in this chapter are an extension of the six state target calculations discussed in the previous chapter. In addition to the previous six states the E,F $^1\Sigma_g^+$ state has also been included. This state has been shown by da Silva *et al* (1990) to be of importance in their test calculations in the resonant energy region. Inclusion of this state also means that none of the lowest states have been excluded. Indeed, above the highest state included here, the C $^1\Pi_u$ state, there is a gap of 1.7 eV before the next highest i $^3\Pi_g$ and I $^1\Pi_g$ states, if the internuclear distance is taken to be fixed at 1.4 a_o, see figure 4.1.

4.1   Calculation

It was found that the set of STOs used in the previous chapter was not able to adequately represent the E,F $^1\Sigma_g^+$ state. Some experimentation was therefore carried out on the exponent of the $2s\sigma_g$ orbital in order to improve the target representation. Table 4.1 shows the results of this investigation and table 4.2 summarises the set of STOs chosen to be used in the seven state model discussed here. It should be noted that the only difference between this set of STOs and the one used in the previous chapter is that the exponent of the $2s\sigma_g$ orbital has been
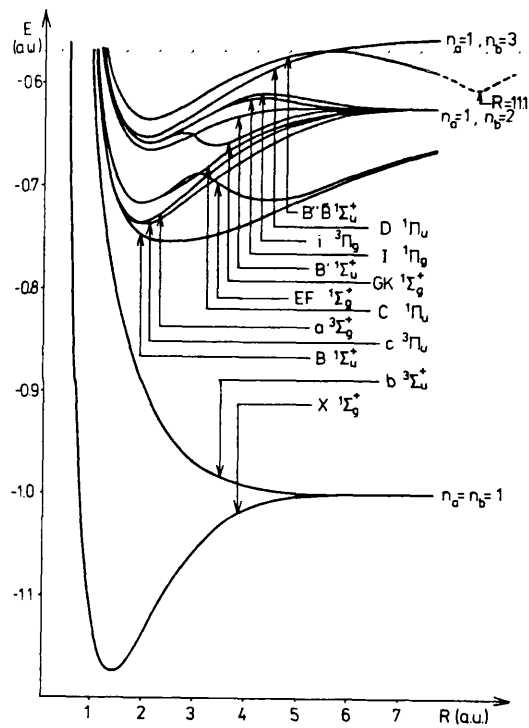
Figure 4.1: Potential energy curves of H_2 taken from Kołos (1978).

Exponent	6 State Basis			7 State Basis	'Exact'
of $2s\sigma_g$	0.800	0.900	0.700	0.600	
$X^1\Sigma_g^+$	-1.16584	-1.16586	-1.16582	-1.1658134	-1.1744744[a]
$b^3\Sigma_u^+$	10.45	10.45	10.45	10.45	10.62[a]
$a^3\Sigma_g^+$	12.77	13.04	12.56	12.47	12.54[b]
$c^3\Pi_u$	12.59	12.59	12.59	12.59	12.73[c]
$B^1\Sigma_u^+$	13.15	13.14	13.15	13.15	12.75[b]
$E,F^1\Sigma_g^+$	14.00	14.48	13.58	13.40	13.14[e]
$C^1\Pi_u$	13.10	13.10	13.11	13.11	13.23[d]

[a]Kołos and Wolniewicz (1965)

[b]Kołos and Wolniewicz (1968)

[c]Kołos and Rychlewski (1977)

[d]Rothenberg and Davidson (1966)

[e]Interpolated from Kołos and Dressler (1985)

Table 4.1: Ground state energies (in Hartrees) and vertical excitation energies (in eV) of H_2 for several different target representations.

Orbital	Exponent	Orbital	Exponent
$1s(\sigma_g)$	1.378	$1s(\sigma_u)$	1.081
$2s(\sigma_g)$	1.176	$2s(\sigma_u)$	0.800
$2s(\sigma_g)$	0.600		
$2p\sigma_g$	1.820	$2p\sigma_u$	1.820
$2p\pi_u$	0.574	$2p\pi_g$	1.084
$3p\pi_u$	0.636	$3p\pi_g$	1.084
$3d\pi_u$	1.511	$3d\pi_g$	2.470

Table 4.2: Exponents of the STOs used in the seven state target representation of H_2.

changed from 0.800 to 0.600.

As in the previous chapter a full CI target calculation was performed for the seven target states and the internuclear separation was fixed at 1.4 a_o. Again the results were no more than 0.4 eV different from the 'exact' quantum chemical results and the diagonal Hamiltonian matrix elements were shifted by the appropriate amount to compensate for this.

The continuum orbitals were generated as described in the previous chapter, with an R-matrix radius of 20 a_o, and all solutions below 5 Ryd with $\ell \leq 6$ and $m \leq 3$ were retained.

It was found that, even for a one state calculation, the new, more diffuse set of STOs suffered from problems with linear dependence if the previous orthogonalisation procedures were used. After some investigation it was found that it

was necessary to Lagrange orthogonalise one orbital from the σ_u and π_g and two orbitals from the σ_g and π_u sets to the target orbitals of the same symmetry. This gave a set made up of 48 σ_g, 38 σ_u, 37 π_u, 35 π_g, 36 δ_g, 25 δ_u, 25 ϕ_u and 23 ϕ_g continuum orbitals. The set of target and continuum orbitals was then Schmidt orthogonalised to the set of target orbitals as in the previous calculation.

Scattering calculations were then performed with an R-matrix propagation radius of 100 a_o and with all diagonal and off-diagonal dipole and quadrupole moments retained. K-matrices, eigenphase sums, T-matrices and integral cross sections were then calculated as before. The resonances were detected and fitted to a Breit-Wigner form using the module RESON.

4.2 Results

Figures 4.2 to 4.9 show the eigenphase sums for the total symmetries $^2\Sigma_g$ to $^2\Phi_g$. They represent scattering calculations separated in energy by 0.01 eV with small gaps at the thresholds, marked by triangles on the base lines. The results have been smoothed by multiples of π where necessary. By comparing these results with those of the previous chapter, shown in dotted lines on these figures, it can be seen that the eigenphases for the seven state calculation are consistently higher than for the six state calculation, as would be expected.

Table 4.3 summarises the resonance positions and widths detected in these calculations. Where necessary a finer energy grid than 0.01 eV has been used to clarify the shape of the eigenphase sums and where possible assignments have been made using the experimental classification scheme (Schulz 1973). In the lowest four symmetries considered here, rapid rises in the eigenphase sum of less than one could not be fitted to a resonance form. Where these effects were seen they have been described in the table as 'features'. In the higher four symmetries
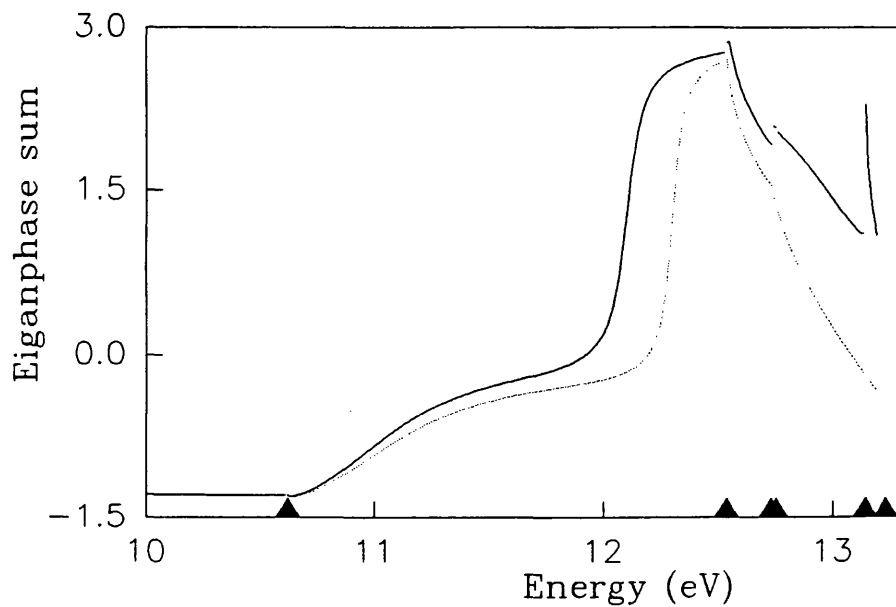
Figure 4.2: $^2\Sigma_g^+$ eigenphase sums for electron-H_2 collisions as a function of scattering energy in eV. Solid curve: seven state model; dotted curve: six state model.
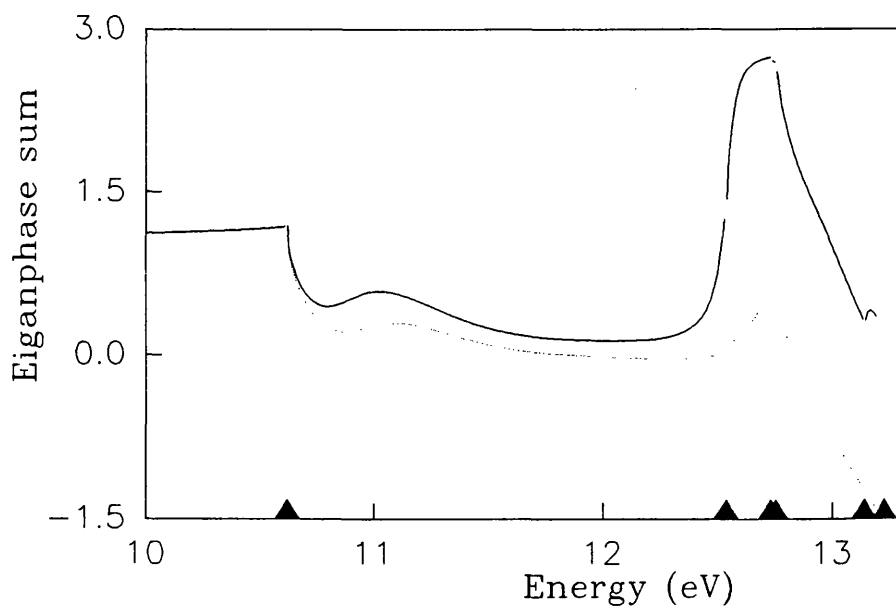
Figure 4.3: $^2\Sigma_u^+$ eigenphase sums for electron-H_2 collisions as a function of scattering energy in eV. Solid curve: seven state model; dotted curve: six state model.
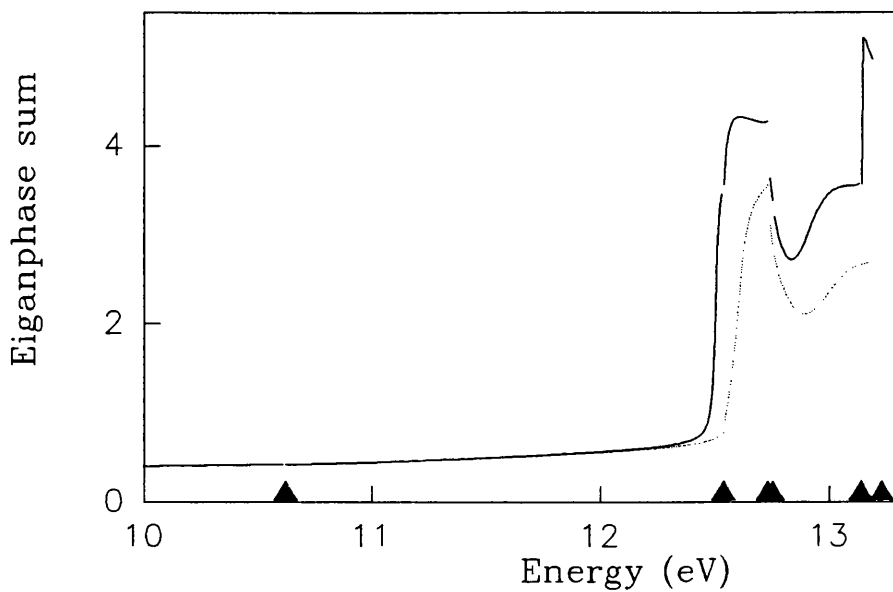
Figure 4.4: $^2\Pi_u$ eigenphase sums for electron-H_2 collisions as a function of scattering energy in eV. Solid curve: seven state model; dotted curve: six state model.
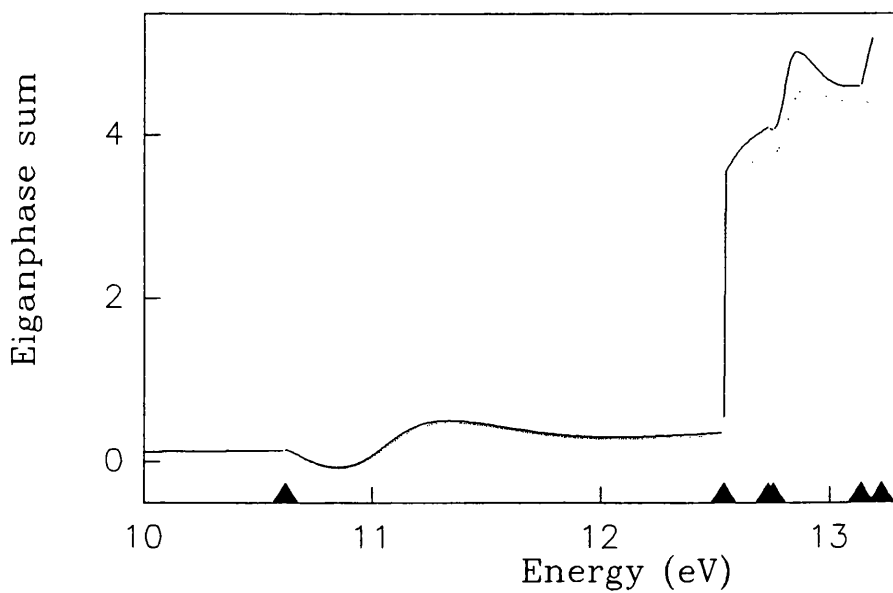
Figure 4.5: $^2\Pi_g$ eigenphase sums for electron-H_2 collisions as a function of scattering energy in eV. Solid curve: seven state model; dotted curve: six state model.
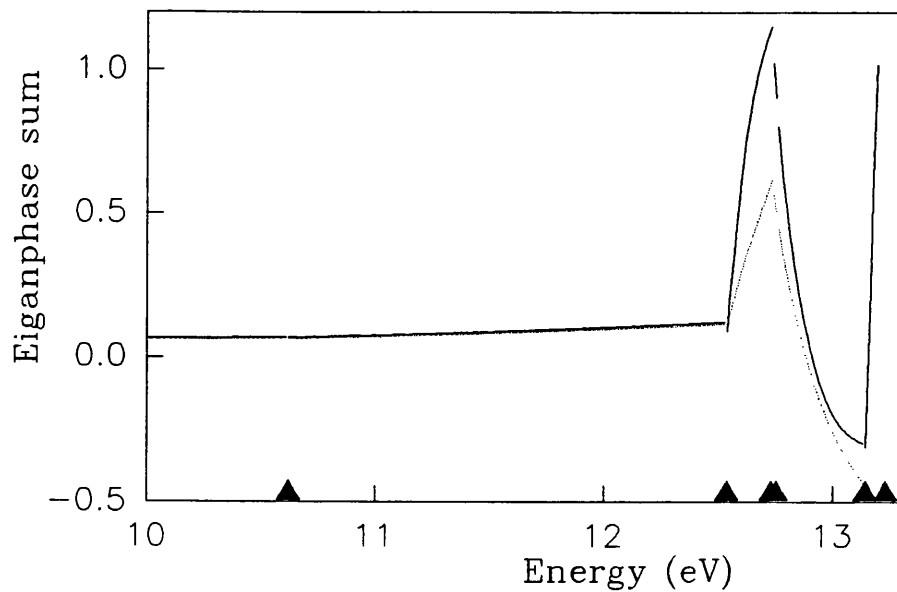
Figure 4.6: $^2\Delta_g$ eigenphase sums for electron-H_2 collisions as a function of scattering energy in eV. Solid curve: seven state model; dotted curve: six state model.
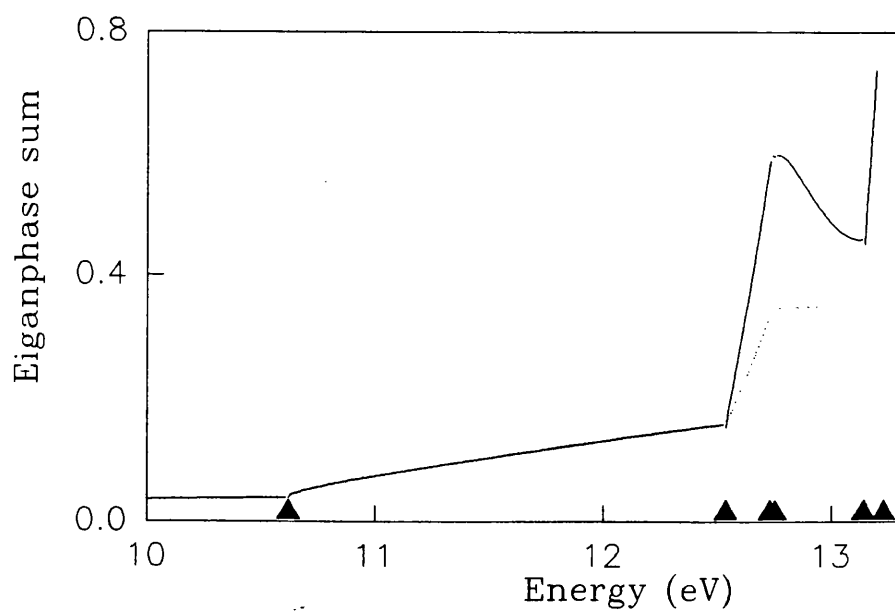
Figure 4.7: $^2\Delta_u$ eigenphase sums for electron-H_2 collisions as a function of scattering energy in eV. Solid curve: seven state model; dotted curve: six state model.
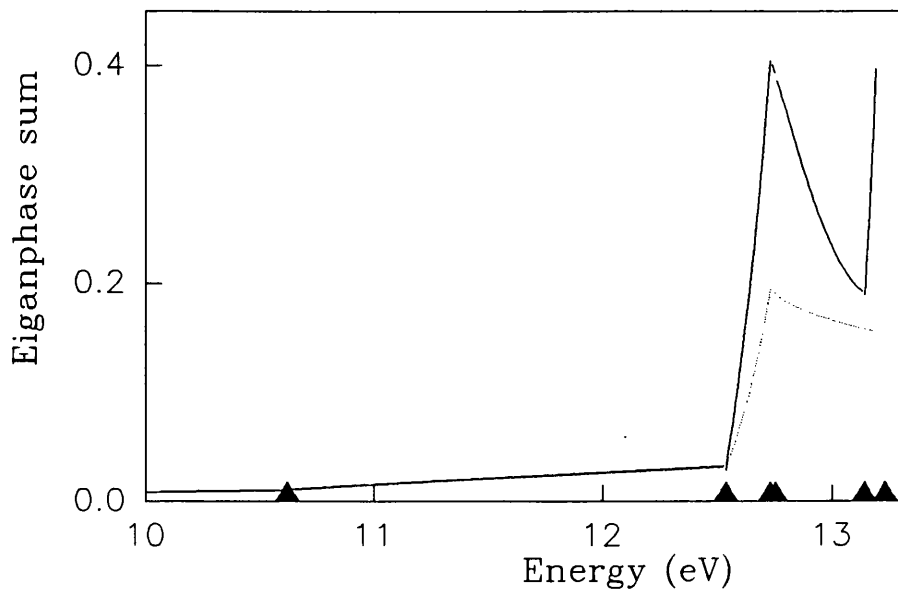
Figure 4.8: $^2\Phi_u$ eigenphase sums for electron-H_2 collisions as a function of scattering energy in eV. Solid curve: seven state model; dotted curve: six state model.
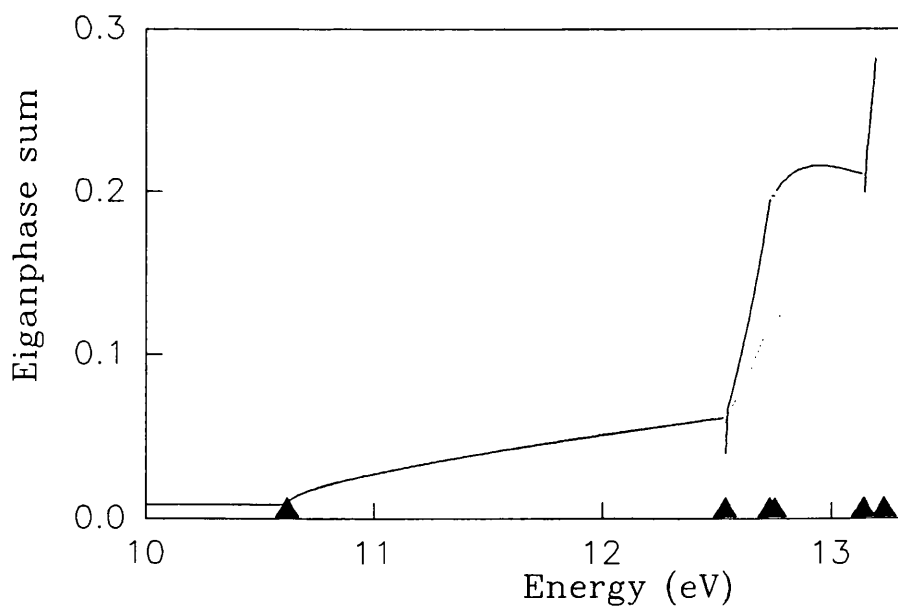
Figure 4.9: $^2\Phi_g$ eigenphase sums for electron-H_2 collisions as a function of scattering energy in eV. Solid curve: seven state model; dotted curve: six state model.

Symmetry	E_{res} (eV)	Γ_{res} (eV)	Assignment
$^2\Sigma_g^+$	10.94	1.24	$1\sigma_g^1 1\sigma_u^2$
	12.10	0.106	$a\ 1\sigma_g^1 2\pi_u^1 2\pi_u^1$
$^2\Sigma_u^+$	10.91		'feature'
	12.54	0.073	$c/e\ 1\sigma_g^1 2\pi_u^1 2\pi_g^1$
$^2\Pi_u$	12.50	0.018	$c/e\ 1\sigma_g^1 2\pi_u^1 2\sigma_g^1$
	12.95	0.175	'feature'
$^2\Pi_g$	11.05	0.46	'feature'
	12.80	0.080	$d\ 1\sigma_g^1 2\pi_u^1 2\sigma_u^1$?
$^2\Delta_g$	12.55	0.21	'resonance'
	13.16	0.058	'resonance'

Table 4.3: Resonance positions, E_{res}, and widths, Γ_{res}, for H_2 using the seven state model.
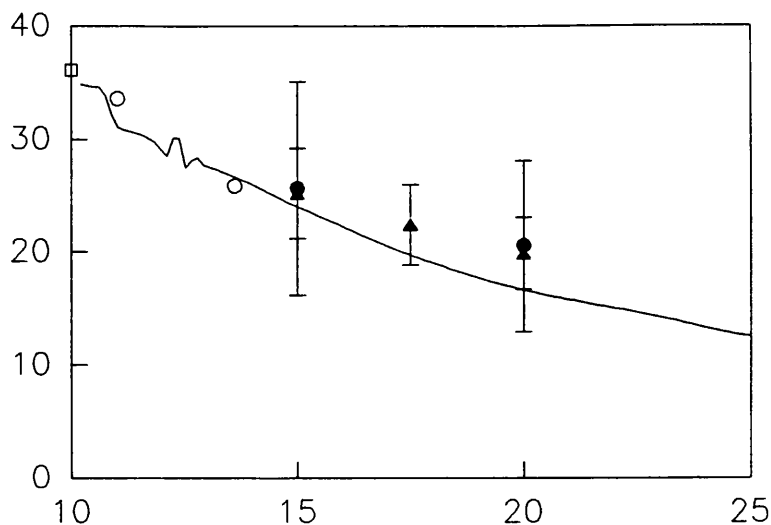
Figure 4.10: Integral cross section, in a_o^2, for elastic scattering as a function of energy, in eV. Theory: full curve, seven-state model; open square, Gibson et al (1984); open circle, Nesbet et al (1986). Experiment: solid circle, Nishimura et al (1985); solid triangle, Khakoo and Trajmar (1986a).

there are eigenphase sums which exhibit resonance-like features, but are not of sufficiently large magnitude to be thought of as true resonances.

Figures 4.10 to 4.16 show the integral cross sections for elastic scattering and for the six electronic excitation processes considered here. These results were obtained by summing up the results from the first eight symmetries and available experimental and previous theoretical results are plotted for comparison.

4.3   Discussion

The eigenphase sums, shown in figures 4.2 to 4.9, for the seven target state model agree well with the corresponding results for the six target state model given in the previous chapter for energies below 12 eV. Above this energy the effect of including the E,F $^1\Sigma_g^+$ state can be clearly seen. Recently da Silva et al (1990) have shown that one of the $^2\Sigma_g$ resonances is particularly sensitive to the inclusion of this state
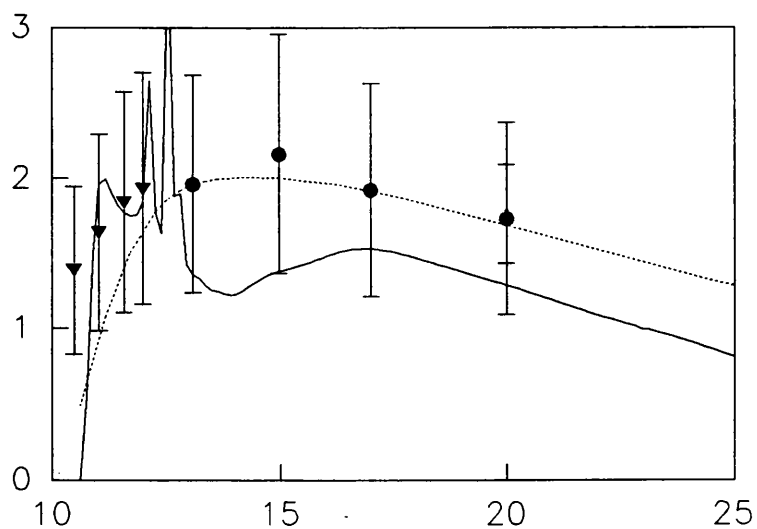
Figure 4.11: Integral cross section, in a_o^2, for excitation to the b $^3\Sigma_u^+$ state, as a function of energy, in eV. Theory: full curve, seven-state model; broken curve, Baluja *et al* (1985). Experiment: solid circle, Nishimura and Danjo (1986); solid triangle, Khakoo *et al* (1987); solid inverted triangle, Hall and Andric (1984).
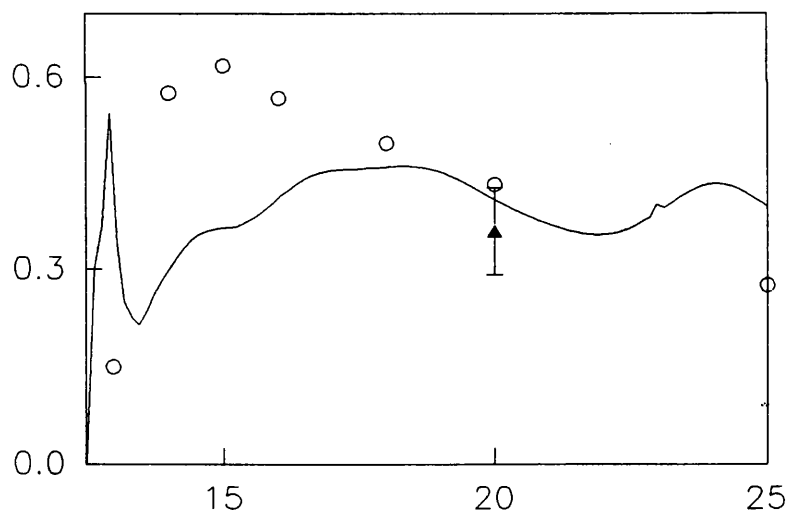
Figure 4.12: Integral cross section, in a_o^2, for excitation from the X $^1\Sigma_g^+$ state to the a $^3\Sigma_g^+$ state, as a function of energy, in eV. Theory: full curve, seven-state model; open circle, Lima *et al* (1988). Experiment: solid triangle, Khakoo and Trajmar (1986b).
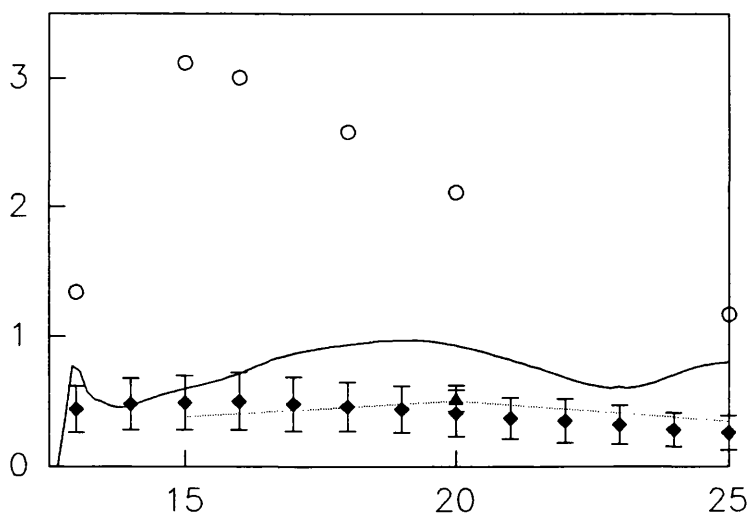
Figure 4.13: Integral cross section, in a_o^2, for excitation from the X $^1\Sigma_g^+$ state to the c $^3\Pi_u$ state, as a function of energy, in eV. Theory: full curve, seven-state model; dotted curve, Lee *et al* (1982); open circle, Lima *et al* (1988). Experiment: solid diamond, Mason and Newell (1986b); solid triangle, Khakoo and Trajmar (1986b).
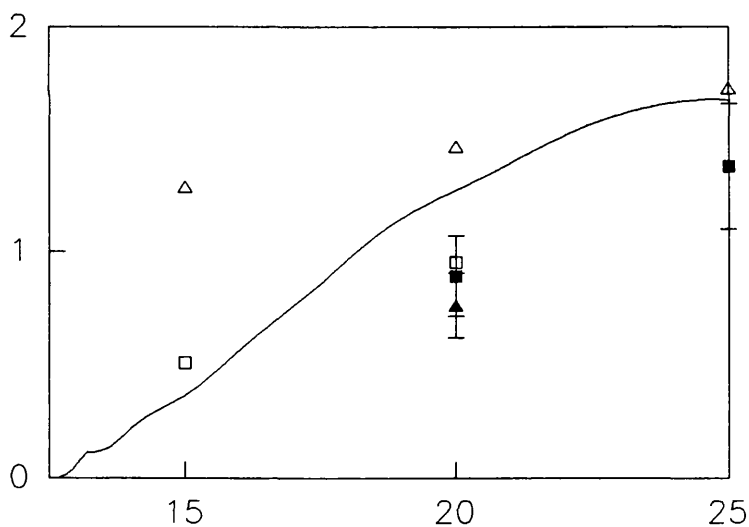
Figure 4.14: Integral cross section, in a_o^2, for excitation from the X $^1\Sigma_g^+$ state to the B $^1\Sigma_u^+$ state, as a function of energy, in eV. Theory: full curve, seven-state model; open square, Gibson *et al* (1987); open triangle, Redmon *et al* (1985). Experiment: solid square, Ajello *et al* (1984); solid triangle, Khakoo and Trajmar(1986b).
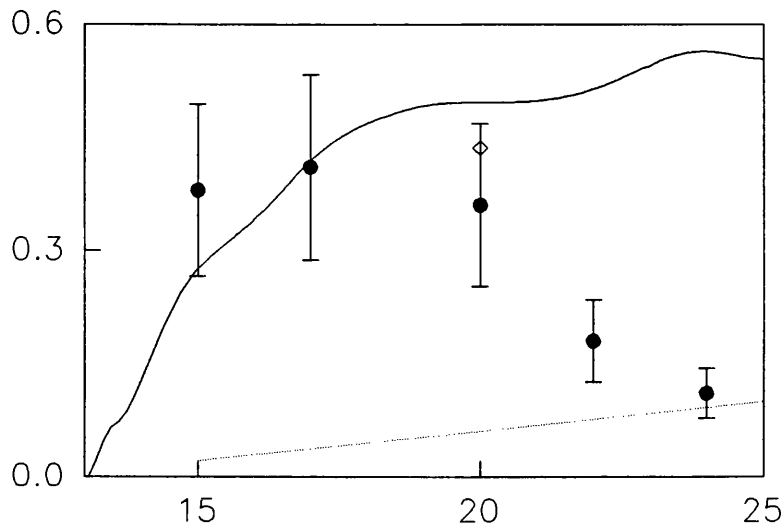
Figure 4.15: Integral cross section, in a_o^2, for excitation from the X $^1\Sigma_g^+$ state to the C $^1\Pi_u$ state, as a function of energy, in eV. Theory: full curve, seven-state model; dotted curve, Lee et al (1982); open diamond, Arrighini et al (1980). Experiment: solid circle $lower$ $limit$ of Watson and Anderson (1977).
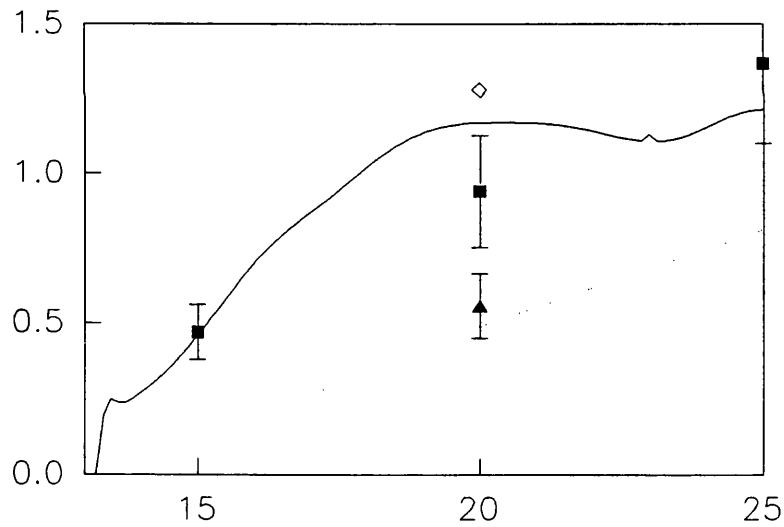
Figure 4.16: Integral cross section, in a_o^2, for excitation from the X $^1\Sigma_g^+$ state to the B $^1\Sigma_u^+$ state, as a function of energy, in eV. Theory: full curve, seven-state model; dotted curve, Lee et al (1982); open diamond, Arrighini et al (1980). Experiment: solid square, Ajello et al (1984); solid triangle, Khakoo and Trajmar (1986b).

Symmetry	Label	6 state	7 state	Eliezer et al (1967)	Buckley and Bottcher (1977)	DeRose et al (1988)
$^2\Sigma_g^+$	$1\sigma_g^1 1\sigma_u^2$	10.96	10.94	10.68	10.94	
$^2\Sigma_g^+$	a	12.30	12.10	12.32	12.16	
$^2\Sigma_u^+$	c/e		12.54		12.41	≤ 12.31
$^2\Pi_u$	c/e	12.60	12.50		12.70	

Table 4.4: Resonance positions for H_2 in comparison with previous calculations.

even though it is a closed state at the energy in question. The possibility that inclusion of higher lying states could have a significant effect on these eigenphase sums cannot, therefore, be ignored. This sensitivity to the model used is likely to be caused by a large number of resonances overlapping. Small changes in their positions and widths would have a large effect on the eigenphase sums because of interference effects.

Table 4.3 shows the seven state target calculation resonance features. It should be noted that the 'feature' in the $^2\Sigma_u^+$ symmetry of the six state calculation has been resolved into a resonance in the seven state calculation. Adding the extra state also had the effect of lowering the positions of the resonances and, except for the 'a' $^2\Sigma_g^+$ resonance, reducing their widths.

Table 4.4 compares the most significant features from table 4.3 with the results of Chapter 3 and with other theoretical calculations which used L^2 methods to study resonances.

The agreement between the seven state calculations and those of Buckley and

81

Bottcher (1977) is good. The calculations of DeRose *et al* (1988) only provide an upper bound on the position of the $^2\Sigma_u$ resonance, but, unlike the other L^2 calculations, they estimate the resonance width. Their value of 0.67 eV is much larger than the seven state calculation of 0.073 eV and if it were correct the resonance would be too wide for vibrational structure to be observed. DeRose *et al* (1988) also found two other lower lying resonances for this symmetry, which have not been found here or elsewhere.

Experimentally the resonances discussed here are sufficiently narrow for vibrational effects to give rise to resonance series. In order to make comparisons between these results and the results of this chapter it was necessary to know the parent state of the resonance considered and to shift the resonance position by the difference between the vertical excitation energy and the adiabatic excitation energy of the parent state. Schulz (1973) gives the parent state of the 'a', 'c', 'd', and the 'e' resonances as the c $^3\Pi_u$ state and shifting the results given in table 4.3 by the appropriate amount gives the results in table 4.5.

The energy position of the resonances is in reasonable agreement with the experimental values which would add support to the assignment of the c $^3\Pi_u$ state as the parent. The width of the 'a' and 'c' resonances calculated here are much larger than the results of Joyez *et al* (1973). However, both Joyez *et al* (1973) and Böse and Linder (1979) found that the widths were dependent on the isotope of hydrogen used. These considerations are beyond the capabilities of the present fixed nuclei calculations.

The resonance found in the $^2\Pi_g$ symmetry is in the same symmetry and has approximately the correct width to be considered the 'd' resonance of Weingartshofer *et al* (1970). The present results also give some evidence for the 'e' resonance, however, in order to clarify the situation a detailed study of the differential cross sections of these excitation process is needed. This was carried out and the results

	Position		Width		
Symmetry	This work	Schulz (1973)	This work	Joyez *et al* (1973)	Weingartshofer *et al* (1970)
$^2\Sigma_g^+$	11.09	11.28–11.34	0.106	≤ 0.016	
$^2\Sigma_u^+$	11.53		0.073		
$^2\Pi_u$	11.49	11.43–11.50	0.018	≤ 0.016	0.08

Table 4.5: Seven state Resonance positions and widths for H_2 in comparison with experimental results. The results of this work have been shifted as described in the text. All energies are in eV.

are presented in the next chapter.

A great deal of experimental and theoretical data exists for the integral cross sections of the elastic and electronic excitation processes considered here. For this reason only the most recent and reliable data have been included in figures 4.10 to 4.16.

It can be seen from these figures that previous theoretical calculations of integral cross sections are not able to produce resonance information. The different techniques used to study resonances have already been discussed. The experimental points are also too far apart and not accurate enough to resolve the structure produced by the present calculations as can be seen in figure 4.10. This is also particularly noticeable in figure 4.11 where the present calculations show a great deal of structure which the two state calculations of Baluja *et al* (1985) were not able to produce. Unfortunately, the available experimental results are not accurate

enough to distinguish between the two.

The results for excitation to the a $^3\Sigma_g^+$ state shown in figure 4.12 are interesting in that the two theoretical sets of results agree with each other at the only available experimental point, but differ at all other points. The present results display a sharp threshold peak, whereas the results of Lima *et al* (1988) predict a more slowly rising, broad peak. This effect is typical of the difference between calculations which do and do not include multichannel effects.

The results of Lima *et al* (1988) shown in figure 4.13 greatly overestimate the integral cross section. More recent calculations by Lee *et al* (1990) show that the inclusion of correlation effects is not enough to significantly improve the results. Only the inclusion of polarisation effects can do this. However, the distorted wave calculations of Lee *et al* (1982) give very good results for this excitation process, but not for the processes shown in figures 4.15 and 4.16.

The present results show very different shapes for excitation to singlet states from excitation to triplet states. Unlike excitation to the triplet states, the cross sections for the excitation to singlet states show little structure at threshold energies and tend to increase with increasing energy. In figure 4.14 this steady increase in cross section is also predicted by Gibson *et al* (1987) and by the impact-parameter method of Redmon *et al* (1985) which neglects exchange. As would be expected these impact-parameter results agree better with the present results as the scattering energy increases.

For the other excitation to singlet state processes considered here the present results agree well with the lower estimate experimental values of Watson and Anderson (1977) for excitation to the E,F $^1\Sigma_g^+$ state shown in figure 4.15 and with the renormalised results of Arrighini *et al* (1980) for excitation to the C $^1\Pi_u$ state shown in figure 4.16.

The results presented here show some features above the energy of the highest

threshold included in the calculations. In particular there would appear to be a resonance at around 23 eV. These features should be treated with care since they are likely to be pseudoresonances caused by neglecting open channels. From simple flux arguments, it must also be assumed that at high energies the present calculations will tend to overestimate the total cross sections. This is demonstrated in figure 4.11 where the two state calculation predicts a much higher cross section at high energies than the seven state calculation.

In this chapter integral cross section results have been presented for electronic excitation from the ground to the first six excited states of H_2 using a full CI seven target state model. In general the integral cross sections have agreed well with experimental data and represent an improvement on previous theoretical calculations. A richness of structure has been displayed in several excitation processes which previous calculations have not been able to predict and no previous calculations are consistently nearer to experimental results for all the excitation processes considered here.

The ability to produce estimates for resonance positions and widths lead to an investigation into the differential cross sections of these excitation process discussed in the next chapter. The experimental data for differential cross sections is much more accurate than for integral cross sections and it is only by studying the differential cross sections that the observed angular distributions of the resonance series can be understood.

Chapter 5

Differential cross sections for H_2

In this chapter the seven CI target state model of H_2, discussed in the previous chapter, has been used to calculate differential cross sections for elastic scattering and for electronic excitation from the X $^1\Sigma_g^+$ ground state to the b $^3\Sigma_u^+$, a $^3\Sigma_g^+$, c$^3\Pi_u$, B $^1\Sigma_u^+$, E,F $^1\Sigma_g^+$ and the C $^1\Pi_u$ states of hydrogen.

The study of differential cross sections is a more stringent test of a model than the study of integral cross sections since the available experimental data for differential cross sections is more accurate. This is because it is necessary to extrapolate differential cross sections to 0° and 180° before integration in order to produce integral cross section. Since it is difficult experimentally to obtain differential cross sections at angles much below 10° or above around 130° this can produce large errors as was seen in the previous chapter.

A study of the differential cross sections is also necessary to explain the observed angular distributions at resonant energies in electron-H_2 scattering. A consistent explanation for this structure and an accurate classification scheme for the resonances is not possible from a study of the integral cross sections alone.

Experimental results for non resonant differential cross sections have been reviewed recently by Tawara *et al* (1990) and resonance studies have been reviewed

by Schulz (1973) with more recent studies including those of Spence (1974), Wein-gartshofer *et al* (1975), Böse and Linder (1979), Huetz and Mazeau (1983) and Mason and Newell (1986b). Theoretically there have been many studies on non resonant differential cross sections, including those of Arrighini *et al* (1980), Fliflet and McKoy (1980), Lee *et al* (1982), Gibson *et al* (1987), Lima *et al* (1988) and Lee *et al* (1990), but there have been no calculations on resonant excitation differential cross sections. Where possible comparison has been made between these studies and the results produced here. Particular attention has been payed to values of energy for which experimental data is available.

5.1   Calculation

The results in this chapter are an extension of those in the previous chapter. Within the set of STOs given there a full CI target calculation was performed on the lowest seven electronic states of H_2 with a fixed internuclear separation of 1.4 a_o. Numerical basis functions with solutions below 5 Ryd with $\ell \leq 6$ and $m \leq$ 3 were retained. The molecular orbitals were orthogonalised by first Lagrange orthogonalising one orbital from the σ_u and π_g and two orbitals from the σ_g and π_u sets of continuum orbitals to the target orbitals of the same symmetry and then Schmidt orthogonalising the complete set of target and continuum orbitals.

A full CI calculation was then performed in the inner region and scattering information was obtained in the outer region by propagating the R-matrix to a radius of 100 a_o and then applying asymptotic expansion techniques (Noble and Nesbet 1984). All diagonal and off-diagonal dipole and quadrupole moments were retained. This method produced K-matrices from which T-matrices were constructed and from these the differential cross section were calculated using the program module DCS (Malegat 1990) described in Chapter 2.

87

Symmetry	E_{res} (eV)	Γ_{res} (eV)	Assignment
$^2\Sigma_g^+$	10.94	1.24	$1\sigma_g^1 1\sigma_u^2$
	12.10	0.106	a
$^2\Sigma_u^+$	12.54	0.073	c/e
$^2\Pi_u$	12.50	0.018	c/e
$^2\Pi_g$	12.80	0.080	d ?

Table 5.1: Resonance positions, E_{res}, and widths, Γ_{res}, for H_2 using the seven state model of Chapter 4.

5.2 Results

The differential cross sections presented here have been produced by summing the results for the first eight symmetries up to $^2\Phi_g$ and have been calculated at 50 evenly spaced angles between 0° and 180°. The energy points have been chosen to correspond with previous experimental data points and particular attention has been paid to the energies of resonance features found in the previous chapter and summarised in table 5.1.

Figure 5.1 shows the differential cross section for elastic scattering at several energies in comparison with previous theoretical and experimental results. At 20 eV the differential cross section summed over the first six symmetries are shown as well as the sum up to $^2\Phi_g$. At lower energies these cross sections are indistinguishable and so they have not been plotted. This is also true of figure 5.2 which shows the results obtained for excitation from the ground to the b $^3\Sigma_u^+$ state of H_2.
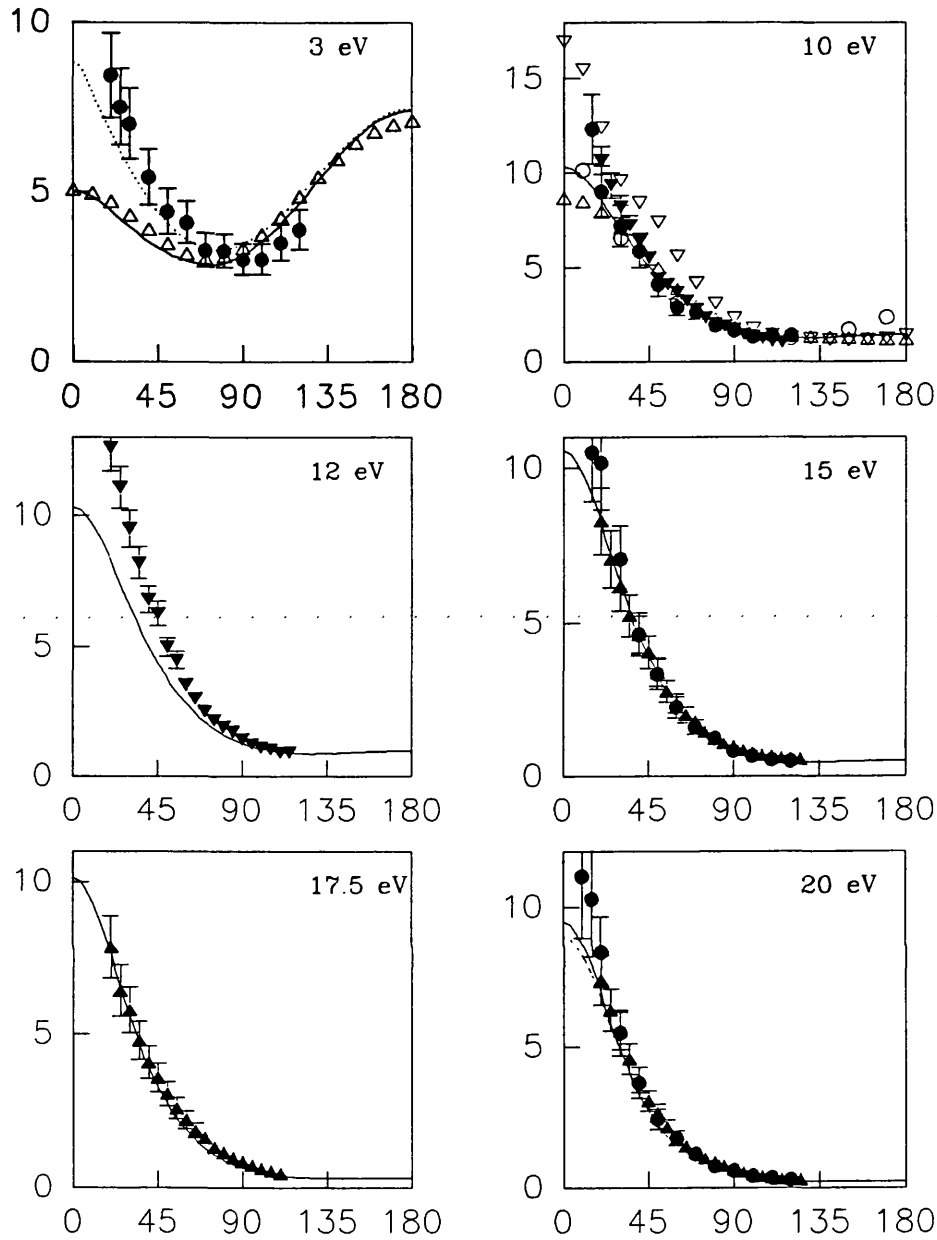
Figure 5.1: Elastic differential cross sections, in a_o^2, at 3 eV, 10 eV, 12 eV, 15 eV, 17.5 eV and 20 eV, as a function of angle in degrees. Theory: solid line, present work including symmetries up to $^2\Phi_g$; dashed line, present work including symmetries up to $^2\Delta_u$; dotted line, Snitchler et al (1991); open circles, Hara (1969); open inverted triangle, Truhlar and Brandt (1976) model 3; open triangle, Gibson et al (1984). Experiment: filled triangle, Khakoo and Trajmar (1986a); filled circle, Nishimura et al (1985); filled inverted triangle, Furst et al (1984).
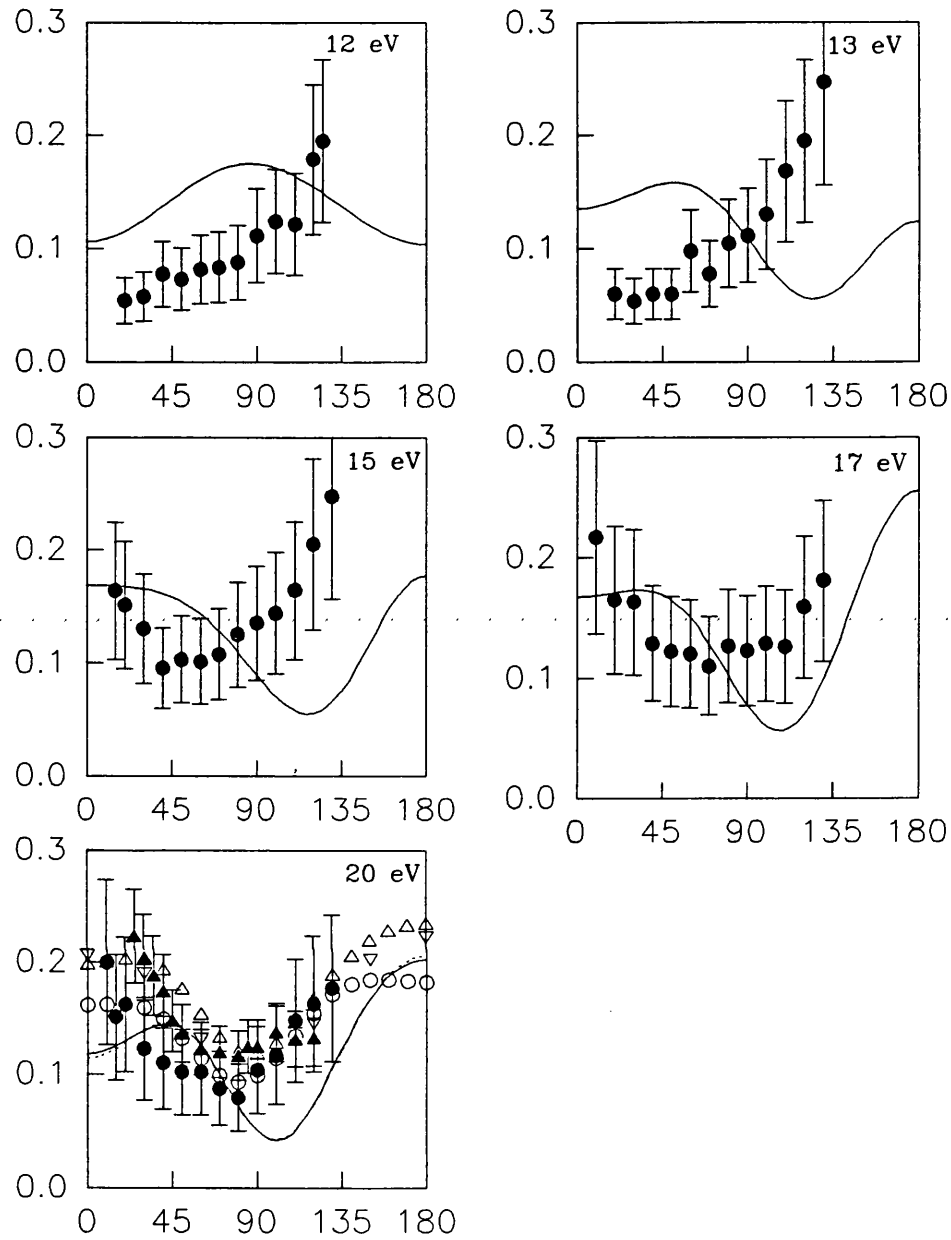
Figure 5.2: Differential cross sections, in a_o^2, for excitation to the b $^3\Sigma_u^+$ state at 12 eV, 13 eV, 15 eV, 17 eV and 20 eV, as a function of angle in degrees. Theory: solid line, present work including symmetries up to $^2\Phi_g$; dashed line, present work including symmetries up to $^2\Delta_u$; open triangle, Fliflet and McKoy (1980); open circle, Lima *et al* (1988); open inverted triangle, Lee *et al* (1990). Experiment: filled triangle, Khakoo *et al* (1987); filled circle, Nishimura and Danjo (1986).
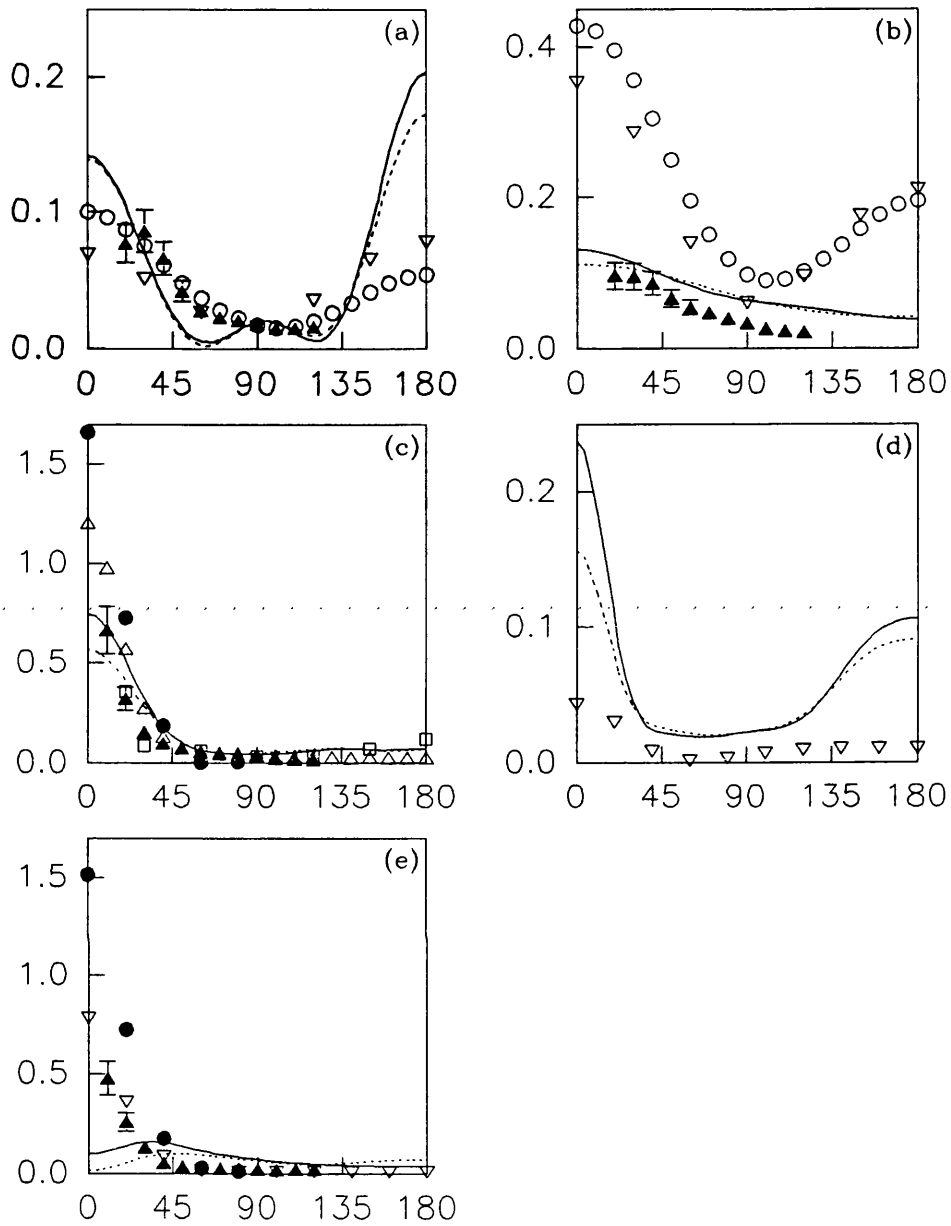
Figure 5.3: Differential cross sections, in a_o^2, for electronic excitation to the a $^3\Sigma_g^+$, c

$^3\Pi_u$, B $^1\Sigma_u^+$, E,F $^1\Sigma_g^+$ and C $^1\Pi_u$ states at 20 eV, as a function of angle in degrees.

Theory: solid line, present work including symmetries up to $^2\Phi_g$; dashed line,

present work including symmetries up to $^2\Delta_u$; solid circle, Arrighini *et al* (1980);

open square Gibson *et al* (1987); open circle, Lima *et al* (1988); open inverted

triangle, Lee *et al* (1982) and Lee *et al* (1990). Experiment: solid triangle, Khakoo

and Trajmar (1986b).
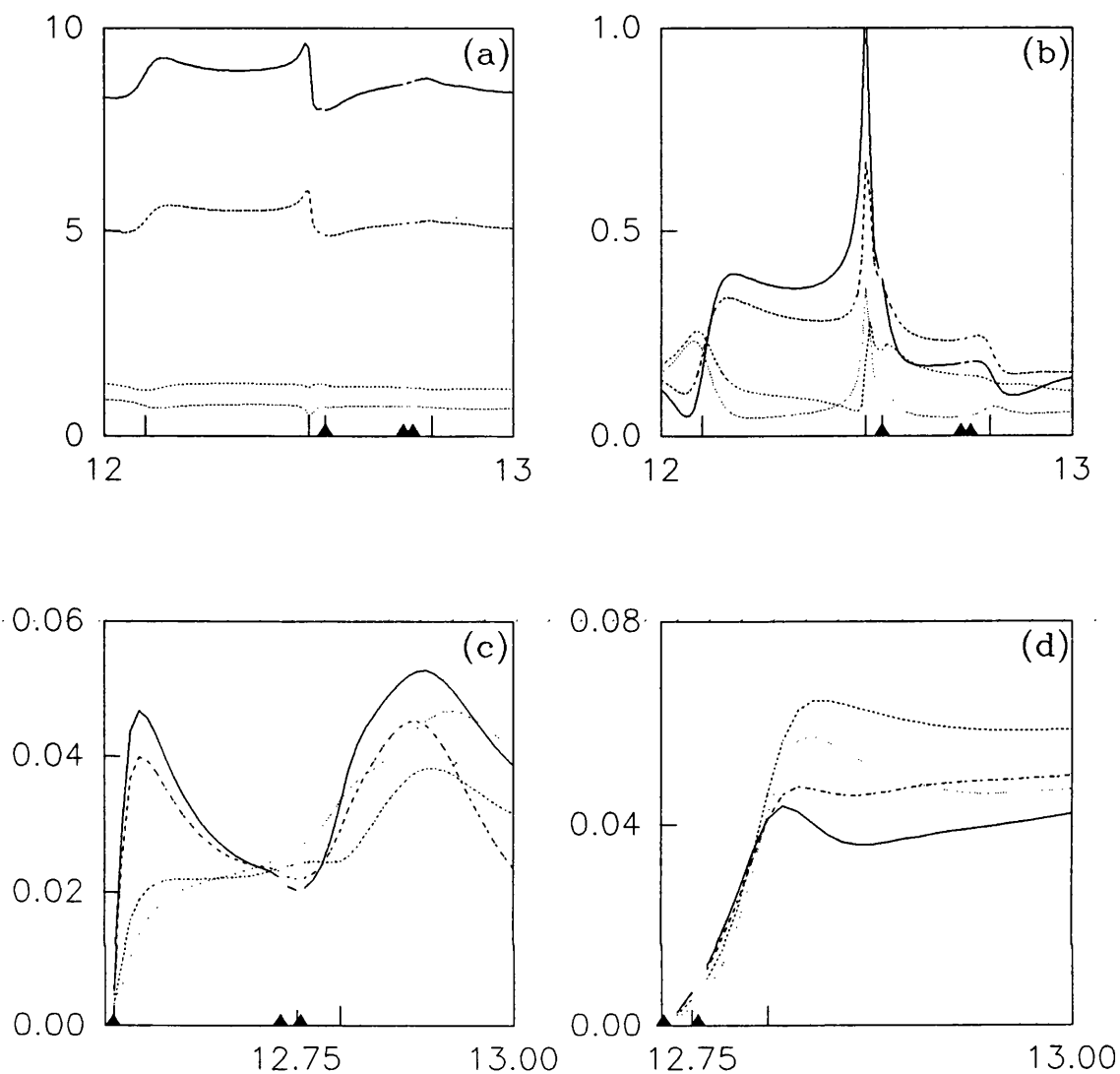
Figure 5.4: Differential cross sections, in a_o^2, as a function of energy, in eV, for elastic scattering and for excitation to the b $^3\Sigma_u^+$, a $^3\Sigma_g^+$ and c $^3\Pi_u$ state. Solid line, at 120°; long dashed line, at 90°; short dashed line, at 40°; dotted line, at 0°. The filled triangles on the base line indicate threshold positions and the vertical lines indicate the resonance positions.
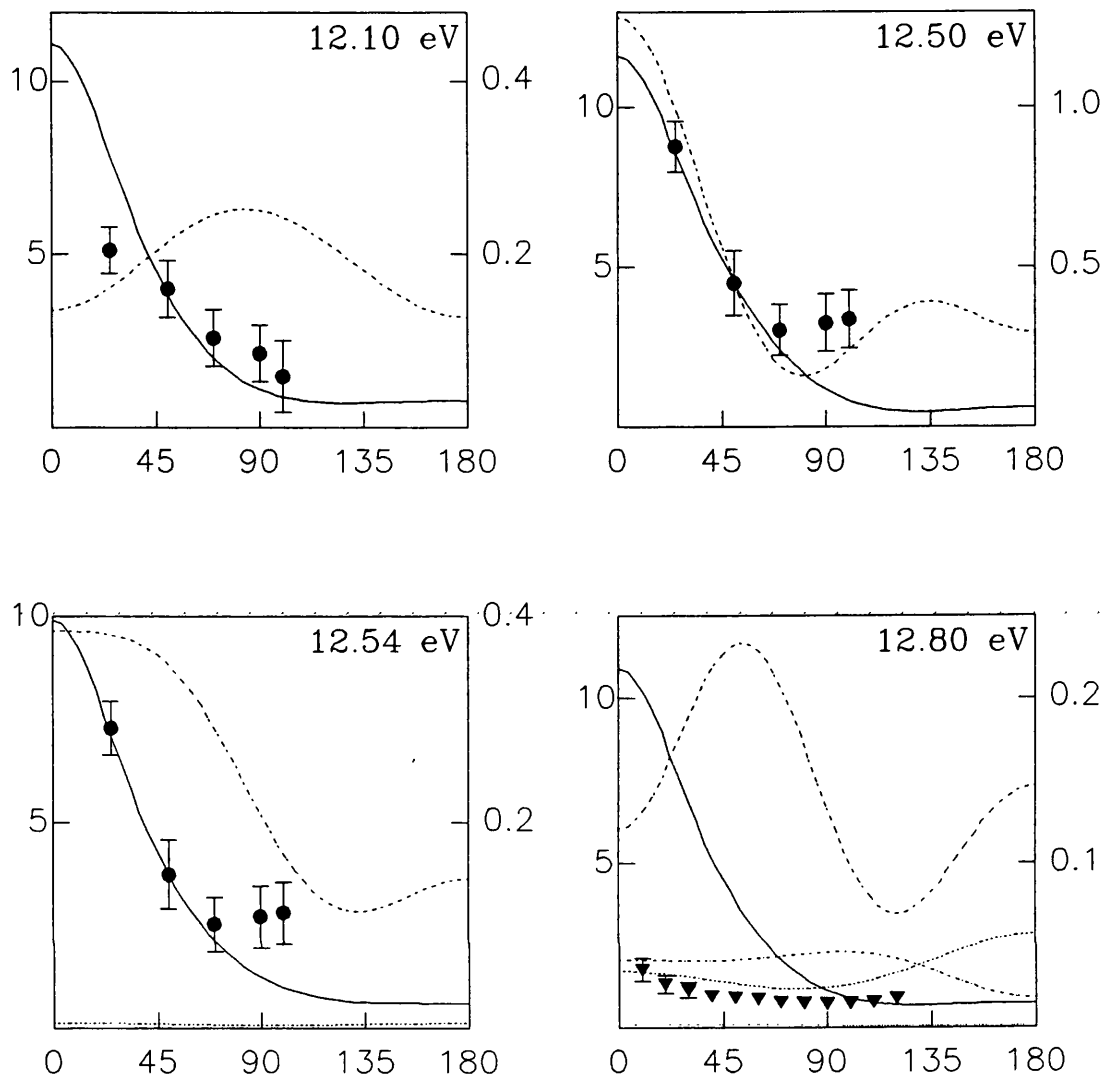
Figure 5.5: Differential cross sections, in a_o^2, at the resonant energies of 12.10 eV, 12.50 eV, 12.54 eV and 12.80 eV, as a function of angle in degrees. This work: solid line, elastic scattering; long dashed line, excitation to the b $^3\Sigma_u^+$ state; medium dashed line, excitation to the a $^3\Sigma_g^+$ state; short dashed line, excitation to the c $^3\Pi_u$ state; dotted line, excitation to the B $^1\Sigma_u^+$ state. Experiment: solid circle, Joyez et al (1973) for electronically elastic scattering, normalised to the 50° data point; solid inverted triangle, Weingartshofer et al (1970), for excitation to the B $^1\Sigma_u^+$ state.

Figure 5.3 shows the differential cross sections for excitation to the higher lying electronically excited state considered here. Results produced by summing over both six and eight partial waves have been presented as well previous theoretical and experimental results. These results are at the higher end of the incident electronic energy for which these calculations are valid.

The shape of the differential cross sections with respect to energy (sometimes called the excitation functions) are shown in figure 5.4. The four energy regions shown here correspond to the resonance positions given in table 5.1 and all eight symmetries up to $^2\Phi_g$ have been included in these results. The differential cross sections at the resonance positions are shown in figure 5.4 for elastic scattering in comparison with the experimental, electronically elastic, but vibrationally inelastic, results of Joyez et al (1973) and for excitation to the B $^1\Sigma_u^+$ state in comparison with the experimental results of Weingartshofer et al (1970).

5.3 Discussion

The agreement between the present calculations and previous experimental results for elastic scattering (figure 5.1) is very good except at low energies and small angles. The most likely source of error at low energies is the neglect of vibrational motion. Indeed at 3 eV Danby (1991) has shown that the inclusion of vibrational effects increases the differential cross section by approximately 12% in the 0° to 30° range compared with a model with internuclear separation fixed at the equilibrium geometry. At 3 eV the results of Snitchler et al (1991), which include vibrational and rotational motion, are in much better agreement with the experimental results than those of Gibson et al (1984) and the present results which assume a fixed internuclear separation.

Another source of error in the present results is lack of long range polarisa-

tion effects. In previous R-matrix calculations these effects have been corrected for by the use of polarised pseudo-state (Gillan *et al* 1988, Danby and Tennyson 1990), but in this calculation the inclusion of the B $^1\Sigma_u^+$ and C $^1\Pi_u$ states have a similar effect at low energies. The parallel and perpendicular components of the polarisability, $\alpha_{\parallel}$ and $\alpha_{\perp}$, can then be found from the equations:

$$\alpha_{\parallel} = \frac{2|\mu(^1\Sigma_u^+)|^2}{E(^1\Sigma_u^+) - E_o}, \tag{5.1}$$

$$\alpha_{\perp} = \frac{2|\mu(^1\Pi_u)|^2}{E(^1\Pi_u) - E_o}, \tag{5.2}$$

where $\mu(^1\Sigma_u^+)$ and $\mu(^1\Pi_u)$ are the dipole moments going from the ground to the $^1\Sigma_u^+$ and $^1\Pi_u$ states respectively and $E(^1\Sigma_u^+)$ and $E(^1\Pi_u)$ are the energies of these states. The effective polarisabilities, α_0 and α_2, are then given by:

$$\alpha_2 = \frac{2}{3}(\alpha_{\parallel} - \alpha_{\perp}), \tag{5.3}$$

and

$$\alpha_0 = \alpha_{\parallel} - \alpha_2. \tag{5.4}$$

The present target representation has effective polarisability of $\alpha_0 = 5.172$ a.u. and $\alpha_2 = 0.809$ a.u. compared with the accurate theoretical values of 5.179 a.u. and 1.202 a.u. (Kołos and Wolniewicz 1967).

The agreement between the present results at 10 eV is very good, but at 12 eV it is less pleasing. This is probably due to the closeness of the resonance at 12.10 eV, since at higher energies the agreement is again very good. At 20 eV the present results are no longer converged with respect to the number of partial waves included. This is probably the major source of error at small angles between these results and the available experimental results.

Agreement between the present results and experimental results is not as good for inelastic processes as for the elastic process, see figures 5.2 and 5.3. The only excitation process for which there is experimental data below 20 eV is excitation

95

from the ground to the b $^3\Sigma_u^+$ state shown in figure 5.2. For this process the agreement is worse in the 12eV to 13 eV energy region. This is probably due to the closeness of several resonance features which would have the result of making the differential cross section extremely sensitive to even small changes in energy and internuclear distance. The shape of the differential cross section at these two energies is different from those at higher energies for both experimental and theoretical results. At higher energies the present results agree better with the experimental results, almost to within the experimental errors, but the dip in the differential cross section predicted by these calculations is consistently at a higher angle than for the observed differential cross section.

It can be seen that at 20 eV the present results are not converged with respect to the number of symmetries summed over for any of the processes considered here, see figure 5.3. This could be corrected for using an approximation such as the Born approximation (e.g. Norcross and Padial 1982). This approximation considers the long range effect of spin conserving interactions and would not, therefore, affect the singlet to triplet excitation processes. As the agreement for singlet to singlet processes is no worse than for singlet to triplet processes this approach was not used.

Although the results presented in figure 5.3 are at the higher energy limit of the validity of these calculations the agreement with experiment is moderately good and in general these calculations represent an improvement on previous theoretical predictions. For example for excitation to the c $^3\Pi_u$ state the present calculations are closer to the experimental results in both shape and magnitude than those of Lima et al (1988) and Lee et al (1990). The present results are somewhat larger than the experimental results of Khakoo and Trajmar (1986b). This is partly due to the broad pseudoresonance at 17.5 eV in the $^2\Pi_u$ symmetry which was caused by neglecting channels open at this energy.

For excitation to the C $^1\Pi_u$ state the present results are of the same shape as, but greater magnitude than, the experimental results of Khakoo and Trajmar (1986b). This was also true for the integral cross section discussed in the previous chapter. For the integral cross section the seven state model results were in better agreement with those of Ajello *et al* (1984), but differential cross sections are not available for comparison.

The differential cross section for excitation to the a $^3\Sigma_g^+$ state demonstrates the difficulty in obtaining integral cross sections from experimental differential cross section results. All the theoretical results predict a rapid increase in the differential cross section at large and small angles, but from the experimental data points it would be very difficult to extrapolate accurately to 0° and 180° in order to obtain an integral cross section.

Figure 5.4 clearly shows that both the apparent position and the width of the resonances depends not only on the exit channel used for observation, but also on the angle of observation. For example the resonance at 12.80 eV does not appear to affect the shape of the resonance for elastic scattering, but for excitation to the b $^3\Sigma_u^+$ state this is not the case. This observation is in agreement with that of Huetz and Mazeau (1983). The position of the thresholds have been marked on these figures, but they do not seem to affect the differential cross sections considerably.

The differential cross sections at resonant energies, shown in figure 5.5, demonstrate that the angular distributions do not, in general, have the shape of the lowest partial wave contributing to that resonance, but are made up of contributions from several partial waves. In particular only the 12.10 eV differential cross section angular distribution for excitation to the b $^3\Sigma_u$ is symmetric about 90°. The present results are in good agreement with the normalised experimental results of Joyez *et al* (1973) since these results are electronically elastic, but rotationally and vibrationally inelastic. The agreement with the results of Weingartshofer *et*

al (1970), however, is not good.

5.4   Conclusions

Results have been presented here for the differential cross sections for elastic scattering of H_2 by electron impact and for electronic excitation from the ground to the first six excited states of H_2 using the full CI seven state target representation discussed in the previous chapter.

Agreement between the present calculations and previous experimental results is very good for elastic scattering in the 10 eV to 20 eV energy range, but is only moderate for the inelastic processes considered here. As well as neglecting closed channels, these calculations also neglect many channels, including ionisation, which are open at 20 eV. This may produce several effects such as the production of pseudo-resonances, neglect of short-range polarisation effects and the overestimation of integral cross sections due to lack of channels taking flux from the calculations. It would be difficult to estimate how great the effects of these errors might be without further extensive tests.

At the higher energies considered here it has already been pointed out that the present calculations are not converged with respect to the number of total symmetries included in the calculation and this is a significant source of error at these energies. Probably the most major source of error, especially at low energies and at resonant energies, is caused by the neglect of nuclear motion. At the resonance energies even small changes in the energy could produce a large difference in the differential and integral cross sections.

These calculations have shown that a great deal of care must be exercised when resonance positions and widths are being analysed. Both the magnitude and the shape of the differential cross section changes not only with the angle of

observation, but also with the exit channel monitored, thus producing different apparent resonance positions and widths according to which excitation process is under observation.

Chapter 6

Bound states of Diatomic

Molecules

In this chapter results are presented which have been produced by the computer module BOUND. Previously quantum chemical techniques have been applied to small molecules to calculate the low lying bound states and more recently these techniques have been adapted to calculate the higher lying Rydberg series of bound states (Kaufmann *et al* 1989). The code developed here, however, is based on the R-matrix method of determining atomic bound states (Seaton 1985) which has proved successful at producing large amounts of atomic ion data (Berrington and Seaton 1985). The advantage of this method over the quantum chemical techniques is that, once a suitable R-matrix has been constructed, it is theoretically possible to determine all the bound states converging to the relevant ionisation threshold.

An R-matrix method was developed by Ojha and Burke (1983) in order to calculate the bound states of argon. This method was later adapted for the calculation of the bound states of molecules by Tennyson *et al* (1986). The disadvantage of this method is that it can only search for bound states that are close in energy to the R-matrix poles. While the bound state energies and wavefunctions produced

for these states were good (Tennyson 1988), this method can not be applied to the higher lying Rydberg states.

6.1 Modules BOUND and TDIP

The program module BOUND was written using the theory based on Seaton (1985) and described for the molecular case in Chapter 2. Channel data and the surface amplitudes at the R-matrix boundary are input to the module which then determines the upper and lower energy bound for a systematic search for the bound states of the system.

For neutral target, or if requested for positive ion targets, the module will then set up an even grid of energy points between the end values in order to perform the search. Alternatively, for positive ion targets, the module will calculate the effective quantum number of the energy limits and set up a search over values of the principal quantum numbers included within the limits. For the lowest value of the principal quantum number a grid of energy points, evenly spaced in effective quantum numbers, is set up. For successive values of the principal quantum number there is an option to reduce the number of grid points which has already been described in Chapter 2.

For each energy grid point BOUND calculates the R-matrix and the outer region functions with calls to the modules VIBRMT, RPROP and CFASYM and then calculates the determinant of the matrix B defined by equations (2.55) and (2.56). BOUND then searches for zeros in the determinant of B by searching for changes in sign of the determinant between adjacent grid points. The possibility of two zeros between grid points is investigated by fitting the determinant to a quadratic form. Once a bound state has been detected BOUND then obtains an estimate for its energy position by repeated application of the Newton-Raphson

method. The final energy position is obtained using the Taylor series expansion method described in Chapter 2 and the bound state wavefunction is determined by applying equation (2.39).

From the input channel data an estimate of the number of bound states expected for a given value of principal quantum number is calculated and a warning printed if fewer bound states are found.

The module TDIP was written to calculate the transition dipoles of a system. TDIP takes the bound state wavefunction information from BOUND and the transition moments computed in TMT and performs the matrix multiplication described by equation (2.61). The perpendicular transition dipoles are multiplied by a factor of $2^{-1/2}$ in order to conform with the convention of Whiting et al (1980).

6.2 Results

6.2.1 CH

Table 6.1 shows results obtained for the bound states of CH compared with those of Tennyson (1988). The results of Tennyson (1988) were obtained using the R-matrix bound state method of Ojha and Burke (1983). The present results were obtained using BOUND and using the same target and scattering representation as the CC3P model of Tennyson (1988). Tennyson (1988) studied several models for the $e^- + CH^+ \rightarrow CH$ process for total symmetries of $^2\Sigma$ and $^2\Pi$ and at several internuclear separations between 1.5 and 4.0 a_o. In this work only the most sophisticated model at the equilibrium internuclear separation of 2.137 a_o was used for comparison.

In this model the CH^+ target is represented by an SCF calculation within a set of 12 σ, 7 π and 3δ STOs on the ground and the first two electronically excited states of CH^+. The R-matrix radius was taken to be 10 a_o and in the $N + 1$

State	Present (work)	Tennyson (1988)	van Dishoeck (1987) Calculated	Herzberg and Johns (1969) Observed
C $^2\Sigma$	4.53	4.53	4.02	3.98
2 $^2\Sigma$	6.82	6.76	6.39	
3 $^2\Sigma$	8.34	8.51	7.96	8.00
4 $^2\Sigma$	9.01			
5 $^2\Sigma$	9.24			
6 $^2\Sigma$	9.26			
7 $^2\Sigma$	9.62			
8 $^2\Sigma$	9.77			
9 $^2\Sigma$	9.83			
10 $^2\Sigma$	9.95			
2 $^2\Pi$	7.74	7.81	7.34	7.31
3 $^2\Pi$	8.28	8.45	7.94	7.96
4 $^2\Pi$	8.98		8.05	
5 $^2\Pi$	9.26	9.29		
6 $^2\Pi$	9.60			
7 $^2\Pi$	9.63			
8 $^2\Pi$	9.78			
9 $^2\Pi$	9.95			
10 $^2\Pi$	9.98			
Ionisation potential	10.83	10.83		10.64

Table 6.1: Vertical electronic excitation energies and ionisation potential, in eV, for the X $^2\Pi$ state of CH at its equilibrium geometry.

calculation the three excited electronic states were included in the close coupling expansion and polarisation was represented by including all two particle, one hole configurations from the target ground state. The continuum functions were generated numerically and all solutions with energy below 9 Ryd were retained. The continuum orbitals were Lagrange orthogonalised to the lowest three σ orbitals and the whole set of target and continuum orbitals were Schmidt orthogonalised. All dipole and quadrupole moments were retained and in the outer region solutions were found by first propagating the R-matrix to 100 a_o and then using asymptotic expansion techniques.

Previous calculated and observed values are also given in table 6.1 for comparison.

6.2.2 *HeH*

The bound state results presented in tables 6.2 and 6.3 were obtained using the representation of Sarpal *et al* (1991a) for the study of electron scattering from HeH^+.

From a suitable set of STOs Sarpal *et al* (1991a) generated target molecular orbitals using an SCF calculation. From these molecular orbitals the lowest three states of HeH^+ were represented by a CI expansion. This is the same procedure that was used in previous chapters to represent the H_2 target states, however, for HeH^+ a full CI expansion could not be used. By including 4 σ and 1 π orbitals in the CI expansion Sarpal *et al* (1991a) found that a good representation of the target energies could be produced. This reduced the number of σ and π components form 106 and 84 to 11 and 6 respectively. Calculations were carried out at 13 geometries with internuclear separations between 1.0 and 4.0 a_o. The vibrational energy levels were then calculated using the fourth order polynomial method of Le Roy (1971). The lowest six vibrational states of the ground state of

Assignment	Energy	μ	T_e	T_e(exp.)
1s $X^2\Sigma$	-3.232158	-0.334		
2s $A^2\Sigma$	-3.094013	0.129	31339	31695
2p $B^2\Pi$	-3.080895	0.036	28460	28888
2p $C^2\Sigma$	-3.035538	-0.435	18506	18837
3s $D^2\Sigma$	-3.011379	0.117	13205	13307
3p $E^2\Pi$	-3.008489	0.046	12570	12647
3d $F^2\Sigma$	-3.007627	0.023	12381	12430
3d $G^2\Pi$	-3.007228	0.012	12294	12355
3d $H^2\Delta$	-3.006284	-0.013	12086	12136
3p $^2\Sigma$	-2.993210	-0.450	9217	
4s $^2\Sigma$	-2.984321	0.114	7267	
4p $^2\Pi$	-2.983156	0.044	7011	7058
4d $^2\Sigma$	-2.982844	0.024	6943	
4d $^2\Pi$	-2.982665	0.013	6903	6931
4f $^2\Sigma$	-2.982561	0.007	6880	
4f $^2\Pi$	-2.982537	0.005	6875	
4f $^2\Delta$	-2.982478	0.001	6862	
4f $^2\Phi$	-2.982351	-0.007	6835	
4d $^2\Delta$	-2.982263	-0.013	6815	6850
4p $^2\Sigma$	-2.976391	-0.456	5526	
5g? $^2\Delta$	-2.973717	0.287	4940	
5s $^2\Sigma$	-2.972142	0.113	4594	
5p $^2\Pi$	-2.971571	0.045	4469	
5d $^2\Sigma$	-2.971411	0.025	4434	

5d $^2\Pi$	-2.971317	0.014	4413
5f $^2\Sigma$	-2.971260	0.006	4400
5f $^2\Pi$	-2.971248	0.005	4398
5g $^2\Pi$	-2.971229	0.003	4394
5f $^2\Delta$	-2.971211	0.000	4390
5g $^2\Sigma$	-2.971208	0.000	4389
5g $^2\Phi$	-2.971202	-0.001	4388
5d? $^2\Delta$	-2.971200	-0.001	4387
5f $^2\Phi$	-2.971155	-0.007	4379

Table 6.2: Bound states of HeH in Hartrees at the fixed equilibrium internuclear separation of 1.455 a_o. T_e is the energy in cm^{-1} relative to the ground state of the ion, -2.951208 Hartrees; μ is the quantum defect number. The last column gives the ionisation potentials deduced from the experimental data of Ketterle (1990).

Vibrational Level	Sarpal *et al* (1991b)			Present work
	B $^2\Pi$	E $^2\Pi$	G $^2\Pi$	
0	-3.07321			-3.07324
1	-3.05882			-3.05900
2	-3.04583			-3.04633
3	-3.03426			-3.03520
0		-3.00095		-3.00090
0			-2.99973	-2.99981
1		-2.98690		-2.96790
1			-2.98574	-2.98516
2		-2.97428		-2.97579
2			-2.97315	-2.97531
3		-2.96312		-2.96426
3			-2.96200	-2.96397
	H $^2\Delta$			
0	-2.99874			-2.99884
1	-2.98463			-2.98483
2	-2.97186			-2.97510
3	-2.96050			-2.96387

Table 6.3: Bound states of HeH in Hartrees for the lowest lying Π and Δ symmetries and their lowest lying vibrational states.

HeH were included in these calculations.

An R-matrix radius of 10 a_o was used and the continuum orbitals calculated numerically as has already been described. All solutions below 10 Ryd were retained and the lowest six σ and π and the lowest three δ and ϕ correlation functions were included in the CI expansion of the $N + 1$ electron system. All dipole and quadrupole moments were retained in the outer region calculation. For the scattering calculation a propagation radius of 300 a_o was used, but for the bound state calculation, which uses a slightly different method of solution in the outer region (see Chapter 2), a propagation radius of 50 a_o was needed. For the Σ and Π total symmetries the lowest ten R-matrix poles were treated non-adiabatically and for the Δ and Φ symmetries seven and five poles respectively were treated non-adiabatically.

Table 6.2 shows the bound states calculated, by Dr. B. K. Sarpal, using BOUND at the fixed equilibrium internuclear separation of 1.455 a_o. These results have been published as Sarpal *et al* (1991b) and the lowest 33 electronic states of *HeH* have been assigned and compared with experimental data. Table 6.3 compares the vibrational results of Sarpal *et al* (1991b), calculated using a Le Roy fit for the potential energy curves and solving the 1D nuclear Schrödinger equation for the vibrational energy levels, with the results obtained using BOUND to include the vibrational motion 'non-adiabatically'.

6.2.3 H_2

Table 6.4 shows the transition energies, transition dipoles and oscillator strengths calculated for H_2 using BOUND to calculate the bound state and the program module TDIP to calculate the transition dipoles and oscillator strengths. These results are then compared with previous theoretical results for transition dipoles, in table 6.5, and for oscillator strengths, in table 6.6.

State (a.u.)	E	ν	Fraction in inner region	Transition dipole	Oscillator strength f	$\nu^3 f$
$^1\Sigma_g$	-1.168391	(0.9135)	1.0000			
$^1\Sigma_u$	-0.703953	1.9266	0.9995	-0.9807	0.297762	2.129301
	-0.627599	2.9272	0.8240	0.4323	0.067382	1.690048
	-0.601673	3.9267	0.2782	-0.3084	0.035933	2.175676
	-0.600569	3.9953	0.4325	-0.0073	0.000020	0.001301
	-0.589849	4.9263	0.1301	0.2202	00018705	2.236224
$^1\Pi_u$	-0.686564	2.0644	0.9986	-0.7344	0.346449	3.048232
	-0.622402	3.0670	0.7265	0.3781	0.104084	3.002661
	-0.600555	3.9962	0.4311	0.0029	0.000006	0.000405
	-0.599491	4.0659	0.2889	-0.2740	0.056940	3.827266
	-0.589281	4.9956	0.2385	-0.0005	0.000000	0.000025

Table 6.4: Bound state energies, effective quantum numbers ν, transition dipoles and oscillator strengths, f, for excitation from the ground state to the lowest lying $^1\Sigma_u$ and $^1\Pi_u$ of H_2 at the fixed equilibrium internuclear separation of 1.4 a_o. The fraction of the wavefunction in the inner region and the function $\nu^3 f$ are also shown.

These results were obtained using the H_2^+ target representation of Tennyson (1991). This uses the σ orbitals of Shimamura et al (1990) and the π orbitals of Cohen and Bardsley (1980) to represent the X $^2\Sigma_g^+$, A $^2\Sigma_u^+$ and the B $^2\Pi_u$ states of H_2^+. The continuum functions were calculated numerically and all solutions with energy less that 7 Ryd were retained. An R-matrix radius of 14 a_o was used and a propagation radius of 30 a_o was used for the calculation of the bound states of H_2. Bound state calculations were carried out at 10 internuclear separations between 1.0 and 3.5 a_o and the transition dipoles calculated using the module TDIP. Table 6.5 shows the transition dipoles calculated for fixed internuclear separation at the equilibrium geometry, of 1.4 a_o, for transitions from the ground to the $^1\Sigma_u$ and to the $^1\Pi_u$ states of H_2. Figures 6.1 and 6.2 show the variation of the transition dipole with respect to changes in the internuclear separation for the lowest five transitions to each of these symmetries.

6.3   Discussion

6.3.1 CH

The results obtained for the bound states of CH, shown in table 6.1, were used as a test case for the development of the module BOUND. The results of Tennyson (1988) were produced using the method of Ojha and Burke (1983). For each symmetry only the lowest three bound states have been given. The method used here, however, was able to produce a very large number of bound states, the lowest ten for each symmetry are given in the table. The results produced by the two different methods are in reasonable agreement with each other. The slight differences are due to the different methods of searching for the poles and also to the fact that the solution of the outer region problem has been improved since the calculations of Tennyson (1988). Where the two sets of results differ, the present

State	Previous Theory		Bauschlicher and Langhoff (1991)			Present work	
Ground state energy (a.u.)	-1.1745^a						-1.1684
	Δ E	Dipole	Δ E	length	velocity	Δ E	Dipole
$^1\Sigma_u$	0.4686^c	0.9821^e	0.4686	0.9802	0.9796	0.4638	0.9807
	0.5459^d	0.3966^d	0.5455	0.3973	0.3971	0.5400	0.4323
						0.5659	0.3084
						0.5670	0.0073
						0.5777	0.2202
$^1\Pi_u$	0.4862^b	0.7432^e	0.4866	0.7212	0.7170	0.4809	0.7344
			0.5510	0.3324	0.3302	0.5451	0.3781
						0.5670	0.0029
						0.5678	0.2740
						0.5783	0.0005

[a] Kołos and Wolniewicz (1965)

[b] Rothenberg and Davidson (1966)

[c] Kołos and Wolniewicz (1968)

[d] Wolniewicz (1975)

[e] Dressler and Wolniewicz (1985)

Table 6.5: Transition dipoles in atomic units for excitation from the ground state to the lowest lying $^1\Sigma_u$ and $^1\Pi_u$ of H_2 at the fixed equilibrium internuclear separation of 1.4 a_o. The excitation energies ΔE are given in Hartrees.

State	Arrighini *et al* (1980) Δ E		Present work Δ E	
$^1\Sigma_u$	0.4678	0.2907	0.4638	0.2978
	0.5427	0.0611	0.5400	0.0674
	0.5685	0.0207	0.5659	0.0359
			0.5670	0.0000
			0.5777	0.0187
$^1\Pi_u$	0.4852	0.3492	0.4809	0.3464
	0.5486	0.0940	0.5451	0.1041
			0.5670	0.0000
	0.5717	0.0427	0.5678	0.0569
			0.5783	0.0000

Table 6.6: Oscillator strengths for excitation from the ground state to the lowest lying $^1\Sigma_u$ and $^1\Pi_u$ of H_2 at the fixed equilibrium internuclear separation of 1.4 a_o. The excitation energies ΔE are given in Hartrees.

Figure 6.1: Transition dipoles in a.u. as a function of internuclear separation, in a_o, for excitation from the ground to the first five excited $^1\Sigma_u$ states of H_2. Open circle, first state; open inverse triangle, second state; open square, third state; open triangle, fourth state; open diamond, fifth state.
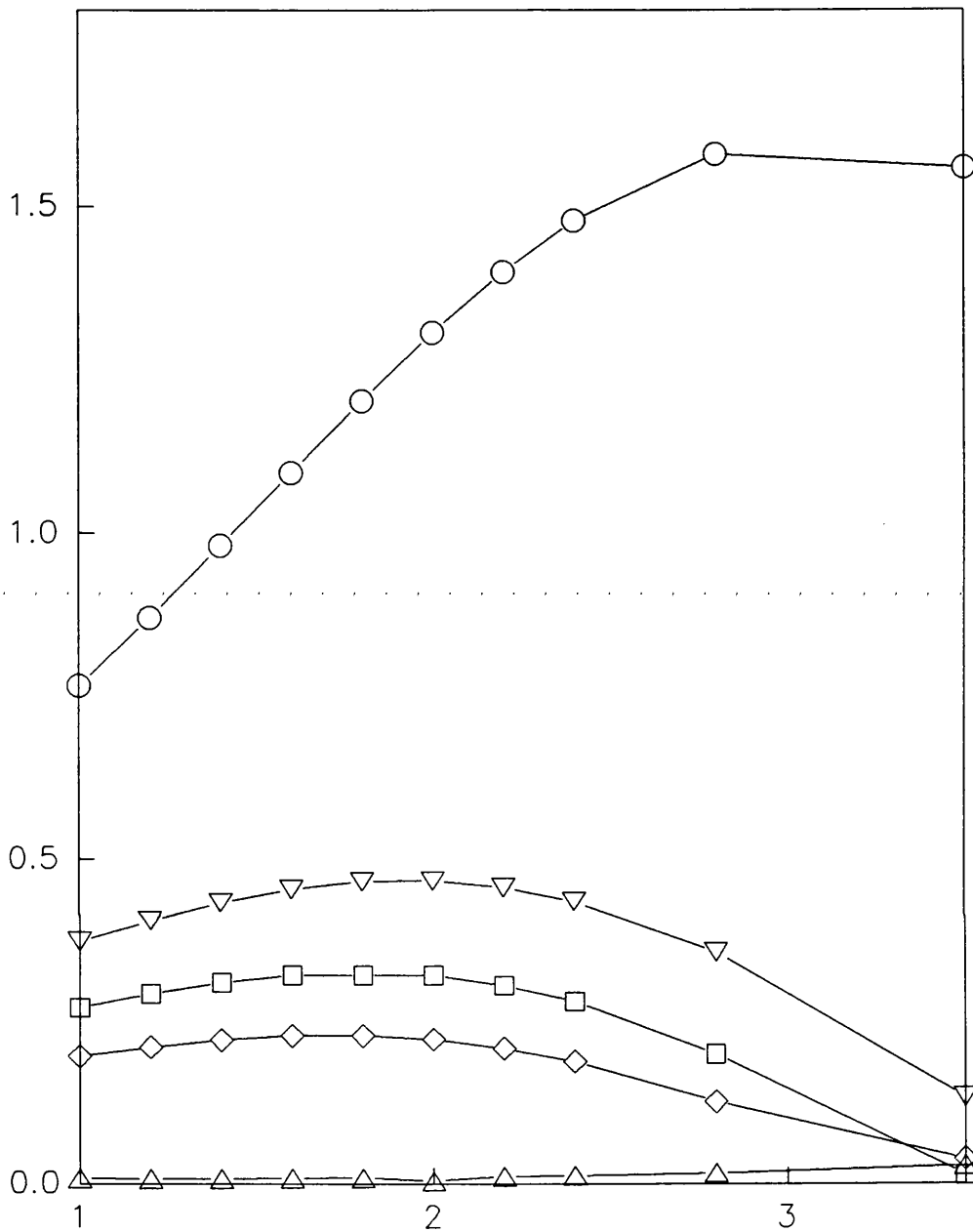
Figure 6.2: Transition dipoles in a.u. as a function of internuclear separation, in a_o, for excitation from the ground to the first five excited $^1\Pi_u$ states of H_2. Open circle, first state; open inverse triangle, second state; open square, third state; open triangle, fourth state; open diamond, fifth state.
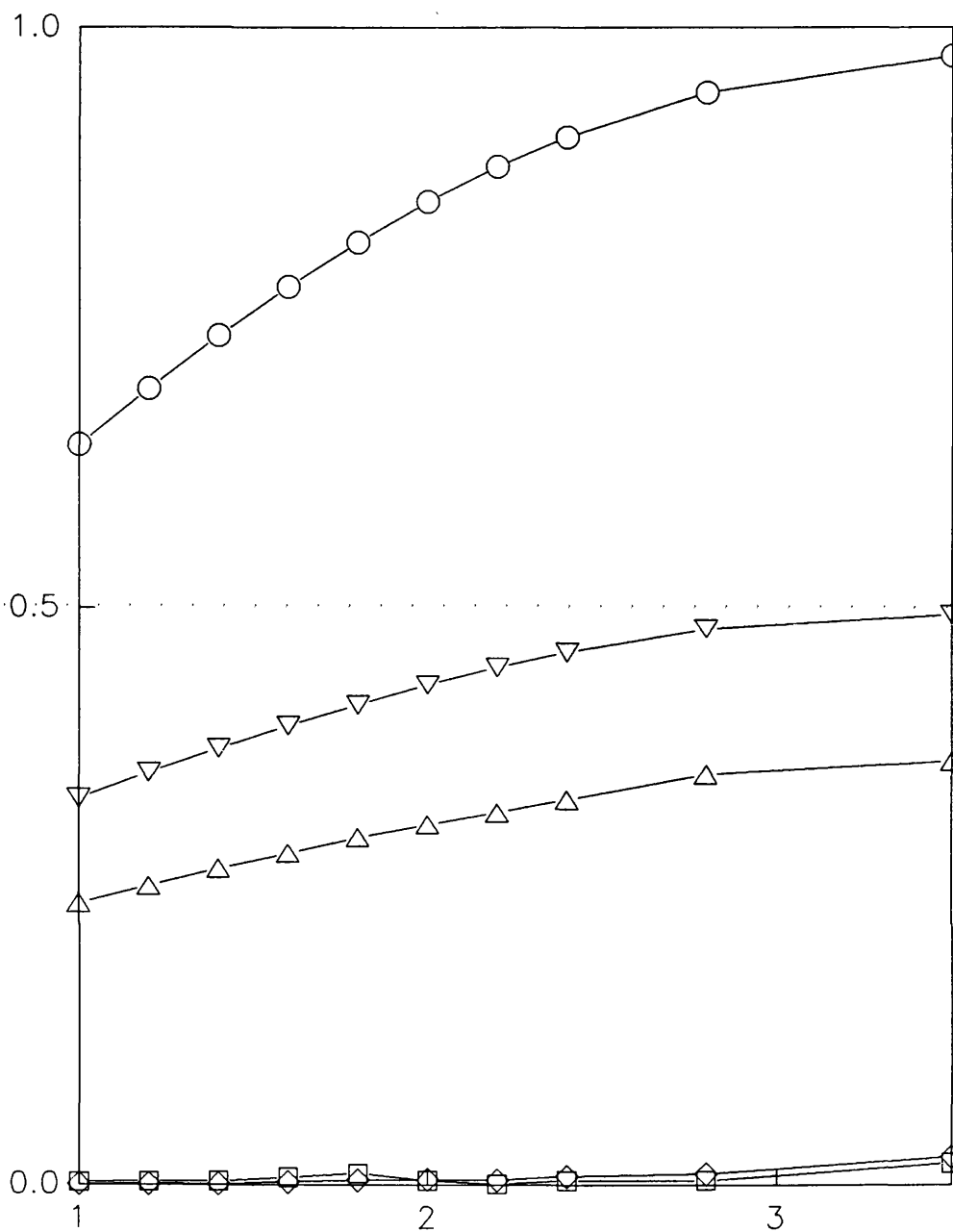
results are in slightly better agreement with the observed results of Herzberg and Johns (1969) and the calculations of van Dishoeck (1987). The module BOUND also has the clear advantage of being able to calculate far more bound states than the method of Ojha and Burke (1983).

6.3.2 HeH

The agreement between the results obtained using a Le Roy fit and those found from the vibrational BOUND calculation of the bound states of HeH is good, see table 6.3. This is particularly pleasing as it demonstrates that the atomic approach of Seaton (1985) can not only be applied to fixed nuclei molecular calculations, but it can also be applied to the vibrational states of molecules.

Essentially there is no difference between these two calculations. The adiabatic method of Sarpal *et al* (1991) first finds the bound states of the system at a grid of internuclear separation points. It then performs a fitting procedure after which the vibrational motion is accounted for. In the present method the inner region calculations are performed at a grid of internuclear separation points, then the nuclear motion is included which yields the vibrational surface amplitudes from which the vibrational R-matrix and hence the vibrational bound state can be calculated. The method presented here has the advantage that if, in the future, coupling between electronic states can be included in the calculation, this method will produce non-adiabatic results. Until then, this method makes the calculation of vibrational bound states much more straight forward.

In the present calculations it proved very difficult to use this approach for the $^2\Sigma$ symmetry. This was because the ground X $^2\Sigma$ state of HeH is dissociative. This meant that there are always open vibrational channels at the energies considered and the states are, therefore, not truly bound states, but resonances. The present computer package can not yet deal with this case.

6.3.3 H_2

The bound state method of Seaton (1985), described in detail in chapter 2, relies on the outer region functions, represented by the matrix $\mathbf{P}$, obeying the orthonormality condition:

$$< \mathbf{P}|\mathbf{P} >_O = 1, \tag{6.1}$$

in the outer region. This condition is satisfied if, at the R-matrix boundary:

$$\mathbf{P}^T\mathbf{Q}' - \mathbf{Q}^T\mathbf{P}' = 1, \tag{6.2}$$

where $\mathbf{Q}$ is defined in chapter 2, $\mathbf{P}'$ denotes the derivative of $\mathbf{P}$ with respect to energy and $\mathbf{P}^T$ denotes the transpose of $\mathbf{P}$. However, the outer region functions used in the present calculations did not satisfy equation (6.2). On evaluating the left hand side of this expression the matrix obtained was found to be diagonally dominant, but the off diagonal terms were as much as 5% of the diagonal elements. The results shown in table 6.4 were obtained by multiplying the outer region functions by a suitable matrix in order to obtain a matrix with diagonal elements equal to one on the evaluation of the left hand side of equation (6.2). The fraction of the contribution from the inner region to the total wavefunction of the system is given in table 6.4 in order to assess the effect of this error. It can be seen that for low lying states the effect of an error in the outer region would be negligible, but for higher states the effect would be more serious. In the future this problem may be solved by calculating the integral on the left hand side of equation (6.1) and using the result to renormalise the final total wavefunctions. However, this integral is not trivial to calculate because of the use of propagation techniques to obtain the outer region functions.

The function $\nu^3 f$ is also given in table 6.4. This function should vary smoothly as transitions to higher states are considered. It can be seen that for a specific quantum defect the present results would appear to follow this behavior.

The results shown in table 6.5 are in very good agreement with previous theoretical results for transitions between the ground and the first $^1\Sigma_u$ and $^1\Pi_u$ states of H_2. Agreement between the other states for which there are previous theoretical results available is within about 10%. The present results tend to overestimate the transition dipoles for these transitions. The major source of error is likely to be the error in the outer region function normalisation, since as the contribution from the outer region increases the agreement becomes less good.

The results shown in table 6.6 are in good agreement with the oscillator strengths of Arrighini et al (1980). As with the present work the calculations of Arrighini et al (1980) are scattering calculations, however, Arrighini et al (1980) have only included the singlet states of H_2. As with the transition dipoles, the present results would appear to overestimate the oscillator strengths for the higher states, which is again probably caused by the error in the outer region functions.

From figures 6.1 and 6.2 it would seem that the magnitude of the transition dipole varies unpredictably as higher states are considered. However, on closer inspection of the effective quantum numbers, the first, second, third and fifth $^1\Sigma_u$ states shown would appear to belong to the same series, with quantum defect equal to 0.073. This is also true for the first, second and fourth states shown for the $^1\Pi_u$ transitions, which have a quantum defect of approximately 0.066 and represent 'p' wave transitions, and for the third and fifth $^1\Pi_u$ transitions, which have a quantum defect of 0.004 and represent 'f' wave transitions.

In the modules BOUND and TDIP there are clearly some areas which need improvement. In particular the outer region normalisation requires a more rigorous approach and the outer region contribution to the transition moment must be included, see Seaton (1986). However, the development of these two modules has made it possible to calculate large amounts of bound state information from a single diagonalisation of the Hamiltonian matrix in the inner region, for both fixed nuclei

and vibration calculations on diatomic molecules. This has meant that transition dipoles can now be calculated to higher lying excited states than was previously possible. Once the improvements already mentioned have been implemented it is hoped that these two modules will be used to calculate transition dipoles, both from the ground state to much high lying excited states and from excited state to excited state.

Chapter 7

Conclusions

In this work the molecular R-matrix method has been used to study electronic excitation of H_2, by electron impact, at the fixed equilibrium internuclear separation of 1.4 a_o. The target molecule was at first represented by a full CI, six coupled electronic target state test model. This model was used to produce integral cross sections which revealed a large amount of resonance structure.

An improved seven electronic target state model was developed to include the E,F $^1\Sigma_g$ state of H_2 which was found to be important in the test calculations of da Silva *et al* (1990). This model was a significant advance on previous studies of this system, since more than two states were included at a time. Improved representation of correlation and polarisation also lead to resonance features, which could not previously be studied in this way.

This seven state model was used to produce integral cross sections for electronic excitation processes and a study of the resonance positions and widths made. It became apparent that the resonance structure could only be understood by a study of the differential cross sections. This was then performed and it was shown that great care must be exercised when classifying resonances since the apparent peak position and width vary, not only with the exit channel monitored, but also the angle of

observation.

Although the agreement between the present results and previous experimental and theoretical results was good for the integral cross sections this agreement was not as pleasing for the differential cross sections. The major cause of error is considered to be the lack of vibrational and rotational motion in this fixed geometry calculation. It is clear that any future investigation should include this in the target and scattering representations.

In this work a computer module has also been developed to calculate the bound states of molecules. This module represents an improvement on previous modules, which could calculate only the low lying bound states, since it can produce large numbers of Rydberg bound states. The module was been tested on the $e^- + CH^+ \rightarrow CH$ at fixed geometry and shown to give good agreement with previous calculated and observed results. It was also tested on the $e^- + HeH^+ \rightarrow HeH$ system at fixed geometry, where the lowest 33 electronic bound states could be assigned, and for a vibrational calculation, where good agreement with an alternative method was obtained.

The development of the bound state module also made it possible to develop a second module to produce transition dipoles and oscillator strengths of molecules. These two modules were then used to calculate the bound states and transition dipoles of H_2. Few previous results exist for the transition dipoles to electronically excited states of H_2, but where they do the present results are in reasonable agreement with them.

It is hoped that in the future the bound state code will be developed to calculate truly non-adiabatic results from which transition dipoles to high lying bound states can be computed.

References

Ajello J M, Shemansky D, Kwok T L and Yung Y L 1984 *Phys. Rev.* A **29** 636–53

Ajello J M, Srivastava S K and Yung Y L 1982 *Phys. Rev.* A **25** 2485–98

Armour E A G and Baker D J 1987 *J. Phys. B: At. Mol. Phys.* **20** 6105–19

Armour E A G, Baker D J and Plummer M 1991 *J. Phys. B: At. Mol. Opt. Phys.* **23** 3057–74

Arrighini G P, Biondi F and Guidotti C 1980 *Mol. Phys.* **41** 1501–14

Arthurs A M and Dalgarno A M 1960 *Proc. Roy. Soc.* A **256** 540–51

Baluja K L, Burke P G and Morgan L A 1982 *Computer Phys. Comm.* **27** 299–307

Baluja K L, Noble C J and Tennyson J 1985 *J. Phys. B: At. Mol. Phys.* **18** L851–5

Bardsley J N and Cohen J S 1978 *J. Phys. B: At. Mol. Phys.* **11** 3645–54

Bauschlicher C W Jr.and Langhoff S R 1991 *Theor Chim Acta.* **79** 93–103

Berrington K A, Burke P G, Butler K, Seaton M J, Storey P J, Taylor K T and Yu Yan 1987 *J. Phys. B: At. Mol. Phys.* **20** 6379–97

Berrington K A and Seaton M J 1985 *J. Phys. B: At. Mol. Phys.* **18** 2587–99

Bloch C 1957 *Nucl. Phys.* **4** 503–28

Böse N and Linder F 1979 *J. Phys. B: At. Mol. Phys.* **12** 3805–17

Buckley B D and Bottcher C 1977 *J. Phys. B: At. Mol. Phys.* **10** L635–40

Buckley B D, Burke, P G and Noble C J 1984 *Electron-molecule collisions* eds I Shimamura and K Takayanagi (Plenum, New York) pp 495–556

Buckman S J, Brunger M J, Newman D S, Snitchler G, Alston S, Norcross D W, Morrison M A, Saha B C, Danby G and Trail W K 1991 *Phys. Rev. Lett.* **65** 3253–6

Burke P G 1982 *In Physics of Electronic and Atomic collisions* ed S Datz (Amsterdam: North Holland) p201

— 1979 Lecture notes from NATO Advanced Study Institute 'Quantum Dynamics of Molecules', Trinity Hall Cambridge, U.K.

Burke P G, Hibbert A and Robb W D 1971 *J. Phys. B: At. Mol. Phys.* **4** 153–161

Burke P G, Mackey I and Shimamura I 1977 *J. Phys. B: At. Mol. Phys.* **10** 2497–2512

Burke P G and Noble C J 1986 *Comments At. Mol. Phys.* **18** 181–207

Burke P G and Robb W D 1975 *Adv. At. Mol. Phys.* **11** 143–214

Burke P G and Seaton M J 1984 *J. Phys. B: At. Mol. Phys.* **17** L683–7

Burke P G and Shimamura I 1990 *Molecular Processes in Space* eds T Watanabe, I Shimamura, M Shimizu and Y Itikawa (Plenum, New York) pp 17–39

Burke P G 1982 *In Physics of Electronic and Atomic collisions* ed S Datz (Amsterdam: North Holland) p201

Burke P G and Sinfailam A L 1970 *J. Phys. B: At. Mol. Phys.* **3** 641–659

Buttle P J A 1967 *Phys. Rev.* **160** 719–29

Chang E S and Fano U 1972 *Phys. Rev.* A **6** 173–185

Clark C W and Taylor K T 1982 *J. Phys. B: At. Mol. Phys.* **15** L213–9

Cohen J S and Bardsley J N 1980 unpublished work

Collins L A and Robb W D 1980 *J. Phys. B: At. Mol. Phys.* **13** 1637–1649

Collins L A, Robb W D and Morrison M A 1978 *J. Phys. B: At. Mol. Phys.* **11** L777–81

Collins L A and Schneider B I 1981 *Phys. Rev.* A **24** 2387–2401

Comer J and Read F H 1971 *J. Phys. B: At. Mol. Phys.* **4** 368–88

Dalgarno A and Davison W D 1966 *Adv. At. Mol. Phys.* **2** 1–32

Danby G 1991 *private communication*

Danby G and Tennyson J 1990 *J. Phys. B: At. Mol. Opt. Phys.* **23** 1005–16

da Silva A J R, Lima M A P, Brescansin L M and McKoy B 1990 *Phys. Rev.* A **41** 2903–5

DeRose E F, Gislason E A, Sabelli N H and Sluis K M 1988 *J. Chem. Phys.* **88** 4878–83

Dressler K and Wolniewicz L 1985 *J. Chem. Phys.* **82** 4720-1

Eliezer I, Taylor H S and Williams J K 1967 *J. Chem. Phys.* **47** 2165-77

Fliflet A W and McKoy V 1980 *Phys. Rev.* A **21** 1863-75

Fraga S and Ransil B J 1961 *J. Chem. Phys.* **35** 1967-77

Furst J, Mahgerefteh M and Golden D E 1984 *Phys. Rev.* A **30** 2256-60

Gibson T L, Lima M A P, McKoy V and Huo W M 1987 *Phys. Rev.* A **35** 2473-8

Gibson T L, Lima M A P, Takatsuka K and McKoy V 1984 *Phys. Rev.* A **30** 3005-11

Gillan C J, Nagy O, Burke P G, Morgan L A and Noble C J 1987 *J. Phys. B: At. Mol. Opt. Phys.* **20** 4585-603

Gillan C J, Noble C J and Burke P G 1988 *J. Phys. B: At. Mol. Phys.* **21** L53-9

Hall R I and Andric L 1984 *J. Phys. B: At. Mol. Phys.* **17** 3815-25

Hara S 1969 *J. Phys. Soc. Japan* **27** 1009-19

Herzberg G and Johns J W C 1969 *Astrophys. J.* **158** 399-418

Huetz A and Mazeau J 1983 *J. Phys. B: At. Mol. Phys.* **16** 2577-92

Huo W M and Weatherford C A 1991 *Phys. Rev.* A *to be published*

Joyez G, Comer J and Read F H 1973 *J. Phys. B: At. Mol. Phys.* **6** 2427-40

Kaufmann K, Baumeister W and Jungen M 1989 *J. Phys. B: At. Mol. Opt. Phys.* **22** 2223-40

Ketterle W 1990 *J. Chem. Phys.* **93** 6935-41

Khakoo M A and Trajmar S 1986a *Phys. Rev.* A **34** 138-45

— 1986b *Phys. Rev.* A **34** 146-56

Khakoo M A, Trajmar S, McAdams R and Shyn T W 1987 *Phys. Rev.* A **35** 2832-7

Kolos W 1978 *J. Mol. Structure.* **46** 73-92

Kolos W and Rychlewski J 1977 *J. Mol. Spectrosc.* **66** 428-40

Kolos W and Wolniewicz L 1965 *J. Chem. Phys.* **43** 2429-41

— 1967 *J. Chem. Phys.* **46** 1426-32

— 1968 *J. Chem. Phys.* **48** 3672-80

Lee M-T, Lucchese R R and McKoy V 1982 *Phys. Rev.* A **26** 3240–8

Lee M-T, Machado L E, Leal E P, Brescansin L M, Lima M A P and Machado F B
C 1990 *J. Phys. B: At. Mol. Opt. Phys.* **23** L233–7

Le Roy R J 1971 *J. Chem. Phys.* **54** 5433–4

Lima M A P, Gibson T L, McKoy V and Huo W M 1988 *Phys. Rev.* A **38** 4527–36

Lima M A P, Gibson T L, Huo W M and McKoy V 1985 *J. Phys. B: At. Mol. Phys.*
18 L865–70

Mason N J and Newell W R 1986a *J. Phys. B: At. Mol. Phys.* **19** L203–7

— 1986b *J. Phys. B: At. Mol. Phys.* **19** L587–91

Malegat L 1990 *Computer Phys. Comm.* **60** 391–404

McConkey J W, Trajmar S and King G C M 1988 *Comments At. Mol. Phys.* **22**
17–49

McCurdy, Jr. C W, Rescigno T N and McKoy V 1976 *J. Phys. B: At. Mol. Phys.*
9 691–8

McLean A D 1971 *Conf. Potential Energy Surfaces in Chemistry* ed W A Lester Jr
(San Jose: IBM Research Laboratory) p 87

McNaughten P, Thompson D G and Jain A 1990 *J. Phys. B: At. Mol. Opt. Phys.*
23 2405S–24S

Miller W H and Jansen op de Haar B M D D 1987 *J. Chem. Phys.* **86** 6213–20

Morgan L A 1984 *Computer Phys. Comm.* **31** 419–22

Morgan L A 1986 *J. Phys. B: At. Mol. Phys.* **19** L439–45

— 1990 *Proc. 16th Int. Conf. on Physics of Electronic and Atomic Collisions* ed
A Dalgarno *et al* (Plenum: New York) Invited Papers and Progress Reports pp
96–102

Morgan L A, Burke P G and Gillan C J 1990 *J. Phys. B: At. Mol. Opt. Phys.* **23**
99–113

Morrison M A 1979 *Electron-molecule and Photon-molecule Collisions* ed T N Rescigno,

124

V McKoy and B I Schneider pp 15–51 (Plenum: New York) 1979

Morrison M A and Collins L A 1981 *Phys. Rev.* A **23** 127–38

Nesbet R K, Noble C J and Morgan L A 1986 *Phys. Rev.* A **34** 2798–808

Nishimura H and Danjo A 1986 *J. Phys. Soc. Japan* **55** 3031–6

Nishimura H, Danjo A and Sugahara H 1985 *J. Phys. Soc. Japan* **54** 1757–68

Noble C J 1982 *Daresbury Laboratory Technical Memorandum*

Noble C J and Nesbet R K 1984 *Computer Phys. Comm.* **33** 399–411

Norcross D W and Padial N T 1982 *Phys. Rev.* A **25** 226–38

Ojha P C and Burke P G 1983 *J. Phys. B: At. Mol. Phys.* **16** 3513–29

Pasquerault D, Defrance A and Hagene M 1985 *J. Phys. B: At. Mol. Phys.* **18** L871–3

Redmon M J, Garrett B C, Redmon L T and McCurdy C W 1985 *Phys. Rev.* A **32** 3354–65

Rescigno T N, McCurdy C W Jr. and McKoy V 1974 *J. Phys. B: At. Mol. Phys.* **7** 2396–402

Rescigno T N and Schneider B I 1988 *J. Phys. B: At. Mol. Opt. Phys.* **21** L691–5

Rothenberg S and Davidson E R 1966 *J. Chem. Phys.* **44** 730–7

Sarpal B K, Tennyson J and Morgan L A 1991a *J. Phys. B: At. Mol. Opt. Phys.* **24** 1851–66

Sarpal B K, Branchett S E, Tennyson J and Morgan L A 1991b *J. Phys. B: At. Mol. Opt. Phys.* **24** 3685–99

Schadee A 1978 *J. Quant. Spectrosc. Radiat. Transfer* **19** 451–3

Schneider B I 1975 *Chem. Phys. Lett.* **31** 237–241

Schneider B I and Collins L A 1981 *J. Phys. B: At. Mol. Phys.* **14** 101–6

Schneider B I and Collins L A 1985 *J. Phys. B: At. Mol. Phys.* **18** L857–63

Schneider B I, LeDourneuf M and Burke P G 1979 *J. Phys. B: At. Mol. Phys.* **12** L365–9

Schulz G J 1973 *Rev. Mod. Phys.* **45** 423–86

Seaton M J 1966 *Proc. Phys. Soc.* **88** 801–14

— 1985 *J. Phys. B: At. Mol. Phys.* **18** 2111–31

— 1986 *J. Phys. B: At. Mol. Phys.* **19** 2601–10

— 1987 *J. Phys. B: At. Mol. Phys.* **20** 6363–78

Shimamura I 1978 *Proc. 10th Int. Conf. on Physics of Electronic and Atomic Collisions* (North Holland) pp 213–30

Shimamura I, Noble C J and Burke P G 1990 *Phys. Rev.* A **41** 3545–54

Snitchler G, Alston S, Norcross D, Saha B, Danby G, Trail W and Morrison M A 1991 *private communication*

Spence D 1974 *J. Phys. B: At. Mol. Phys.* **7** L87–90

Takatsuka K and McKoy V 1981 *Phys. Rev.* A **24** 2473–80

— 1984 *Phys. Rev.* A **30** 1734–40

Takayanagi K and Geltman S 1965 *Phys. Rev.* A **138** 1003–10

Tawara H, Itikawa Y, Nishimura H and Yoshimo M 1990 *J. Phys. Chem. Ref. Data* **19** 617–36

Tennyson J 1986 *J. Phys. B: At. Mol. Phys.* **19** 4255–63

— 1988 *J. Phys. B: At. Mol. Opt. Phys.* **21** 805–16

— 1990 *private communication*

— 1991 *private communication*

Tennyson J, Berrington K A and Burke P G 1987 *Computer Phys. Comm.* **47** 207–12

Tennyson J and Morgan L A 1987 *J. Phys. B: At. Mol. Phys.* **20** L641–6

Tennyson J and Noble C J 1984 *Computer Phys. Comm.* **33** 421–4

Tennyson J, Noble C J and Burke P G 1986 *Int. J. Quantum Chemistry* **29** 1033–42

Truhlar D G and Brandt M A 1976 *J. Chem. Phys.* **65** 3092–101

van Dishoeck E F 1987 *J. Chem. Phys.* **86** 196–214

Watson J Jr and Anderson R J 1977 *J. Chem. Phys.* **66** 4025–30

126

Weingartshofer A, Clarke E M, Holmes J K and McGowan J W 1975 *J. Phys. B: At. Mol. Phys.* **8** 1552–69

Weingartshofer A, Ehrhardt H, Hermann V and Linder F 1970 *Phys. Rev.* A **2** 294–304

Whiting E E, Schadee A, Tatum J B, Hougen J T and Nicholls R W 1980 *J. Mol. Spectrosc.* **80** 249–56

Wigner E P 1946a *Phys. Rev.* **70** 15–33

— 1946b *Phys. Rev.* **70** 606–618

Wigner E P and Eisenbud L 1947 *Phys. Rev.* **72** 29–41

Wolniewicz L 1975 *Chem. Phys. Lett.* **31** 248–50

Wolniewicz L and Dressler K 1985 *J. Chem. Phys.* **82** 3292–9